FUNCTIONAL CHARACTERIZATION OF *gnb3b* AND *guk1b* FOR PHOTORECEPTOR INTEGRITY IN A ZEBRAFISH MODEL FOR RETINITIS PIGMENTOSA

HUSVINEE SUNDARAMURTHI

NATIONAL UNIVERSITY OF SINGAPORE

2016

FUNCTIONAL CHARACTERIZATION OF *gnb3b* AND *guk1b* FOR PHOTORECEPTOR INTEGRITY IN A ZEBRAFISH MODEL FOR RETINITIS PIGMENTOSA

HUSVINEE SUNDARAMURTHI

(B.Sc.(HONS.), NANYANG TECHNOLOGICAL UNIVERSITY)

A THESIS SUBMITTED

FOR THE DEGREE OF DOCTOR OF PHILOSOPHY

DEPARTMENT OF BIOLOGICAL SCIENCES

NATIONAL UNIVERSITY OF SINGAPORE

2016

Declaration

I hereby declare that this thesis is my original work and it has been written by me in its entirety. I have duly acknowledged all the sources of information which have been used in the thesis.

This thesis has also not been submitted for any degree in any university previously.

_____

Husvinee Sundaramurthi

21 January 2016

Acknowledgements

First and foremost, I would like to express my sincere gratitude to my supervisor, Assoc. Prof. Christoph Winkler for giving me this wonderful opportunity to carry out my doctoral studies in his lab. I am especially thankful for providing me with the independence and sufficient freedom to pursue my research. I greatly appreciate the continuous guidance, critics and oppurtunities that he has given me over these past years, which has made me a better researcher.

I would also like to thank my TAC members, Assoc. Prof. Cynthia He and Prof. Gong Zhiyuan, who took time off their heavy work schedule to listen to my project and give me helpful suggestions. I am very thankful to Joanne, who joined the project as a FYP student, and was a great help in screening of the mutant lines. I would like to say a big thanks to her, for going out of her way to stay on in the lab after her FYP, to help me with my project. I would like to acknowledge Eugene, who helped me with the screening of *guk1b* mutants.

I am sincerely thankful to Mdm Loy and Keshma for spending hours on end with me to teach and train me for EM - from sample preparation to imaging. Special thanks to Martin for making the *guk1b* gRNA used in the generation of the mutant line and for patiently teaching me various experimental techniques when I was new to the lab. Additionally, I want to thank Leslie and Angela for all the extensive discussions we had over TALEN design and generation; Thuy for teaching me the ropes of cryo-sectioning; Mr Balan from the fish facility for always having available fish/embryos; Sudha, Shermaine and Wen hui for the various help in setting up fish and collecting embryos; and Manish for always fixing my laptop Wi-Fi network connection without complaining. I am grateful for the financial support that I have received from DBS, NUS to pursue my graduate studies and to Reena and Priscilla for all the administrative paper work support.

Anita, Angela, Zoltan and Martin: thank you very much for your advice, constant encouragement in various stages of my PhD and always being willing to lend a listening ear. I am extremely grateful for my lab partners-in-crime, Tingsheng and Sudha, you know what you did/still do; Vicky for being my confidante and always being there for me. I would like to thank all of my colleagues, both former and present, for helping me in any possible way, creating a friendly and pleasant work atmosphere, making the past 4 years in the lab enjoyable and eventful.

Last but not least, I would like to thank my entire family for the unconditional love, unwavering support and time, without whom my life wouldn't be the same.

I dedicate this thesis to my mum and dad - for giving me the chance to become who I am today.

Publications

1. Yin, J., Brocher, J., Linder, B., Hirmer, A., **Sundaramurthi, H.**, Fischer, U., and Winkler, C., *The 1D4 antibody labels outer segments of long double cone but not rod photoreceptors in zebrafish.* Investigative Ophthalmology & Visual Science, 2012. **53**(8): p. 4943-51.

Conferences

1. 9th European Zebrafish Meeting, Oslo, Norway (2015)

Poster: A Zebrafish Model For Retinitis Pigmentosa: Identification Of Novel Candidates That Are Required For Photoreceptor Integrity

2. SNA Symposium 'Neurons and Glia: Advances in Health and Disease' National University of Singapore, Singapore (2013)

Poster: A zebrafish model for Retinitis pigmentosa: Identification of novel genes required for photoreceptor maintenance

3. 17th Biological Sciences Graduate Congress, Chulalongkorn University, Thailand (2012)

Presenter: A zebrafish model for human eye disorders: Identification and characterization of novel Retinitis Pigmentosa disease genes

Contents

Summary

Retinitis Pigmentosa (RP) is a debilitating inherited eye disease affecting approximately 1 in 5000 people worldwide. RP patients exhibit rod and cone photoreceptor degeneration with intra-retinal pigment deposition that ultimately results in blindness. Mutations in the pre-mRNA splicing factors Prpf8 and Prpf31 have been shown to cause RP. However, it remains unclear how deficiencies in these ubiquitously expressed proteins lead to a retina specific phenotype. To address this, a transcriptome analysis of *prpf8/31* deficient zebrafish retinas was performed previously and several novel candidates with potential implications for the pathophysiology of RP were identified (Brocher et al., unpublished). In the present study, two of the novel candidate genes, *gnb3b* and *guk1b*, were selected for further functional characterization using gene knock-down and knock-out strategies in a zebrafish model.

Gnb3b encodes the beta subunit of the heterotrimeric G protein transducin, and is possibly involved in the phototransduction signalling cascade. *gnb3b* morphants showed irregularities in the outer segments of cone photoreceptors, whereas rods appeared normal. *gnb3b* mutants, on the other hand, had similarly malformed cone photoreceptors, but rod outer segments were also mildly affected at larval stages. Interestingly, homozygous *gnb3b* mutants showed with high larval lethality and did not survive into adulthood. The second analysed gene, *guk1b*, encodes a kinase required for catalyzing the formation of GDP from GMP, as part of cGMP recycling during phototransduction. *guk1b* morphants reflected a characteristic RP phenotype, with degenerating rod photoreceptors and pigment deposition. Contrarily, in larval and adult *guk1b* mutants, rods appeared mostly unaffected with only slight shortening of the outer segments and absence of intra-retinal pigment deposition. In contrast, the outer segment of cone cells exhibited strong structural deficits in both larvae and adults. In conclusion, the obtained data suggests that *gnb3b* and *guk1b* are essential for the maintenance of photoreceptors, especially cones, and their structural integrity.

List of Figures

List of Tables

List of Abbreviations

^{0}C	degree celsius
3D	3-Dimensional
adRP	autosomal dominant RP
ATP	adenosine triphosphate
bp	base pairs
Ca^{2+}	calcium ions
Cas9	clustered regularly interspaced short palindromic repeats -associated genes
cGMP	cyclic GMP
CRISPR	clustered regularly interspaced short palindromic repeats
dpf	days post fertilization
EM	electron microscopy
ERG	electroretinogram
EtOH	Ethanol
Gα	G alpha subunit
Gβ	G beta subunit
Gγ	G gamma subunit
GC	guanylyl cyclase
gDNA	genomic DNA
GDP	guanosine diphosphate
GMP	guanosine monophosphate
gnb3b	guanine nucleotide binding protein (G protein), beta polypeptide 3b
gRNA	guide RNA
GTP	guanosine triphosphate
guk1b	guanylate kinase 1b
HDR	homology directed repair
hpf	hours post fertilization
hrs	Hours
IBMX	3-isobutyl-1-methylxanthine
indels	insertion/deletion
IPL	inner plexiform layer
LCA	Leber's congenital amaurosis
MeOH	Methanol
mins	Minutes
MO	morpholino oligonucleotides
MQ water	Milli Q water
Na^{+}	sodium ions
NDP-K	nucleoside diphosphate kinase
NHEJ	non-homologous end joining
NMD	nonsense mediated decay
OKR	optokinetic response
OPL	outer plexiform layer
PCR	polymerase chain reaction
PDEs	phosphodiesterases
ph3	phosphorylated-histone 3
PG	pigment granules
prpf	pre-mRNA processing factors
RFLP	restriction fragment length polymorphism
Rge	retinopathy globe enlarged
RP	retinitis pigmentosa
rpm	revolutions per minute
RT	room temperature
RT-PCR	reverse transcriptase-PCR
s/sec	Seconds
SNP	single nucleotide polymorphism
snRNP	small nuclear ribonucleoprotein
TALEN	transcription activator-like effector nuclease
Temp.	Temperature
TUNEL	terminal deoxynucleotidyl transferase dUTP nick end labelling
USH2A	Usher syndrome 2A
Vol.	Volume
WISH	whole mount in situ hybridization

1. Introduction

1.1. Retinitis pigmentosa (RP) disease manifestation

Retinitis pigmentosa (RP) is an inherited retinal degenerative disease with a worldwide prevalence of approximately 1 in 5000 people (Chizzolini et al., 2011; Anasagasti et al., 2012). The age of onset ranges between early childhood to adulthood. Patients suffering from RP have initial night blindness, followed by peripheral vision loss and ultimately complete blindness (Hamel, 2006; Natarajan, 2011). The various stages of disease progression in RP are mainly attributed to primary loss of rods (tunnel vision) followed by cone photoreceptors with intra-retinal pigment deposition (Hamel, 2006). This disease displays locus heterogeneity whereby mutations in more than one gene or multiple mutations in a single gene results in RP (RetNet, http://www.sph.uth.tmc.edu/RetNet/). Additionally, patients with similar mutations can exhibit different disease onset, disease manifestation and severity of symptoms even within the same family (Daiger et al., 2007).

RP can be further classified as a non-syndromic (does not affect other organs), syndromic (affects other sensory systems) or systemic (affects multiple organs) eye disease. Non-syndromic RP has different modes of inheritance, namely autosomal dominant, autosomal recessive and X-linked recessive forms. Rare forms of RP with inheritance patterns such as X-linked dominant, digenic or mitochondrial do occur as well (Daiger et al., 2007). The autosomal dominant form of RP occurs with a frequency of about 30 to 40% of cases, the recessive form in 50 to 60%, and the X-linked trait approximately in 5 to 15% of cases (Hartong et al., 2006; Ferrari et al., 2011; Anasagasti et al., 2012).

1.1.1. Genetics of autosomal dominant RP (adRP)

In a review article by Hartong et al., it was highlighted that almost 50% of adRP cases have an unknown molecular etiology, while 25% of the cases were due to alterations in the rhodopsin gene (Fig. 1) (Hartong et al., 2006). The remaining 25% of the causal genes identified so far were from various gene families. In most cases, the genes affected were involved in various retina related functions such as visual transduction, retinal metabolism, photoreceptor growth, development and maintenance.

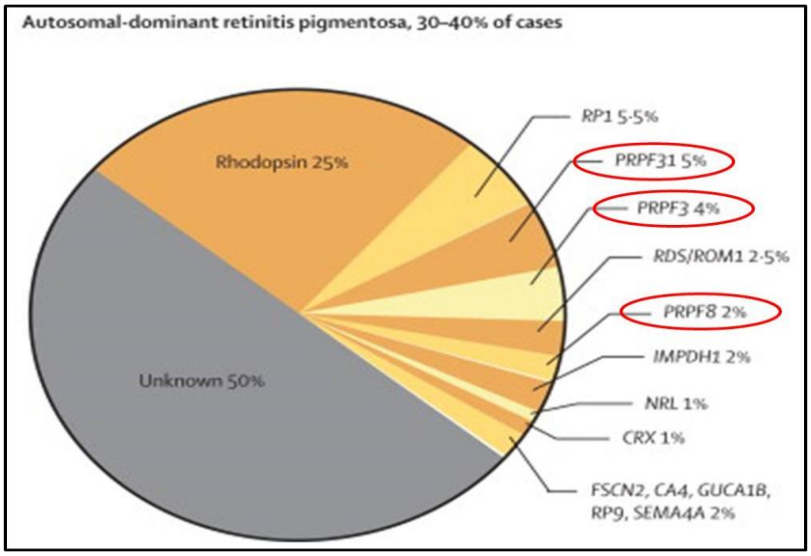

Figure 1: Pie chart depicting the incidence of various types of autosomal dominant RP (adRP) disease genes. About 50% of the cases have unknown molecular etiology. 25% of the cases are caused by mutations in the rhodopsin gene and the remaining 25% of the cases are made up of genes from various gene families. Genes circled in red encode ubiquitously expressed pre-mRNA splicing factors (adapted and modified from Hartong et al., 2006).

Interestingly, it was shown that more than 12% of the mutations occurred in genes that encoded for ubiquitously expressed splicing factors such as *pap1*, *snrn200*, *prpf3*, 6, *8* and *31* (Fig. 1, red circles) (Hartong et al., 2006; Ferrari et al., 2011; Benaglio et al., 2014). Pre-mRNA processing factors 3, 8 and 31 (Prpf3, 8 and 31) are conserved, essential members of the splicing machinery, and mutations in them result in an eye-specific phenotype. This raised the question of how such widely expressed genes result in a tissue specific phenotype without causing devastating systemic disorders.

1.1.2. Pre-mRNA splicing and the role of Prpf8 and Prpf31

In the splicing pathway, Prpfs are required for the proper formation of the U4/U6.U5 tri-snRNP complex as well as for the catalytic activation of the spliceosome. Briefly, the U1 snRNP (small nuclear ribonucleoprotein) recognizes and binds to the 'GU' dinucleotide at the 5' intron site while U2 snRNP binds to the branch point 'A', towards the 3' end forming the pre-spliceosome complex A (Fig. 2A). Following this, the U4/U6.U5 tri-snRNP complex joins with complex A to make up the pre-catalytic complex B.

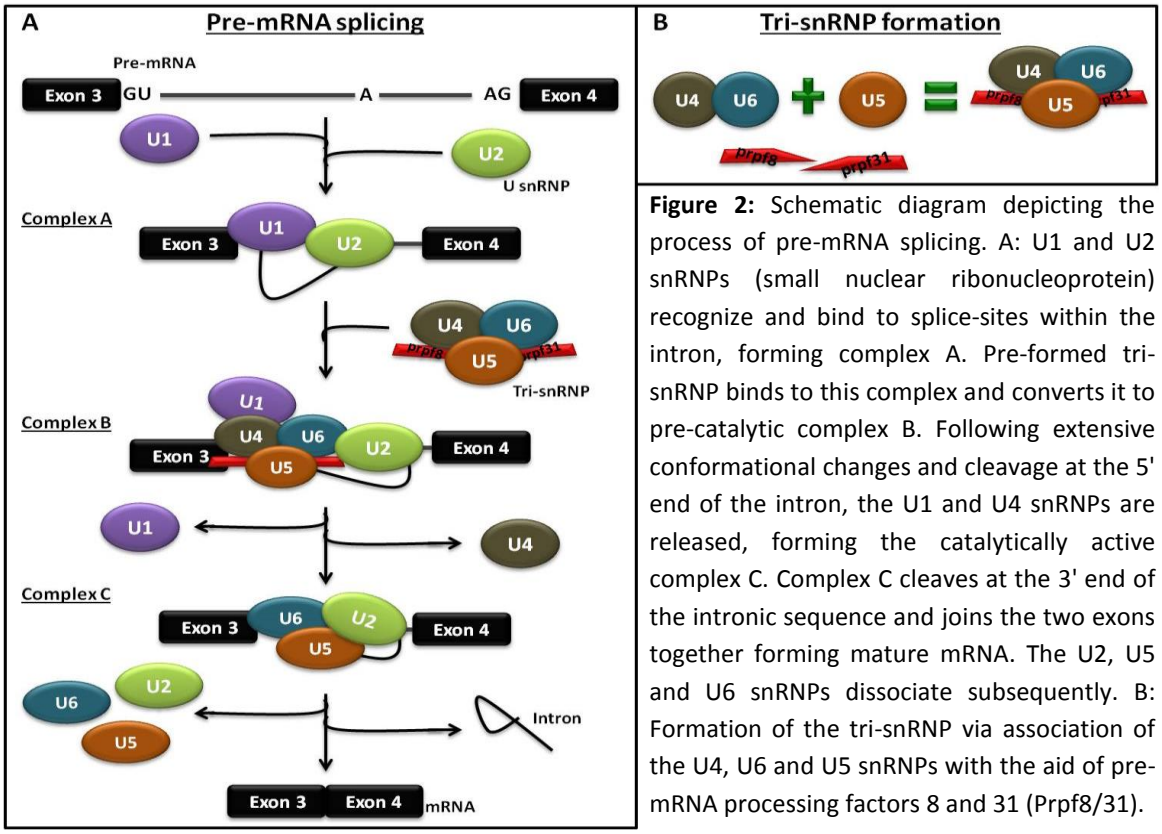

Figure 2: Schematic diagram depicting the process of pre-mRNA splicing. A: U1 and U2 snRNPs (small nuclear ribonucleoprotein) recognize and bind to splice-sites within the intron, forming complex A. Pre-formed tri-snRNP binds to this complex and converts it to pre-catalytic complex B. Following extensive conformational changes and cleavage at the 5' end of the intron, the U1 and U4 snRNPs are released, forming the catalytically active complex C. Complex C cleaves at the 3' end of the intronic sequence and joins the two exons together forming mature mRNA. The U2, U5 and U6 snRNPs dissociate subsequently. B: Formation of the tri-snRNP via association of the U4, U6 and U5 snRNPs with the aid of pre-mRNA processing factors 8 and 31 (Prpf8/31).

Subsequently, structural rearrangements and cleavage takes place, whereby the 5' intron end gets cleaved and links to the branch point forming a lariat. The U1 and U4 snRNPs get dissociated from the complex parallely (catalytic complex C). Finally, the catalytically active complex C cleaves at the 3' end removing the intron, disassembles the U2, U5, U6 snRNPs and joins the exons together, making up the mature mRNA (Jurica and Moore, 2003; Chen and Manley, 2009). The released snRNPs get recycled for subsequent rounds of splicing.

Initially, the U4 and U6 snRNPs are bound together with several other splicing related co-factors. In the presence of Prpf6/8/31, the U5 snRNP coupled to its specific co-factor proteins, is brought together to associate with the U4/U6 snRNP, making critical interactions to form a stable tri-snRNP complex (Fig. 2B) (Liu et al., 2006). It was found that the main role of Prpf31 was to tether the U4/U6 snRNP with U5 snRNP by acting as a bridge (Makarova et al., 2002). On the other hand, Prpf8 is highly conserved and forms the core component of the U5 snRNP protein. Prpf8 is involved in the interaction with the 5' and 3' splice-sites of the pre-mRNAs as well as for unwinding of U4/U6 snRNA (McKie et al., 2001; Grainger and Beggs, 2005).

One can postulate that deficiencies in these factors will lead to improper formation of the tri-snRNP and thereby affect spliceosomal complex formation and/or activity. Consequently, this will result in splicing deficits and altered protein production, which can have a detrimental effect on the organism.

1.1.3. Deficiencies in components of splicing factors lead to retina specific defects

Studies conducted in cell lines and zebrafish models, have demonstrated that Prpfs play a significant role in regulating pre-mRNA splicing, and that without sufficient amounts it results in retina-specific defects. In a *prpf31* deficient zebrafish model, it was observed that morphants presented with visual deficits, and several photoreceptor specific transcription factors were found to be down-regulated (Linder et al., 2011; Yin et al., 2011). The defects seen were attributed to be possible consequences of either nonsense mediated decay (NMD) of the target transcripts, dominant-negative effects that altered protein activity, or to the formation of cytotoxic aggregates.

Tanackovic et al. (2011) wanted to understand why the retina was more severly affected upon deficiency of widely expressed Prpfs. They measured the levels of snRNAs (components of the spliceosome) and mRNAs in various human tissues and cell lines and revealed that the retina

contained approximately seven times more snRNAs and had the highest amount of mature mRNAs (Tanackovic et al., 2011). This supports the hypothesis put forward by Vithana et al. (2001) whereby rods have a higher demand for spliced opsin mRNA for maintenance of structural integrity and phototransduction. In mutants with compromised splicing, cells are unable to meet this demand, making the rod photoreceptors more susceptible to degeneration (Vithana et al., 2001).

Taken together, this led to the idea of analysing the transcriptomes of *prpf8* and *31* zebrafish morphants for identification of novel candidate genes that could possibly be involved in the pathogenesis of retinal specific diseases (Linder et al., 2011).

1.2. Transcriptome analysis of *prpf8/31* morphant zebrafish retinas

Translation-blocking *prpf8* and *prpf31* morpholinos were injected into one-cell stage zebrafish embryos and total RNA from 3 days post fertilization (dpf) larval retinas was isolated for microarray transcriptome analysis (Linder et al., 2011; Brocher et al., unpublished). It was found that the majority of gene transcripts (93% for *prpf8* and 97% for *prpf31*) were unaffected in both morphant lines. The remaining 7% and 3% of transcripts were differentially (up and down) regulated in *prpf8* and *prpf31* morphants, respectively. Summarised in the table below is the list of gene transcripts showing differential expression with a cut-off of > 1.5 fold change (Table 1). The right panel depicts genes that are up-regulated. Notably, it was found to be made up of splicing factors forming the components of the splicing machinery (coloured in blue). This up-regulation was proposed to be a compensation trigger for the deficient splicing machinery (Linder et al., 2011).

Conversely, among the top-most down-regulated transcripts (left panel, in red), the majority of them have already been determined to be known genes involved in the pathomechanism of RP. Additionally, a small number of retina specific novel genes (highlighted in grey) were identified with potential involvement in RP disease manifestation.

Down-regulated genes

downregulated	FC	
Gene symbol	Prp31	Prp8
opn1lw1	13.21	7.43
opn1sw1	10.99	11.25
opn1mw1	10.92	11.02
Wu:fk54a10	10.27	8.68
opn1sw2	8.91	10.78
gnat2	8.07	11.65
opn1lw2	6.97	6.74
arr3l	6.26	5.50
rds4	6.24	8.65
gnb3	5.20	9.50
zgc:73075	5.03	4.59
gnat2	4.78	9.01
rs1	4.60	4.59
pde6c	4.49	9.26
Transcribed locus	4.48	3.58
guk1	4.44	4.88
rho	4.28	3.46
gngt2	4.20	3.83
sf3a3	4.08	3.80
rcv1	3.97	3.80
Data Not Found	3.63	3.56
zgc:73153	3.42	4.11
zgc:73359	3.23	4.82
zgc:114180	3.23	3.29
gnb5	3.16	3.92
nme2l	3.15	5.86
Discontinued	3.11	4.84
Transcribed locus	3.10	3.37
LOC560585	3.06	1.93
pde6c	3.06	6.30
rds2	3.05	6.40
pde6c	3.04	5.99
zgc:153443	3.02	5.31
rds4	3.02	5.55

Up-regulated genes

upregulated	FC	
	Prp31	Prp8
ccng1	4.50	5.55
Transcribed locus	4.41	17.50
tp53	4.14	6.04
zgc:136826	3.79	5.68
wu:fb51a10	3.32	2.78
13orf22l	2.80	2.69
LOC100000578	2.66	1.70
Data Not Found	2.39	1.54
LOC797854	2.38	1.89
Discontinued	2.38	1.99
scfd2	2.32	N/A
lsm7	2.32	1.71
eftud2	2.30	2.28
snrpd3	2.29	1.96
mmp2	2.25	2.81
Transcribed locus	2.24	N/A
Transcribed locus	2.23	2.50
lsm8	2.19	1.60
prpf31	2.18	1.61
Transcribed locus	2.15	2.02
snrpg	2.14	1.56
snrpe	2.14	1.54
Transcribed locus	2.12	1.83
wu:fi18h02	2.08	2.33
LOC794136	2.06	2.73
zgc:158463	2.06	1.54
snrpd1	2.05	2.40
LOC571762	2.04	N/A
Transcribed locus	2.02	N/A

Table 1: Transcriptome analysis of zebrafish larval retinas obtained from *prpf8/31* morphants at 3 dpf (Brocher et al., unpublished). Most of the transcripts were found unaffected upon *prpf8/31* knock-down (not shown). Transcripts labelled in blue are components of the splicing machinery. In the category of strongly down-regulated genes (left panel), the top regulated targets were identified to be transcripts that are already known to be involved in the pathomechanism of RP (coloured in red). Also novel retina specific genes were identified to be down-regulated (highlighted in grey). Novel target genes selected for further functional characterization in this thesis are labelled with green asterisks.

From the list of novel retina transcripts, two genes, guanine nucleotide binding protein (G protein) beta polypeptide 3b (*gnb3b*) and guanylate kinase 1b (*guk1b*) were selected for the present study, for functional characterization in a zebrafish model. Both *gnb3b* and *guk1b* showed a relatively strong down-regulation with a fold change of > 5 and > 4 in both *prpf8/31* morphants, respectively. These genes were selected based on their potential roles played in the rod and cone phototransduction cascade, and I hypothesize that any disruption in this pathway could lead to retinal diseases.

1.2.1. Gnb3b and Guk1b in the phototransduction signalling cascade

The selected two genes have potential functionality in the phototransduction cascade, which takes place in the outer segments of rod and cone photoreceptors. This raised the question on

how deficiency in these two genes might impact this pathway and possibly affect vision as a consequence. During phototransduction, a photon gets absorbed by opsins in respective rod and cone photoreceptor cells. This triggers a conformational change from 11-cis retinal to all-trans retinal (Shichida and Matsuyama, 2009) and mediates the activation of the heterotrimeric G protein, transducin, following the exchange of guanosine diphosphate (GDP) to guanosine triphosphate (GTP). Subsequently, the activated G alpha (Gα) subunit dissociates from the G beta and G gamma (Gβγ) subunit and moves along to activate phosphodiesterases (PDEs) (Fig. 3). In turn, the activated PDEs start hydrolysing cyclic GMP (cGMP) molecules into guanosine monophosphate (GMP), thereby closing the cGMP-gated ion channels.

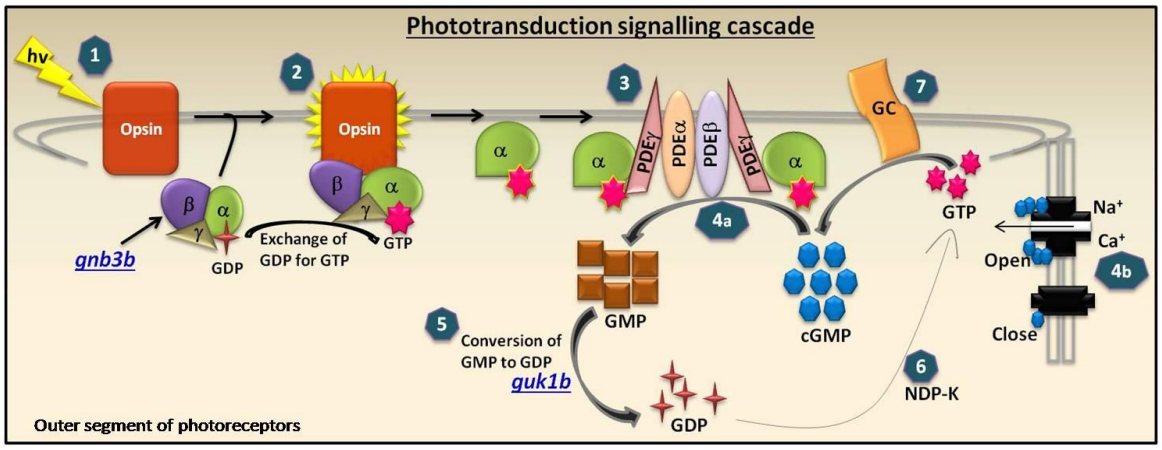

Figure 3: Step-wise diagram illustrating the phototransduction signalling cascade. 1. Absorption of a photon by opsins elicits a conformational change from 11-cis retinal to all-trans retinal. This triggers the activation of transducin (heterotrimeric G protein, *gnb3b*) via exchange of GDP to GTP. 2. The activated Gα subunit dissociates from the Gβγ subunit and interacts with PDEs, in turn activating them (3). Activated PDEs proceed to degrade cGMP molecules into GMP (4a), resulting in the closure of cGMP-gated ion channels (4b), and hence hyperpolarization of the photoreceptors. To re-establish homeostasis, GMP molecules are resynthesized into cGMP, with guanylate kinase (*guk1b*) initiating the first step (5) towards cGMP production. NDP-K converts GDP into GTP (6) and GC catalyzes the production of cGMP (7) in the subsequent steps. hv: photon, Gαβγ: heterotrimeric G protein - transducin, PDE: phosphodiesterase, GC: guanylyl cyclase, NDP-K: nucleoside diphosphate kinase (adapted and modified from Ridge et al., 2003).

As a result, the influx of Na^+ and Ca^{2+} ions gets stalled and a decrease in intracellular positive ion concentration causes the photoreceptors to be hyperpolarized. Hyperpolarization of photoreceptors lead to reduced neurotransmitters release and this signal is transmitted to the brain, where the visual information gets processed.

gnb3b is predicted to encode the β subunit of transducin that acts upstream (Fig. 3, step 2) in the phototransduction pathway while g*uk1b* acts further downstream, catalyzing the conversion of GMP into GDP (Fig. 3, step 5) (Ridge et al., 2003). One can postulate that disruption in either one of these two genes can lead to the dysregulation of the phototransduction pathway. It is speculated that without *gnb3b*, the heterotrimeric G protein complex may not be able to form properly. Hence, signal transduction will not proceed accordingly, leading to constitutively open ion channels. Consequently, this will cause an increase in the influx of positive ions into the photoreceptors, resulting in photoreceptor degeneration. Previous studies have shown that either an increase or decrease in Ca^{2+} levels trigger photoreceptor degeneration, leading to retinal diseases (Krizaj and Copenhagen, 2002; Vallazza-Deschamps et al., 2005).

On the other hand, it can be expected that a loss of *guk1b* will cause the cGMP-gated ion channels to be closed permanently as the source of cGMP molecules will no longer be replenished. In doing so, the photoreceptors can be anticipated to be in a constitutively hyperpolarized situation. In two retinal diseases, Oguchi disease and Leber's congenital amaurosis (LCA), a persistent hyperpolarization of the photoreceptors leads to a drop in Ca^{2+} levels. In these patients, the observed extensive photoreceptor degeneration may be a result of Ca^{2+} triggered apoptosis (Perrault et al., 1996; Fain and Lisman, 1999). Concurrently, increased oxygen toxicity due to the loss of outer segments and reduced oxygen consumption could further aggravate photoreceptors degeneration (Travis, 1998).

1.2.2. Role of guanine nucleotide binding protein (G Protein), β polypeptide 3 (Gnb3) in the retina

Gnb3 encoding for the β-subunit of the heterotrimeric G protein transducin, is conserved across vertebrate species with its expression observed in cone photoreceptors and some bipolar cells (Larhammar et al., 2009; Dhingra et al., 2012). Studies conducted in chicken and mouse *gnb3* mutants revealed that the mutant chickens suffered from progressive vision loss while in mice,

the visual capacity was found to be intact with reduced light sensitivity (Tummala et al., 2006; Nikonov et al., 2013). Missense mutations in Gβe of *Drosophila*, corroborated the mouse phenotype, and also showed defective termination of the light response as well as mislocalization of the α subunit (Dolph et al., 1994). In human patients, a single base pair polymorphism in GNB3 is associated with Alzheimer's disease, hypertension, obesity, insulin resistance, dyslipidemia and more (Weinstein et al., 2006). Though, this polymorphism or other mutations in GNB3 have yet to be implicated in retina-related diseases in humans.

These studies attest that the novel candidate *gnb3b* will be an interesting target to functionally characterize in zebrafish. Analysis of this gene will address issues such as the role of *gnb3b* in photoreceptors and similarities and/or differences in gene function across species.

1.2.3. Guanylate kinase 1 (Guk1) is involved in the re-synthesis of cGMP required for phototransduction

Guanylate kinase is an enzyme that is involved in catalyzing the addition of a phosphate group from adenosine triphosphate (ATP) to GMP, generating GDP (Fig. 4), the first step towards re-synthesis of cGMP (Gaidarov et al., 1993). With the help of nucleoside diphosphate kinase (NDP-K), the GDP molecules are converted into GTP (Abdulaev et al., 1998) and guanylyl cyclase (GC)

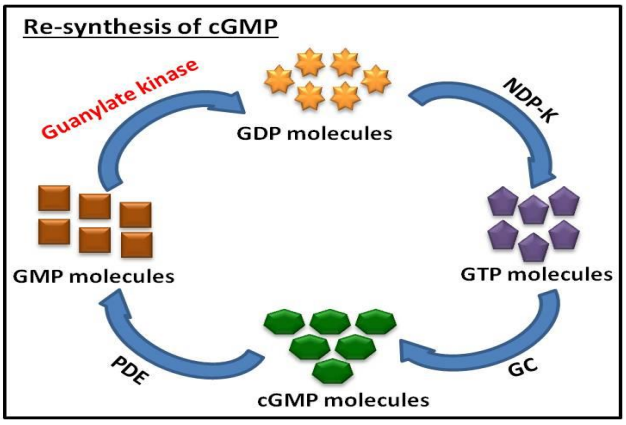

Figure 4: cGMP re-synthesis pathway. First, GMP is converted into GDP via addition of a phosphate group by guanylate kinase. The nucleoside diphosphate kinase (NDP-K) then adds another phosphate to GDP generating GTP molecules. Finally, guanylyl cyclase (GC) converts GTP into cyclic-GMP (cGMP) second messengers. Phosphodiesterases (PDE) break down cGMP back into GMP molecules.

converts the GTPs into cGMP. PDEs break down the cGMP molecules into GMP, and the cycle continues. In the phototransduction cascade, re-synthesis of cGMP second messengers is a

critical step towards re-establishing homeostasis in the photoreceptors (Brady et al., 1996; Fitzgibbon et al., 1996).

Chromosomal localization of the human GUK1 has shown that, this gene lies distal to the retinal gene, RP12, which is implicated in RP, and is placed in the same interval as Usher Syndrome 2A. This suggests a possible involvement in the pathogenesis of retinal diseases (Fitzgibbon et al., 1996). It has been shown that either an increase or decrease in cGMP levels indirectly result in retinal diseases such as photoreceptor degeneration (RP), LCA and macular degeneration (Perrault et al., 1996; Xu et al., 2013; Meighan et al., 2015). These studies underline the importance of having a proper regulation of the cGMP cycle. Improper functionality of any steps preceding or following cGMP synthesis can lead to diseases. As of now, a direct link between deficiencies in GUK1 and retinal diseases has yet to be established. Currently, not much information is available on the functionality of GUK1 in the retina. To address this, *guk1b* was chosen as a suitable novel gene for functional characterization in zebrafish.

Spatio-temporal expression pattern analysis in zebrafish larva by whole mount in-situ hybridization (WISH) was conducted (Brocher et al., unpublished data). *guk1b* expression was found to be restricted to photoreceptors in the retina of 96 hours post fertilization (hpf) larvae. Additionally, from 48 to 72 hpf, strong *guk1b* expression was observed in the heart, which was absent at 96 hpf. Successively, morpholino knock-down of *guk1b* was carried out and the photoreceptor morphology of 4 dpf larvae was analysed (Brocher et al., unpublished data). The overall morphant retinal organization was comparable to that of wildtype but a closer look into specific photoreceptor subtypes revealed structural abnormalities. Red cones immunolabeled with 1D4 showed cells partially lacking their outer segments with gaps in between, whereas double cones (zpr-1) were slightly shorter in length with aberrant outer segments (Fig. 5A, B).

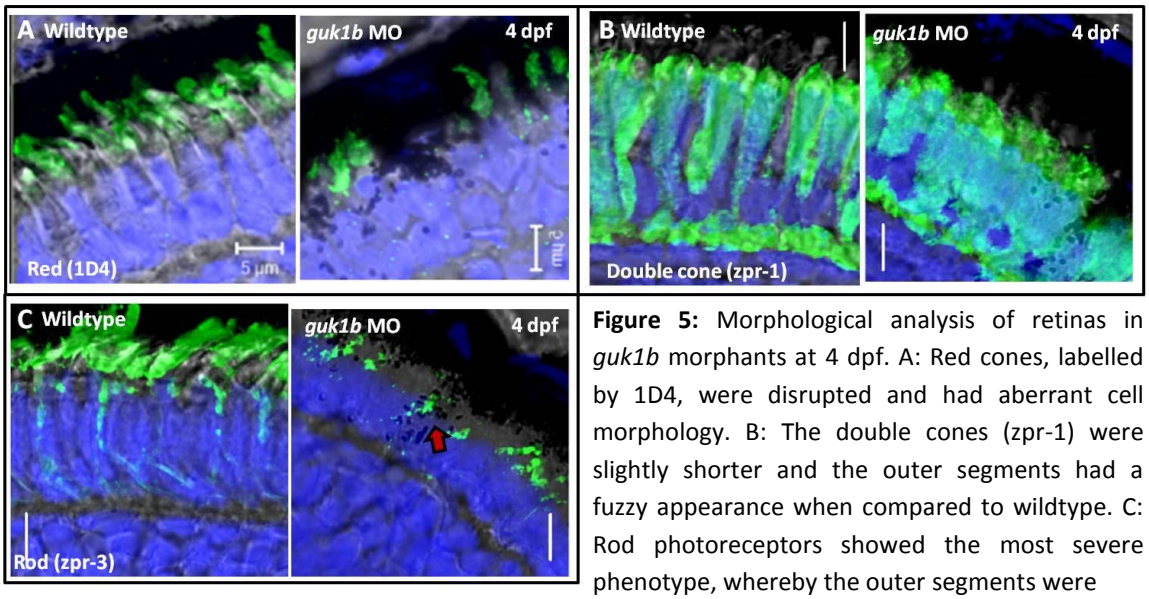

Figure 5: Morphological analysis of retinas in *guk1b* morphants at 4 dpf. A: Red cones, labelled by 1D4, were disrupted and had aberrant cell morphology. B: The double cones (zpr-1) were slightly shorter and the outer segments had a fuzzy appearance when compared to wildtype. C: Rod photoreceptors showed the most severe phenotype, whereby the outer segments were completely devoid of cellular structures and only cell remnants were detected. Additionally, the retinal pigment epithelium was disrupted and pigment deposition was observed within the photoreceptors inner segment (red arrow) (Brocher et al., unpublished).

The rod (zpr-3) cells in *guk1b* morphants were most severely affected, with only remnants of the outer segments detectable and intra-retinal pigment deposition (Fig. 5C, red arrow). Preliminary knock-down analysis of *guk1b* therefore identified this gene as a promising novel candidate as RP disease gene.

1.3. Zebrafish as model organism for biomedical research

In the last 20 years, zebrafish has gained vast popularity in biology as an excellent model organism for *in vivo* studies. The advantages of using zebrafish includes high fecundity, oviparity, transparency of embryos, short generation time (approximately 3 months) to attain sexual maturity, rapid embryonic development (48 hours until hatching) and ease of genome manipulation (Streisinger et al., 1981; Driever et al., 1994; Fadool and Dowling, 2008). Within a lab set-up, zebrafish is a relatively inexpensive organism to maintain and keep in large numbers.

Transparency of embryos is an attractive feature as it allows live imaging of growth and developmental processes while at the same time embryos that are deviating from the norm can be identified and analysed (Fig. 6A). In addition, fluorescence proteins can be driven by

promoters of interest, allowing for spatio-temporal expression analysis to single cell lineage tracing via live imaging and/or immunostaining of desired cell types (Fig. 6B) (Progatzky et al., 2013).

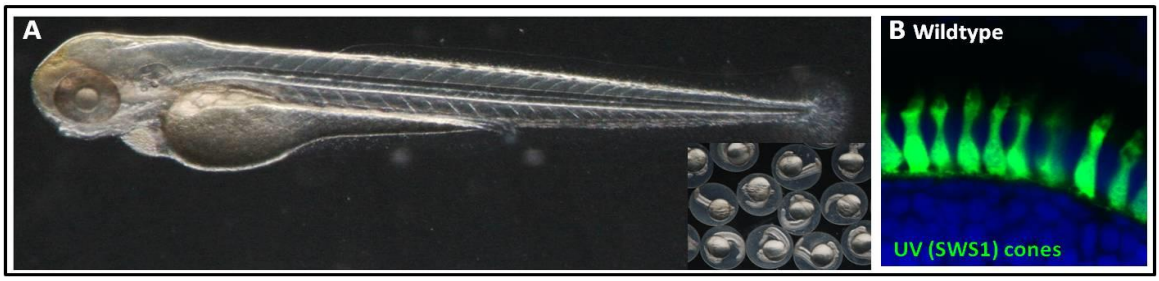

Figure 6: Overview of transparent zebrafish larvae and EGFP expression in UV cone photoreceptors. A: Completely transparent 3 days old larvae with clearly demarcated organs; inset: pool of 1 day old embryos within the chorion. B: Direct imaging of green fluorescent protein expression in UV cones with concurrent nuclei staining in 4 days old wildtype larvae.

Additionally, reverse genetics can be easily performed using tools that are currently available to edit the genome with high rates of efficiencies. This provides a platform for generating mutant forms of genes of interest to address the pathomechanism by mimicking human diseases and phenotypes in *in vivo* models. In recent times, zebrafish is becoming a highly popular model for retinal research (Fadool and Dowling, 2008; Chhetri et al., 2014).

1.3.1. Zebrafish as a model for eye research

The zebrafish retina closely resembles that of humans though differences exist. Features of the zebrafish retina that makes it a suitable model for vision related research includes cone dominant vision as found in the human eye, formation of a functional eye within five days and expression of four different types of cone photoreceptors in the retina. This makes the zebrafish retina tetrachromatic, compared to the human trichromatic eye (Chhetri et al., 2014). Furthermore, the development and function of the retina is highly conserved across vertebrate species such as *Xenopus*, mice, zebrafish and chicken (Centanin and Wittbrodt, 2014). Several techniques are well established for genome editing and screening of visual mutants using behavioural assays. Large scale ENU-mutagenesis screens have been performed in zebrafish with

successful identification of mutants with visual deficits using behavioural assays (Muto et al., 2005). Complementary to forward genetics, tools such as zinc finger nuclease (ZFN), transcription activator-like effector nuclease (TALEN) and clustered regularly interspaced short palindromic repeats/CRISPR-associated genes (CRISPR/Cas9) currently have paved the path for selective targeting of genes of interest. Coupled to behavioural assays such as optokinetic response (OKR), optomotor response (OMR) and escape response, this allows for validation of visual impairment in these mutants (Neuhauss, 2003).

The organization of the zebrafish retina closely follows that of the human eye. The retina encompasses three neural layers (outer nuclear layer, inner nuclear layer, ganglion cell layer) and two plexiform layers (Fig. 7). The outer nuclear layer is made up of rod and four cone photoreceptor subtypes, double cone pair (comprising of red and green cones), long single (blue) cones and short single (UV) cones, arranged in a highly ordered mosaic pattern (Cayouette et al., 2006). Photoreceptors are formed with a structurally distinct outer and inner segment, with rods having an elongated columnar outer segment while cone outer segments are conical in shape and extends to less than half of the rod outer segments (Branchek and Bremiller, 1984). Within the inner segment, cellular components such as ribosomes, mitochondria, endoplasmic reticulum and golgi apparatus can be found. Rod and cone photoreceptors are specialized sensory cilia whereby the absorbed light photons of different wavelength are processed in the outer segment of respective photoreceptor cell types (Fig. 7).

The inner nuclear layer comprises the horizontal, bipolar and amacrine interneuron cell bodies and Müller glia cell bodies. The cell bodies of ganglion cells reside in the ganglion cell layer. Retinal pigment epithelial cells lie adjacent to the outer segment of the photoreceptors and are essential for the maintenance of structural integrity of the retina (Simo et al., 2010). The first cells to differentiate in the retina are ganglion cells, occurring at around 32 hpf. Around 50 hpf, opsins of the rod and cone photoreceptors are expressed and outer segments of the

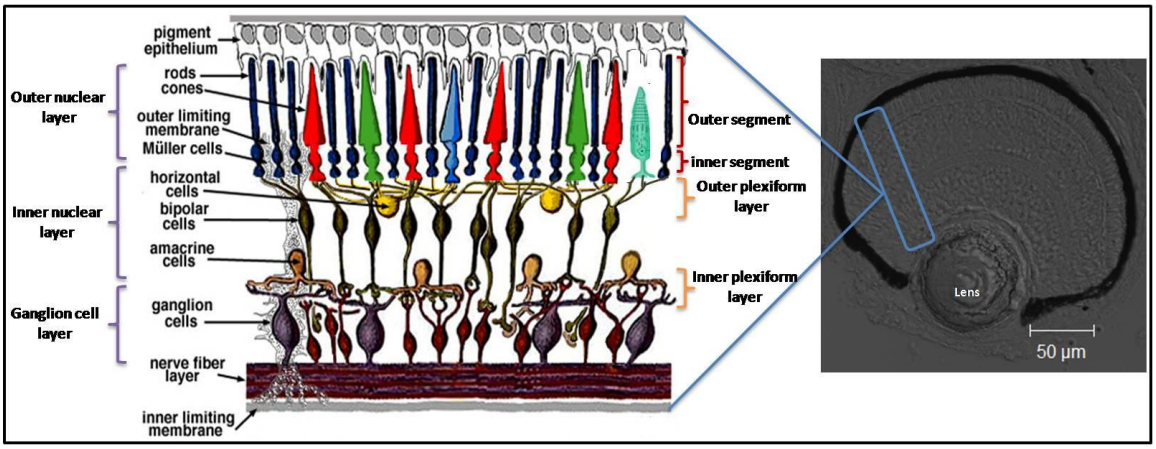

Figure 7: Diagram highlighting the organization of the vertebrate retina (modified and adapted from (Kolb H, 2011)). DIC image on the right shows the overview of a 4 dpf zebrafish larval retina section. The different cell layers of the retina are boxed (blue), starting with the retinal pigment epithelium on top.

photoreceptors become evident in a small ventral patch by approximately 55 hpf (Tsujikawa and Malicki, 2004; Gestri et al., 2012). Afterwards, synaptic terminals and connections are established. The photoreceptors start maturing from 72 hpf and cones are functional by 96 hpf. Rod cells take much longer to develop and become fully functional only at around 15 dpf (Bilotta and Saszik, 2001).

Synaptic connections between neuronal cells are made within the outer and inner plexiform layers (OPL/IPL). Synapses between photoreceptors and bipolar, horizontal cells occur within the OPL while bipolar, amacrine and ganglion cells form synapses in the IPL (Chhetri et al., 2014). Within the retina, light gets processed in the outer segments of the photoreceptors and transmitted to the bipolar cells via OPL, which in turn sends out information to the ganglion cells through the IPL. Ganglion cells then send out signals through the optic nerve to the brain, where the synaptic information gets processed to form vision. The horizontal and amacrine cells play a supportive role in fine tuning the visual input that gets transmitted to the brain (Centanin and Wittbrodt, 2014). Müller glia cells act as the stem cell population necessary for regeneration of the various neural cells upon degeneration (Lenkowski and Raymond, 2014). Overall, the zebrafish proves to be a highly reliable *in vivo* model for modelling human retinal disorders by modulating expression of genes involved in retinal development and maintenance.

1.3.2. Tools available for manipulation of the zebrafish genome

Currently many tools are available for modulating various steps in the development of an organism, from the genomic to the proteomic level. Popular techniques used for the manipulation of the zebrafish genome ranges from knock-down by morpholino oligonucleotides (MOs) to genome editing (knock-out) by either TALEN or the CRISPR/Cas9 system. MOs are suitable for transient dose-dependent knock-down of specific gene function by targeting either the translation start site or the splice-sites. MOs are 25 base long oligos that are made up of a phosphorodiamidate backbone and a morpholine ring that stably binds complementarily to the target RNA (Bill et al., 2009). As shown in Figure 8A (left panel), binding by ATG-site specific MOs result in a translation block by preventing 40S ribosomal assembly and thereby protein production. In contrast, splice-site specific MOs inhibit the binding of splicing factors to the 5' and 3' splice-sites (Fig. 8A, right panel), leading to retention of intronic sequences in the mRNA, thus introducing a premature stop codon that may result in NMD of the mRNA.

MOs do have caveats, such as non-specific binding that causes off-target phenotypes, which are not readily distinguishable from a true phenotype, and a short half-life lasting up to around 50 hpf, after which cell proliferation leads to dilution of MOs and a drop in efficacy (Bedell et al., 2011). Addressing these limitations, gene knock-out strategies were created for improved specificity and analysis of long-term effects. TALEN and CRISPR/Cas9 are the two techniques widely in use for genome editing, be it for knock-out or knock-in strategies.

TALE is a protein from the plant pathogenic bacteria, *Xanthomonas*, and is used to assist the invasion into host cells by regulating the plant genome (Miller et al., 2011). The TALE protein consists of 15 to 20 units of a 33 to 35 amino acid long repeat sequence that recognizes target DNA. Within each repeat unit, two amino acids can be modified to detect individual nucleotides (A, T, C and G), thus creating a complementary sequence to target specific regions within the

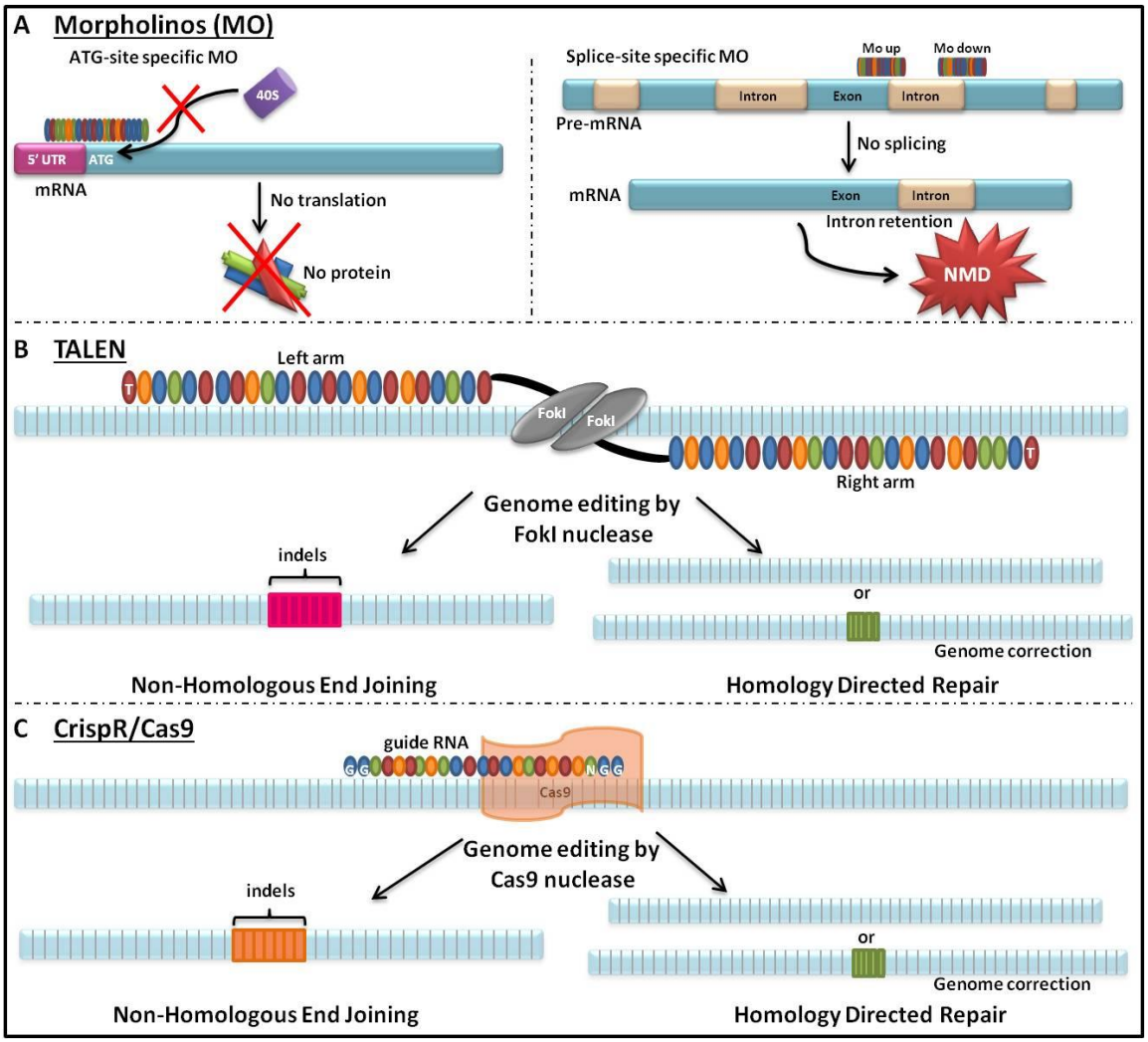

Figure 8: Illustration of transient knock-down by MOs and genome editing tools, TALEN and CRISPR/Cas9. A: Two types of MOs, ATG-specific and splice-site specific, are widely used for transient knock-down of gene expression. In the left panel, ATG-specific MOs prevent the binding of 40S ribosomal assembly and thus lead to inhibition of protein product synthesis. Splice-site specific MOs (right panel) inhibit splicing of intronic sequences leading to their retention in the mature mRNA, and cause nonsense mediated decay (NMD) of the mRNA. B: TALEN mediated genome editing involves two TALE arms each fused to monomeric FokI nuclease binding complementarily to the target region of interest. Dimerization of the nucleases causes double stranded breaks in the genome, introducing indel mutations or correction of genomic sequence via non-homologous end joining or homology directed repair mechanism, respectively. C: A single guide RNA strand complementary to the target site is used in the CRISPR/Cas9 system to bind specifically and recruit the Cas9 nuclease to the target region of interest. Subsequently, cleavage of the genome results in indel mutations or correction of the genome through repair mechanisms.

genome (Cermak et al., 2011; Huang et al., 2011). For genome editing, two arms (right and left) forming a pair of TALE sequences are fused to a monomeric FokI nuclease and are designed to flank the target gene of interest (Fig. 8B). Binding of the TALEN pair to the target site results in

the dimerization of the FokI nuclease and subsequent cleavage of the genomic sequence, introducing alterations (Dahlem et al., 2012).

The second system, CRISPR/Cas9, was more recently developed and has gained extensive popularity in the past few years. This system was first discovered to be utilized by bacteria and archea as a defence mechanism against pathogens. Upon invasion with foreign DNA, the host incorporates short sequences of the foreign DNA (called spacer) into the CRISPR locus, which then gets transcribed into small RNAs (crRNAs) that bind complementarily to the genome of the pathogen (Auer and Del Bene, 2014). This triggers the recruitment of a trans-activating crRNA which guides the Cas9 nuclease to the target site, thereby cleaving and inactivating the pathogen (Fig. 8C) (Hwang et al., 2013).

Currently, these systems have been modified to be used for efficient genome editing in various species, including zebrafish. Successful binding of the selectively designed oligomers to the target sequence allows for the nuclease to induce double stranded breaks, which then get repaired either via non-homologous end joining (NHEJ) or homology directed repair (HDR). NHEJ is error prone and thus introduces insertion/deletion (indel) mutations rendering the resultant protein product truncated and/or non-functional. Homology dependent repair (HDR) on the other hand, repairs the break using an available template DNA thereby reinstating the original genomic sequence or interleaves new sequences into the genome (Fig. 8B, C). With recent advances in technology, the design and generation time for CRISPR/Cas9 takes about one to two days to prepare while for TALEN it usually takes around one to two weeks (Nemudryi et al., 2014). Using these techniques, genome editing has been successfully performed in zebrafish, with a reported germline transmission efficacy rate of approximately 4% and 28% for TALEN and CRISPR/Cas9, respectively (Varshney et al., 2015).

1.4. Objectives of this study

As of now, not much is known about the cellular functions of *gnb3b* and *guk1b* in the retina. These genes were identified to be strongly down-regulated upon knock-down of *prpf8/31* in the zebrafish retina in a preliminary study. This raised the question of whether these two novel candidates could possibly be implicated in RP pathogenesis and play critical roles in photoreceptor maintenance. Therefore, the current study was designed to address the importance of *gnb3b* and *guk1b* in zebrafish photoreceptor maintenance and/or biogenesis.

An initial functional characterization of *gnb3b* was carried out by knock-down of gene expression based on splice-site specific MOs. After that, knock-out mutant lines were generated using the TALEN and CRISPR/Cas9 technologies. Photoreceptor morphology was analysed in homozygous mutants using transgenic reporter lines, *Tg (SWS1:EGFP)* labelling UV cones and *Tg (Rho:EGFP)* labelling rods, and/or immunostaining with zpr-1 (for double cones) and zpr-3 (for outer segments of rod and double cones) at both larval and adult stages. As preliminary MO knock-down data for *guk1b* (Brocher et al., unpublished data) was already available, I proceeded with establishing CRISPR/Cas9 stable mutant lines for this gene. *guk1b* larval and adult mutants photoreceptor morphology was analysed using the experimental techniques described above. Additionally, *guk1b* adult mutants were tested for potential degeneration (TUNEL staining) and regeneration (phosphorylated histone 3 staining) of photoreceptors, and further subjected to electron microscopy (EM) for analysis of the organization of their photoreceptor lamellar disk membranes. In parallel, a biochemical assay that quantifies cGMP levels in the retina was also performed in *gnb3b* and *guk1b* adult mutant retinas.

Together, these studies were designed to gain insight into the roles played by *gnb3b* and *guk1b* in retina photoreceptors and to understand the implications of their loss of function.

2. Material and Methods

2.1. Materials

All chemicals and reagents used in this study were purchased from Sigma Aldrich and all restriction enzymes were from New England Biolabs (NEB), unless otherwise stated. Morpholinos and primers were obtained from Gene Tools, LLC and Integrated DNA Technologies (IDT), respectively. Buffers were autoclaved or sterile filtered with a bottle-top vacuum filter (pore size of 0.22 µm, Corning) before being used.

Detailed information on injected solutions and concentrations; zebrafish strains and antibodies used in this study are summarized in Tables 2 - 4.

Table 2: Sequences and dosages used for injected MOs, TALENs and CRISPR/Cas9 mRNAs.

Injected MOs	**5' - 3' sequence**	**Injected dosage**
gnb3bupMO2	ACT TCA CTT AAA TCA CCT TAT TTC C	3.1 mg/ml
gnb3bdownMO2	AGC ATT GAC CTG ATG AAA GAA GCA A	3.1 mg/ml
p53 MO	GCG CCA TTG CTT TGC AAG AAT TG	5 mg/ml
Control MO	CCT CTT ACC TCA GTT ACA ATT TAT A	6.25 mg/ml
Injected TALEN	**5' - 3' sequence**	**Injected dosage**
gnb3b_St1	TGA CAC AGA CAT GGC GGC AGC	50 - 300 ng/µl
gnb3b_St2	TTG GAC CCG AGG GGC TGG A	
gnb3b_Wd40 1	GTG TCT GTC TCT GTC	
gnb3b_Wd40 2	CGC AAG CTC CAG AAA T	
Injected CRISPR/Cas9	**5' - 3' sequence**	**Injected dosage**
gnb3b gRNA	GGA AAT CTC GTG GCC AGC GG	50 ng/µl
guk1b gRNA	GGA TAG TCT ACA GAA GCG AC	25 or 50 ng/µl
Cas9 mRNA	-	300 ng/µl

Table 3: Zebrafish strains and lines created and used.

Fish strains used in this study			
Wildtype line	**Obtained from**	**Mutant lines**	**Created**
DBS wildtype	NUS Fish facility	*gnb3b*^{del114}	Current study
Transgenic lines	**Created by**	*guk1b*^{del174}	Current study
Tg (RHO:EGFP)	Dr. Yin Jun	*gnb3b*^{del114} *x Tg (SWS1:EGFP)*	Current study
Tg (SWS1:EGFP)	Dr. Yin Jun	*guk1b*^{del174} *x Tg (SWS1:EGFP)*	Current study
		guk1b^{del174} *x Tg (RHO:EGFP)*	Current study
		guk1b^{del175}	Current study

Table 4: List of primary and secondary antibodies used for immunostaining and the cell type labelled.

Cell type labelled	1^0 AB	Dilution	Species	2^0 AB	Dilution	Species
Double cones	zpr-1	1 : 200	Mouse	Alexa 488	1 : 500	Anti-mouse Anti-rabbit
Outer segments of rods and double cones	zpr-3	1 : 100	Mouse	Alexa 633	1 : 500	
Outer segments of red cones	1D4	1 : 50	Mouse	**Stain**	**Cell type**	**Dilution**
TUNEL positive cells	Digoxigenin	1 : 50	Mouse	DAPI (0.5 mg/ml)	Nucleus	1 : 500
Mitotic cells	Phospho-histone 3	1 : 100	Rabbit	Bodipy TR ceramide	Cell membrane	3 : 200
*1^0, 2^0 AB → primary and secondary antibodies, respectively ** Primary antibodies were obtained from ZIRC (zpr-1, zpr-3), Abcam (1D4; *#ab5417*), Millipore (phospho-histone 3 (ph3); *#06-570*) , Roche (anti-Digoxigenin; *#11333062910*)						

2.2. Zebrafish care and maintenance

Zebrafish rearing, breeding and maintenance was carried out in the fish facility of the Department of Biological Sciences, National University of Singapore (DBS, NUS). The protocols used were in accordance with the Institute of Animal Care and Use Committee (IACUC) approval, protocol number R13-574. Adult fish were kept under 14 hr light/10 hr dark cycles, with constant monitoring of water quality, pH, temperature and salinity.

For breeding purposes, fish were set up in mating tanks with males and females separated by dividers overnight. The following morning, the dividers were removed, spawned embryos were collected and raised in 1x Danieau's medium (58 mM NaCl, 0.7 mM KCl, 0.4 mM $MgSO_4$, 0.6 mM $Ca(NO_3)_2$, 5 mM HEPES pH 7.2 and 0.04% methylene blue) in a 28^0C incubator for five days before transferring the larvae to the fish facility. For experiments on larvae older than two days, 0.003% 1-phenyl 2-thiourea (PTU) was added at shield stage to inhibit pigmentation.

2.3. Microinjection of zebrafish embryos

An injection mould was made with 1.5% agarose (1^{st} Base) in 1x Danieau's medium prior to microinjection. The grooves in the mould allowed for placement and alignment of embryos in the desired orientation. Injection needles were made from glass capillaries (Harvard Apparatus)

with a needle puller (Narishige). Details of MOs, TALEN pairs and CRISPR/Cas9 sequences and concentrations used for microinjection are given in Table 2.

gnb3b splice-site specific (UP/DOWN) MOs were dissolved in Milli-Q (MQ) water to a final stock concentration of 25 mg/ml. The working solution was optimized. Throughout this study, a working concentration of 3.1 mg/ml was used for knock-down of *gnb3b*. To inhibit unspecific apoptosis, 5 mg/ml *p53* MO was co-injected with *gnb3b* MOs. MO working solutions were prepared fresh, denatured at 65^0C for 10 mins, centrifuged (Eppendorf) for 3 mins at 14,800 rpm and cooled on ice before injection. TALEN mRNA pairs for *gnb3b* were either co-injected or injected as single pair of TALEN mRNA, into embryos at concentrations ranging from 50 ng/µl to 300 ng/µl. For generation of CRISPR/Cas9 *gnb3b* and *guk1b* mutant lines, 50 ng/µl gRNA each was co-injected with 300 ng/µl of Cas9 mRNA.

The injection needles were filled with approximately 2 µl of working solution and a droplet size of 0.5 - 1 nl was injected into the yolk, directly below the cell cytoplasm, of 1-cell stage embryos under air pressure, using a Femtojet Microinjector (Eppendorf). Injected embryos were transferred into petri-dishes (Greiner Bio-One) containing 1x Danieau's medium and incubated at 28^0C. Unfertilized and dead embryos were removed daily with regular monitoring of injected samples for presence of abnormalities.

2.4. Sample tissue preparation for fixation and genotyping

2.4.1. Fin-clipping of adult caudal fins

Adult fish (2-3 months old) were anesthetized in 0.05% tricaine in 1x Danieau's medium without methylene blue. The anaesthetized fish were placed onto a sterile flat surface and the caudal fins were clipped with a 10 mm scalpel blade (Sigma). Each fin was placed into individual PCR tubes (Axygen) for genomic DNA isolation and the fish were quickly recovered in fresh medium. 70% ethanol (EtOH) was used to sterilize the blade and surface after subsequent fish.

2.4.2. Dissection of adult retinas

Adult fish (6-7 months) were first anesthetized in ice-cold water, and then transferred onto a sterile flat surface. Using a scalpel blade, a dissection cut was made between the gills and body. Forceps were used to gently detach the eyes from the optic nerve and to remove them from the eye socket. The eyes were immediately placed into either 4% paraformaldehyde in 1x phosphate buffered saline with tween-20 (PFA/PBST) or 1x cell lysis buffer for cGMP measurements (see section 2.16.).

2.4.3. Zebrafish sample fixation

Whole embryos and larvae were fixed in 4% PFA/PBST either for 4 hrs at room temperature (RT) on an orbital shaker (Grant Bio) or overnight at 4^0C. If necessary, embryos were dechorionated with forceps before fixation. Dissected adult retinas (6-7 months) were fixed with 4% PFA/PBST in glass vessels on a shaker for 4 hrs at RT. The fixative was then changed to fresh 4% PFA/PBST and samples were incubated overnight at 4^0C.

For long term storage, the fixed samples were washed with 1x PBST for 5 mins, thrice on a shaker at RT. They were then transferred into 100% methanol (MeOH) and washed for 5 mins on a shaker. The samples were replaced with fresh 100% MeOH and stored at -20^0C.

2.5. Genomic DNA isolation

2.5.1. DNA isolation using sodium hydroxide (NaOH)

Single embryos or adult caudal fins were transferred to individual PCR tubes containing 50 µl of 50 mM NaOH (Merck) and incubated at 95^0C for a total of 30 mins with regular vortexing (Scientific Industries) at every 10 min interval. Next, 5µl of 1 M Tris-HCL, pH 8.0 was added for neutralization of the reaction and the isolated genomic DNA (gDNA) was stored at -20^0C.

2.5.2. Isolation using DNA lysis buffer

Samples to be genotyped (single embryos, larval trunks or adult caudal fins) were placed into PCR tubes with 10 µl DNA lysis solution, consisting of lysis buffer (10 mM Tris pH 8.3, 50 mM KCL, 0.3% NP40, 0.3% Tween-20) and freshly added 20 µg/ml proteinase K (recombinant proteinase K, PCR grade, Roche Diagnostics). The samples were incubated for 20 mins at 55^0C, vortexed and quickly spun down. These steps were repeated twice or thrice depending on sample type, with longer incubation time given for fixed tissues. Subsequently, heat inactivation was performed by incubating the samples at 90^0C for 10 mins. For long term storage, the prepared gDNA was stored at -20^0C.

The gDNA was spun down for 2 mins using a table top centrifuge (Heathrow Scientific LLC) at maximum speed before addition into PCR mix as templates for PCR amplification.

2.6. Amplification of target regions of interest

2.6.1. Polymerase chain reaction (PCR)

Primers for PCR amplification were designed using the Primer3 v0.4.0 software. The obtained primers were dissolved in MQ water to a final stock concentration of 100 mM. A list of primers used in this study is given in Appendix 2. *gnb3b* samples were amplified using Phusion High-Fidelity DNA polymerase (Thermo Scientific) and *guk1b* samples with GoTaq polymerase (Promega). Phusion High-Fidelity DNA polymerase was also used for amplification of inserts required for blunt end cloning. PCR reactions were run in an Applied Biosystems Veriti 96-well thermal cycler. Details of the reaction components and cycle conditions are given below in Table 5. Following PCR amplification, either 5 µl or 25 µl of the PCR amplicons were mixed with 6x loading dye (Thermo Scientific) and separated in an agarose gel. Loading dye was not added to samples amplified with GoTaq polymerase as the 5x Green GoTaq buffer already contained loading dye, therefore these samples were directly loaded into agarose gels.

Table 5: PCR reaction mixes and cycling conditions used for amplification of genes of interest.

Reagents	Volume (µl)
5x HF buffer	5
Phusion polymerase	0.3
100% DMSO	0.75
10 mM dNTPs	1
10 mM Forward primer	1
10 mM Reverse primer	1
Template DNA	0.5
MQ water	15.45
Total volume:	**25 µl**

Steps	Temp. (^{0}C)	Time	No. Of Cycles
gnb3b			
Initial denaturation	98	35 s	1
Denaturation	98	10 s	35
Annealing	60	15 s	
Extension	72	20 s	
Final elongation	72	10 min	1
Termination	4	∞	

* Type of template (cDNA/gDNA/plasmid), volume of template, annealing temperature and time were subject to variations depending on primers used.

Reagents	Volume (µl)
5x Green GoTaq buffer	5
GoTaq polymerase	0.2
$MgCl_2$	2
10 mM dNTPs	1
10 mM Forward primer	1
10 mM Reverse primer	1
Template DNA	2
MQ water	12.80
Total Volume:	**25 µl**

Steps	Temp. (^{0}C)	Time	No. of Cycles
guk1b			
Initial denaturation	95	2 min	1
Denaturation	95	30 s	35
Annealing	58	15 s	
Extension	72	35 s	
Final elongation	72	10 min	1
Termination	4	∞	

* Type of template (cDNA/gDNA/plasmid), volume of template, annealing temperature and time were subject to variations depending on primers used.

For semi-quantitative RT-PCR, cDNA was used as the template and the amplification cycle number was subjected to modification to ensure that the PCR amplicons derived were not completely saturated (i.e. 24 cycles for *β-actin* and 28-30 cycles for specific genes). The expression level of the amplicons were then quantified using ImageJ.

2.6.2. Gel electrophoresis

PCR amplified samples were separated in an agarose gel prepared with 1x TAE buffer (50x TAE stock is made up of 242 g of Tris base, 57.1 ml of Glacial Acetic acid and 100 ml of 0.5 M EDTA, pH 8) and 8% SYBR-Safe DNA stain (Invitrogen), and cast into gel trays with 15 or 20-well combs (Bio-Rad). Depending on the expected size of the PCR amplicon, samples were separated with either a 1% gel for fragment sizes larger than 500 base pairs, or a 2% gel for amplicons smaller

than 500 base pairs in length. Once solidified, gels were placed into a gel running chamber (Bio-Rad) filled with 1x TAE buffer and samples were loaded into the wells. 5 µl gene ruler DNA ladder mix (Thermo Scientific) was loaded into a single well and was used as marker to determine the size of separated bands.

RNA samples to be analyzed were mixed in the ratio of 1 µl RNA sample, 1 µl 6x RNA loading dye and 4 µl MQ water, to make up a total volume of 6 µl, and denatured for 10 mins at 80^0C. The RNA samples were chilled on ice for 2 mins before loading into the gel. DNA and RNA samples were separated at a constant current of 100 - 120 V supplied by a power pac (Bio-Rad) for 30 to 45 mins. Gels were visualized using a G-box gel documentation system (Syngene) and analyzed with GeneSnap software (Syngene). If necessary, selected DNA bands were cut out with scalpel blades and gel extracted.

2.7. Restriction fragment length polymorphism (RFLP)

PCR amplicons derived from tissue samples of TALEN or CRISPR/Cas9 lines were subjected to RFLP analysis for identification of mutants and for classification according to their genotype.

Table 6: RFLP reaction mixes and conditions used for screening of TALEN and CRISPR/Cas9 mutants.

***gnb3b* TALEN Pair I**		***gnb3b* TALEN Pair II**	
Reagents	**Volume (µl)**	**Reagents**	**Volume (µl)**
10x cutsmart buffer	5	Neb 3.1	3
PCR product	10	PCR product	10
MwoI (5 U/µl)	1	PciI (10 U/µl)	0.5
MQ water	34	MQ water	16.5
Total volume:	**50 µl**	**Total volume:**	**30 µl**
Samples were incubated at 60^0C for 3 hrs.		Incubate samples at 37^0C for 3 hrs.	
CRISPR/Cas9 mutant screening			
Reagents	***gnb3b* volume (µl)**	**Reagents**	***guk1b* volume (µl)**
10x cutsmart buffer	5	Neb 3.1	3
PCR product	20	PCR product	20
HaeIII (10 U/µl)	1	BsrI (10 U/µl)	1
MQ water	24	MQ water	6
Total volume:	**50 µl**	**Total volume:**	**30 µl**
Incubate samples overnight at 37^0C.		Overnight incubation of samples at 65^0C.	

A list of used primers is given in Appendix 2. *gnb3b* TALEN injected embryos were analysed with MwoI and PciI. HaeIII and BsrI were used for analysis of *gnb3b* and *guk1b* CRISPR/Cas9 lines, respectively. Table 6 summarizes the digestion reaction mix and conditions used. The enzyme digested samples were separated on a 2% agarose/TAE gel.

2.8. Gel extraction and purification

After agarose gel separation, DNA bands of interest were cut out from the gel using a 10 mm scalpel blade under the UV transilluminator (WISD) at a wavelength of 365 nM, and placed into 1.5 ml tubes. Gel extraction was carried out using the Wizard SV Gel & PCR Clean-up System (Promega) according to the manufacturer's protocol. Where necessary, amplified PCR products were also purified directly using the kit. Following isolation, the sample concentration was measured using a Biowave II UV/Visible spectrophotometer (Biochrom) and remaining samples were stored at -20^{0}C.

2.9. Sequencing of DNA samples

PCR amplicons, gel extracted bands and plasmid clones were sequenced to ensure correct sequence of interest and/or to determine the type of introduced indel mutations. The sequencing reactions were carried out using the BigDye Terminator v3.1 Cycle Sequencing Kit (Applied Biosystems) in a PCR machine. Table 7 shows the sequencing reaction and cycle settings used. Following the sequencing reaction, samples were precipitated with 10 µl MQ water, 2 µl 3 M NaOAc, pH 5.2 and 50 µl 100% EtOH and centrifuged at 14,800 rpm for 1 hr at 4^{0}C. The supernatant was removed and replaced with 1 ml of 70% EtOH. Samples were spun down again for 45 mins at 4^{0}C. The supernatant was discarded without disturbing the pellet and the tubes were dried in a 50^{0}C heating block (Thermomixer compact, Eppendorf). The dried pellet was re-dissolved in 15 µl of HiDi-formamide (Life technologies), and transferred into MicroAmp Fast Optical 96-Well Reaction Plates (Thermo Scientific). These samples were

separated with an ABI 3730 KL 96-capillary sequencer (Applied Biosystems) and the chromatogram analyzed using BioEdit v7.2.3.

Table 7: Sequencing reaction reagents and cycle conditions used.

Reagents	Vol. (µl)	Steps	Temperature (^{0}C)			Time	No. of cycles
Template DNA	1		***gnb3b***	***guk1b***	**Plasmid clones**		
5x BigDye sequencing buffer	1	**Initial denaturation**	96	96	96	2 min	1
Forward/Reverse primer	1	**Denaturation**	96	96	96	15 s	30 - 35
BigDye sequencing mix	2	**Annealing**	60	58	58	20 s	
MQ water	5	**Extension**	62	60	60	4 min	
Total volume:	**10 µl**	**Termination**	4	4	4	∞	
Volume of template, annealing temperature and time were primer dependent and subject to changes. For plasmid clones: M13 F/R, pJet F/R or gene specific F/R primers were used. F/R: forward/reverse primers.							

2.10. RNA preparation and clean-up

2.10.1. Qiagen RNeasy Mini Kit

Total RNA was isolated from whole zebrafish larvae and cleaned-up with an RNeasy Mini kit (Qiagen) according to the supplier's protocol, with modifications to the initial sample prep. 15 – 25 embryos or larvae were collected at the desired stage and placed into 1.5 ml tubes containing 20 µl β-mercaptoethanol/RLT buffer (10 µl β-mercaptoethanol (Bio-Rad) per 1 ml RLT buffer). The larvae were homogenized with a pestle on ice, topped up with 330 µl β-mercaptoethanol/RLT buffer and spun at 14,800 rpm for 5 mins. The supernatant was transferred to a new 1.5 ml tube, to which 350 µl 70% EtOH was added. The total 700 µl solution was transferred into a spin column and centrifuged at 14,800 rpm for 25 sec. The flow-through was discarded and the RNA clean-up was continued according to the manufacturer's protocol. Samples were eluted from the column with MQ water, giving a final volume of 60 µl. To the eluted samples, 2 µl DNaseI (Thermo Scientific) and 10 µl 10x DNaseI reaction buffer with $MgCl_2$ (Fermentas) were added and incubated at 37^{0}C for 1 hr. Subsequently, the RNA samples were

cleaned-up using the RNeasy Mini kit. The eluted samples were then precipitated with 6 µl 3 M NaOAc and 132 µl 100% EtOH, and incubated at -80^{0}C for 1 hr. Subsequently, the samples were spun at 14,800 rpm for 1 hr at 4^{0}C. The supernatant was removed, 1 ml 70% EtOH was added and the samples were re-centrifuged for 45 mins at 4^{0}C. The supernatant was discarded and the tubes were dried on a 50^{0}C heating block. The dried pellet was solubilised in 20 µl MQ water and stored at -80^{0}C. Once the RNA was isolated, its concentration was measured using an UV/Visible spectrophotometer before storage.

2.10.2. Alternative RNA isolation method using Trizol

Isolation of RNA with Trizol (Invitrogen) was performed only on larval samples from the *gnb3b* mutant line. The trunk of 3 dpf larvae was dissected for genotyping (refer to section 2.5.2.) and the heads were used for RNA isolation. PCR tubes were prepared with 10 µl Trizol and the individual dissected larval heads were added immediately into Trizol. The samples were then vortexed and snap-frozen in liquid nitrogen. These steps were repeated until a complete dissociation of larval tissue was obtained. Samples were kept at -80^{0}C. Six samples per genotype were thawed and pooled together in a 1.5 ml tube topped up with 190 µl Trizol to make-up a final volume of 250 µl. The samples were centrifuged at 14,800 rpm for 20 mins at 4^{0}C. The supernatant was transferred into a new tube with 50 µl chloroform, vortexed for 30 sec and incubated at room temperature for 2 mins, followed by centrifugation at 14,800 rpm for 20 mins at 4^{0}C. These steps were repeated twice. To the supernatant, 2 µl DNaseI, 1 µl Ribolock RNase Inhibitor (Thermo Scientific) and 30 µl 10x DNaseI reaction buffer with $MgCl_2$ was added, and incubated at 37^{0}C for 1 hr. The samples were then precipitated and stored as before (see section 2.10.1.).

2.11. First strand cDNA synthesis from total RNA

Extracted RNA was reverse transcribed into cDNA using the RevertAid First Strand cDNA Synthesis Kit (Thermo Scientific) following the manufacturer's protocol. For preparation of cDNA, 0.5 - 1 µg of total RNA, random hexamer primers and MQ water were added to make up 12 µl for the positive reaction tubes and 13 µl for the negative control group (Table 8, Step 1). The samples were well mixed and incubated at 70^0C for 5 mins. Next, 5x reaction buffer, 10 mM dNTPs and Ribolock Ribonuclease inhibitor were added to the reaction mix and incubated at 25^0C for 5 mins (Table 8, Step 2).

Table 8: Step-wise protocol for cDNA synthesis and volumes of reagents used.

Step 1	**Volume (µl)**		**Step 2**	**Volume (µl)**		**Step 3**	**Volume (µl)**	
Reagents	**- RT**	**+ RT**	**Reagents**	**- RT**	**+ RT**	**Reagents**	**- RT**	**+ RT**
Total RNA (µg)	0.5 - 1 µg		5x reaction buffer	4 µl	4 µl	Reverse transcriptase	-	1 µl
Random hexamer primers	1 µl	1 µl	10 mM dNTPS	2 µl	2 µl			
MQ water	Top - up		Ribonuclease inhibitor	1 µl	1 µl			
Total Volume	**13 µl**	**12 µl**	**Total Volume**	**20 µl**	**19 µl**	**Total Volume**	**20 µl**	
1. Incubate at 70^0C for 5 mins			2. Incubate at 25^0C for 5 mins			3.Incubate at 25^0C for 10 mins		

Only to the positive reaction tubes (+RT), 1 µl of reverse transcriptase were added, after which all sample tubes with a total volume of 20 µl were incubated at 25^0C for 10 mins (Table 8, Step 3). The reaction mix was then incubated at 42^0C for 1 hr and stopped at 70^0C for 10 mins. The prepared cDNA samples were diluted 2.5 times before using them as templates for PCR amplification of genes of interest (refer to section 2.6.1.).

2.12. Cloning of PCR inserts into vectors and *in vitro* transcription

For cloning of *gnb3b* sense and anti-sense probes for whole mount in situ hybridization (WISH), the target sequences of interest were PCR amplified with Phusion High-Fidelity DNA polymerase using 4 dpf cDNA as template, and cloned into Zero TOPO-BluntII vector (Invitrogen). For cloning of TALEN pairs directed against selected target sequences, various TALE repeat units were

combined into a p-MD18T vector backbone and used as vectors and inserts for ligation (refer to section 2.13.1.). CRISPR gDNA was prepared by cloning of a double stranded DNA (dsDNA) insert into the pDR274 vector (refer to section 2.13.2. for details). CRISPR/Cas9 induced indel mutations in injected F_0 fish were identified by cloning of restriction enzyme digested amplicons into either the CloneJet (Thermo Scientific) or pGem-T Easy vectors (Promega). The PCR amplicons and RFLP digested samples used were separated on agarose gels and purified before cloning into vectors.

2.12.1. Cloning and bacterial transformation

For cloning of inserts into a vector backbone, a ligation mix was prepared with a 3 (insert) : 1 (vector) ratio following the manufacturer's instructions, and incubated at RT between 15 mins to 1 hr (Table 9). In parallel, DH5α *E.coli* competent cells were thawed on ice. All following procedures were conducted on ice, unless stated otherwise. The ligation reaction mix was chilled on ice for 5 mins, before addition into 50 - 100 µl competent cells. The reaction tubes were gently mixed and incubated for 30 - 60 mins on ice.

Table 9: Different vectors used for cloning and their reagents and reaction conditions.

TOPO-BluntII		**TALEN and CRISPR**		**pJet 1.2 Vector**		**pGem-T Easy**	
Reagents	**Vol.**	**Reagents**	**Vol.**	**Reagents**	**Vol.**	**Reagents**	**Vol.**
Salt solution	1	10x reaction buffer	1.5 µl	2x reaction buffer	10	2x rapid ligation buffer	2.5
Vector	1	* Vector	1 : 3 or	Vector	12.5 ng	Vector	25 ng
Insert	3 : 1	* Insert	1 : 10	Insert (3:1)	1	Insert	3 : 1
		T4 DNA ligase	0.5 µl	T4 DNA ligase	1	T4 DNA ligase	0.5
MQ water	Top up	MQ water	Top up	MQ water	Top up	MQ water	Top up
Total Vol.	**6 µl**	**Total Vol.**	**15 µl**	**Total Vol.**	**20 µl**	**Total Vol.**	**5 µl**
* Vector concentration used was 120 ng for TALEN and 37.5 ng for CRISPR.							
Conditions for bacterial transformation and propagation							
Ligate at RT for 30 mins heatshock samples for 30 sec.		Ligation at RT for 15 mins, heatshock for 40 sec (TALEN) and 30 sec (CRISPR).		Ligate for 15 mins at RT and heatshock for 45 sec.		Ligation reaction for 1 hr at RT, heatshock cells for 45 sec.	
→Competent cells transformed with TOPO-BluntII or CRISPR gDNA were plated or cultured in LB-Kanamycin. Cells cloned with TALEN, pJet and pGem-T Easy vectors were plated and propagated with LB-Ampicillin.							

Next, the reaction mix was heat shocked for 30 - 45 sec at 42^{0}C, chilled on ice for 2 mins, followed by addition of 250 µl LB medium (Becton, Dickinson Biosciences). Samples were then incubated for 1 hr at 37^{0}C in a Multitron thermo shaker (INFORS HT), rotating at 225 rpm. Afterwards, all 250 µl of the bacterial culture was plated onto either LB-Kanamycin (50 mg/L) or LB-Ampicillin (100 mg/L) agarose plates and incubated at 37^{0}C overnight.

2.12.2. Clone-test PCR

To test for the successful cloning, about 8 - 16 clones were picked for detection of insert, once single colonies were easily identifiable on the culture plates. A master plate was prepared with the selected clones and incubated at 37^{0}C. For the clone-test PCR, the bacterial clones were mixed with 5 µl MQ water and used as template. Table 10 shows the used reagents and cycling conditions. PCR products were run on 1% agarose gels.

Table 10: Reagents and cycling settings used for clone-test PCR.

Reagents	Volume (µl)
10x Taq reaction buffer	2.5
Taq polymerase	0.3
$MgCl_2$	2
10 mM dNTPs	1
10 mM Forward primer	1
10 mM Reverse primer	1
Plasmid clone DNA	5
MQ water	12.2
Total Volume:	**25 µl**

Steps	Temp. (^{0}C)	Time	No. of Cycles
Initial denaturation	95	10 min	1
Denaturation	95	30 s	28
Annealing	58	30 s	
Extension	72	1 min	
Final elongation	72	5 min	1
Termination	4	∞	

Primers and annealing temperatures were subject to changes; generally M13 F/R, pJET F/R primers or gene-specific primers were used. F/R: forward/reverse primers.

2.12.3. Propagation of bacteria and isolation of plasmid

Following the clone-test PCR, 4 - 6 positively identified clones were propagated from the master plate. Selected clones were added into culture tubes (Becton, Dickinson Biosciences) containing 2 ml of LB-Kanamycin or LB-Ampicillin medium and incubated overnight at 37^{0}C in a thermo shaker, shaking at 225 rpm. Subsequently, the plasmids were isolated from the bacteria using

the Wizard Plus SV Minipreps DNA Purification System (Promega) following the manufacturer's instructions. Once purified, the plasmids were eluted out in 35 µl MQ water and stored at -20^{0}C. The plasmids cloned for WISH probe production, TALEN and CRISPR gDNA preparations, were sequenced to confirm in frame sequence and insert orientation before proceeding with linearization and *in vitro* transcription. Plasmid clones generated for the F_0/F_1 CRISPR/Cas9 mutant fish were sequenced and the fish were sorted out according to the mutation type.

2.12.4. Linearization and clean-up of plasmid DNA

Plasmid clones with correct sequence identity and orientation were selected and linearized for *in vitro* transcription. In the table below, the reagents and volumes used are given.

Table 11: Conditions for plasmid linearization for WISH probe synthesis.

***gnb3b* anti-sense and sense probe**	
Reagents	**Volume (µl)**
Plasmid DNA	5 µg
10x Reaction buffer	20 µl
NotI enzyme (10 U/µl)	3 µl
MQ water	Top up
Total Volume:	**200 µl**

The prepared linearization reaction mix was incubated overnight at 37^{0}C. The next day, 200 µl phenol : chloroform : isoamyl alcohol (25:24:1, pH 8) was added, the tubes were vortexed for 30 sec and centrifuged at 14,800 rpm for 5 mins. The supernatant was transferred to new tubes containing 200 µl of chloroform (Merck). The sample was again vortexed for 30 sec and centrifuged at 14,800 rpm for 5 mins. The supernatant was transferred to new tubes and precipitated with 20 µl 3M NaOAc and 500 µl 100% EtOH, followed by incubation at -20^{0}C for 1 hr. The sample tubes were spun at 4^{0}C for 45 mins, the supernatant was removed and 1 ml 70% EtOH was added and again centrifuged at 4^{0}C for 30 mins at 14,800 rpm. The supernatant was then discarded and the pellets were dried in a 50^{0}C heat block. The purified plasmid pellet was solubilised in 20 µl of MQ water and the concentration was measured using a UV/Visible

spectrophotometer. 2 µl of the linearized plasmid DNA was run in a 1% agarose/TAE test gel to ensure complete linearization before using it as template for *in vitro* transcription. The samples were stored at -20^{0}C.

2.12.5. *In vitro* transcription of riboprobes

Linearized plasmids were mixed with transcription buffer, DIG labelled NTP mix, Ribolock RNase Inhibitor and SP6 or T7 polymerase (Fermentas, see Table 12 for details), and incubated at 37^{0}C for 2 hrs 40 mins. Afterwards, 1 µl DNaseI was added to the reaction mix and incubated at 37^{0}C for an additional 20 mins.

Table 12: Reagents used for *in vitro* transcription of riboprobes.

***gnb3b* anti-sense and sense probe**	
Reagents	**Volume (µl)**
Linearized plasmid DNA	1 µg
5x transcription buffer	4 µl
10x DIG labelled NTP mix	2 µl
Ribolock RNase inhibitor	0.5 µl
SP6 polymerase	1 µl
MQ water	Top up
Total Volume:	**20 µl**

The *in vitro* transcribed RNA samples were cleaned up using the RNeasy Mini kit (Qiagen), in accordance with the manufacturer's protocol and the eluted samples were precipitated as before (see section 2.10.1.). The RNA pellet was dissolved in 25 µl MQ water, 1 µl was used for running on a test gel, 1 µl was used for measurement of concentration and to the remaining 23 µl, 77 µl Hybridization Mix (Hybmix, for preparation refer to Table 17) was added. This probe stock solution was stored at -20^{0}C.

2.12.6. *In vitro* transcription of capped mRNA

Capped TALEN and Cas9 mRNAs were prepared from linearized plasmid using the mMessage mMachine T7 or SP6 kit (Ambion). The reagents and volume used are given in Table 13. The

reaction mix was incubated for 2 hrs at 37^{0}C and then 1 µl of Turbo DNaseI (Ambion) was added and incubated for an additional 30 mins (Step 1 and 2, Table 13).

Table 13: Used reagents, conditions and steps involved in synthesis of capped mRNA.

Step 1		**Step 2**	
Reagents	**Volume (µl)**	**Reagents**	**Volume (µl)**
Linearized plasmid DNA	1 µg	DNaseI	1 µl
10x transcription buffer	2 µl	**Step 3**	
Ribonucleotide mix (capped NTPs)	10 µl	**Reagents**	**Volume (µl)**
10x Sp6/T7 enzyme mix	2 µl	Ammonium acetate	7.5
MQ water	Top up	MQ water	71.5
Total Volume:	**20 µl**	**Total Volume:**	**100 µl**

Next, the digestion reaction was stopped via addition of ammonium acetate STOP solution and MQ water. Synthesized capped mRNA was cleaned up using 100 µl phenol (water saturated; Sigma) and 50 µl chloroform/isoamylalcohol. Samples were vortexed for 30 sec, spun down at 14,800 rpm for 5 mins. The supernatant was transferred to new tubes and 100 µl of chloroform/isoamylalcohol was added to the samples. The samples were vortexed and centrifuged as before. The supernatant was subjected to purification using the RNeasy Mini kit and the RNA was precipitated (refer to section 2.10.1.). The obtained pellet was dissolved in 20 µl of MQ water, and 1 µl was used for running on a test gel and 1 µl for measurement of concentration. The remaining samples were stored at -80^{0}C.

2.13. Design and creation of mutant lines

2.13.1. Generation of two pairs of TALEN mRNA

Using the TAL Effector Nucleotide Targeter 2.0 software, two TALEN pairs, targeting exon 3 and exon 7 of *gnb3b*, were designed. The 'unit assembly' protocol established by Huang et al., was used to generate the TALEN expression vectors (Huang et al., 2011). Plasmids containing the individual TALE repeat units to generate the desired TALE sequence combination were kindly provided by Dr. Karuna Sampath, Temasek Life Science Laboratories (Lim et al., 2013). These plasmids contained combinations of repeat unit sequences that target combinations of any two

nucleotides (pA, pT, pC and pG^{NN}). Selected plasmid combinations were double digested for 4 hrs at 37^0C, to provide a vector backbone and insert (Table 14). The plasmids and inserts were separated in a 2% agarose/TAE gel, gel purified and ligated together with T4 ligase (NEB, Table 9). The ligation reaction mix was transformed into competent cells, and obtained clones propagated and sequenced (refer to section 2.12.1. - 2.12.3.). These steps were carried out in multiple rounds to generate four plasmids with the complete TALE repeat array sequence of interest.

Table 14: Double digestion reaction for generation of TALEN expression vectors.

I. Double digestion of TALE plasmids to act as vector backbone		**II. Double digestion of TALE plasmids to obtain insert sequence**		**III. Double digestion of FokI plasmid as vector backbone**		**IV. Double digestion of plasmid with TALE repeat sequence for insert**	
Reagents	**Vol.(µl)**	**Reagents**	**Vol.(µl)**	**Reagents**	**Vol.(µl)**	**Reagents**	**Vol.(µl)**
Plasmid	1 µg	Plasmid	1 µg	Plasmid	0.5 µg	Plasmid	1 µg
10x Tango buffer	1.5 µl	10x Tango buffer	1.5 µl	10x Tango buffer	1.5 µl	10x Tango buffer	1.5 µl
NheI	0.5 µl	SpeI	0.5 µl	NheI	0.5 µl	NheI	0.5 µl
HindIII	0.5 µl	HindIII	0.5 µl	SpeI	0.5 µl	SpeI	0.5 µl
MQ water	Top up	MQ water	Top up	MQ water	Top up	MQ water	Top up
Total Vol.	**15 µl**	**Total Vol.**	**15 µl**	**Total Vol.**	**15 µl**	**Total Vol.**	**15 µl**
* I provide with vector backbone for insert from II.				** III is the vector backbone for insert IV.			
→ NheI, HindIII and SpeI concentration: 10 U/µl							

In parallel, pCS2 vectors containing the FokI nuclease sequence were double digested (see Table 14) and dephosphorylated with shrimp alkaline phosphatase (SAP, Fermentas, Table 15, Step 2.2). The vector with FokI nuclease was used as backbone for the insertion of the combined TALE repeat units during ligation (see section 2.12.1, Table 9). As before, the insert together with the FokI nuclease was transformed and sequenced (refer to section 2.12.1. - 2.12.3.).

Once the correct sequence combination was confirmed, with each TALE arm associated with a monomeric FokI nuclease, the cloned TALEN plasmids were linearized with NotI and *in vitro* transcribed using mMessage mMachine Sp6 kit to generate capped mRNA (see section 2.12.4 and 2.12.6.). The mRNA was purified and stored at -80^0C. A 1% agarose/TAE test gel was run to confirm successful mRNA synthesis, and the concentration was measured. Working solutions

were freshly prepared from this stock of TALEN capped mRNA for microinjection. The workflow for TALEN generation is illustrated in Figure 16B.

2.13.2. CRISPR/Cas9 mRNA preparation

An optimized protocol established by Hwang et al., was used for CRISPR/Cas9 generation in this study (Hwang et al., 2013). A single CRISPR target site for *gnb3b* was selected using the ZiFit Targeter version 4.2 program and the corresponding oligos were ordered from IDT. The obtained oligos were annealed using gradient annealing to generate dsDNA and then phosphorylated using T4 polynucleotide kinase (PNK, Fermentas) (Step 1.1 and 1.2, Table 15). In parallel, the vector pDR274 (Addgene) was linearized with BsaI-HF (for 2 hrs at 37^0C) and dephosphorylated with SAP for 1 hr at 37^0C, to prevent re-ligation (Step 2.1 and 2.2, Table 15). Details of the reagents and conditions used for preparation of dsDNA, phosphorylation and dephosphorylation of vectors are given in Table 15.

Table 15: Protocol for dsDNA preparation, phosphorylation and dephosphorylation of vectors.

Step 1.1 Annealing		**Cycling Conditions**			**Step 2.1 Linearization of Vector**	
Reagents	**Vol. (µl)**	**Temp. (^{0}C)**	**Time**	**Cycle**	**Reagents**	**Vol. (µl)**
Oligo 1 (2 µg)	3.1	95	10 min	1	pDR274 Vector (10 µg)	10 µg
Oligo 2 (2 µg)	2.9	95 - 16	- 1^0C/min	60	10x cutsmart buffer	50
10x Taq reaction buffer with KCl	1	16	∞	∞	BsaI-HF (20 U/µl)	10
MQ water	3				MQ water	Top up
Total Volume :	**10 µl**				**Total Volume:**	**500 µl**
Step 1.2 PNK phosphorylation		**Cycling Conditions**			**Step 2.2 Dephosphorylation of Vector**	
Reagents	**Vol. (µl)**	**Temp. (^{0}C)**	**Time**	**Cycle**	**Reagents**	**Vol. (µl)**
dsDNA (147 ng)	0.74	37	30 min	1	Lin. pDR274 Vector (2 µg)	2 µg
PNK buffer A	2	75	10 min	1	10x SAP buffer	12
10 mM ATP	2	75 -16	- 3^0C/min	20	SAP enzyme	5
T4 PNK enzyme	1	16	∞	∞	MQ water	Add on
MQ water	14.26					
Total Volume:	**20 µl**				**Total Volume:**	**120 µl**

After dephosphorylation of the vector and phosphorylation of the insert, a ligation reaction mix in a ratio of 1 (vector) : 10 (insert) was prepared consisting of 0.5 µl pDR274 vector, 0.5 µl dsDNA (*gnb3b* insert), 1 µl 10x T4 DNA ligase reaction buffer and 0.5 µl T4 ligase topped up to 10 µl with MQ water (refer to Table 9). This mix was incubated at RT for 15 mins and afterwards added to 50 µl of competent cells for transformation and propagation (see 2.12.1. - 2.12.3.).

The plasmid clones were sequenced and only selected clones were subjected to linearization. Purified plasmid DNA was linearized with DraI (10 U/µl, Thermo Scientific) and cleaned-up with phenol-chloroform as before (see 2.12.4.). The linearized *gnb3b* gDNA plasmid was *in vitro* transcribed using the MAXIscript T7 Transcription kit (Ambion) and treated with Turbo DNaseI, in accordance to the manufacturer's protocol (refer to Table 16). The *gnb3b* gRNA was then purified, precipitated and the obtained pellet was dissolved in 20 µl of MQ water. The gRNA for *guk1b* that was used in this study was prepared by a former PhD student, M. Graf.

Table 16: gRNA synthesis using T7 MAXIscript and polyA tail addition to Cas9 mRNA.

***gnb3b* gRNA synthesis**	
Reagents	**Volume (µl)**
Linearized plasmid DNA	1 µg
10x transcription buffer	2 µl
ATP	1 µl
UTP	1 µl
CTP	1 µl
GTP	1 µl
T7 MAXIscript mix	2 µl
MQ water	Top up
Total Volume:	**20 µl**

Cas9 mRNA - PolyA tail addition	
Reagents	**Volume (µl)**
Transcribed RNA	20
5x reaction buffer	10
10 mM ATP	5
25 mM $MnCl_2$	5
E-PAP (polyA enzyme)	2
MQ water	10
Total Volume:	**52 µl**

The Cas9 nuclease containing vector pMLM3616 (Addgene) was linearized with PmeI (10 U/µl) as per manufacturer's protocol, purified with phenol-chloroform and the DNA precipitated with sodium acetate (refer to section 2.12.4.). The linearized Cas9 vector was *in vitro* transcribed with T7 mMessage mMachine kit (see section 2.12.6., Table 13) and poly-adenylated (polyA tailing kit, Ambion, Table 16). The poly-adenylated Cas9 RNA was purified with phenol-chloroform, RNeasy kit followed by precipitation (refer to section 2.12.6.). The obtained RNA pellet was subsequently dissolved in 20 µl MQ water. The gRNA and Cas9 RNA concentration was

measured and a 1% agarose/TAE gel was run to confirm successful mRNA synthesis. Samples were stored at -80^{0}C, with working solution freshly prepared for each round of microinjection.

2.13.3. Establishment of CRISPR/Cas9 zebrafish mutant lines

Gnb3b and *guk1b* gRNAs were co-injected with Cas9 mRNA into the yolk, below the cell cytoplasm of one-cell stage embryos. The next day, injected larvae were subjected to a preliminary screen for presence of indel mutations in the genome via RFLP assay (see section 2.7.). Once the dosage and concentration of injected gRNA and Cas9 mRNA were optimized, three to four successive rounds of injections were performed and the embryo batches raised into adulthood. Around 2 to 3 months later, when the fish were sexually mature, the injected adult fish were finclipped and genotyped for identification of fin positive potential founders. These fin positive 'potential founders' were incrossed and the F1 embryos screened for germline transmission of mutations.

The founders (F_0) were subsequently incrossed as well as outcrossed to *Tg (SWS1:EGFP)* and *Tg (Rho:EGFP)* transgenic reporter lines, and the siblings raised to adulthood. The F_1 larvae with transgenic background were screened for EGFP fluorescence at 4 dpf before raising into adults. Two to three months later, the F_1 adult fish were finclipped, genotyped and sequenced. EGFP transgenic fish siblings carrying the same mutation alleles were pooled together. The F_1 heterozygous fish carrying same mutations were incrossed and the F_2 progeny raised and sorted out according to their genotype (wildtype, heterozygous and homozygous). Morphological analyses of the mutants were performed at both larval and adult stages. Figure 9 describes the steps involved in the generation of a stable CRISPR/Cas9 mutant line.

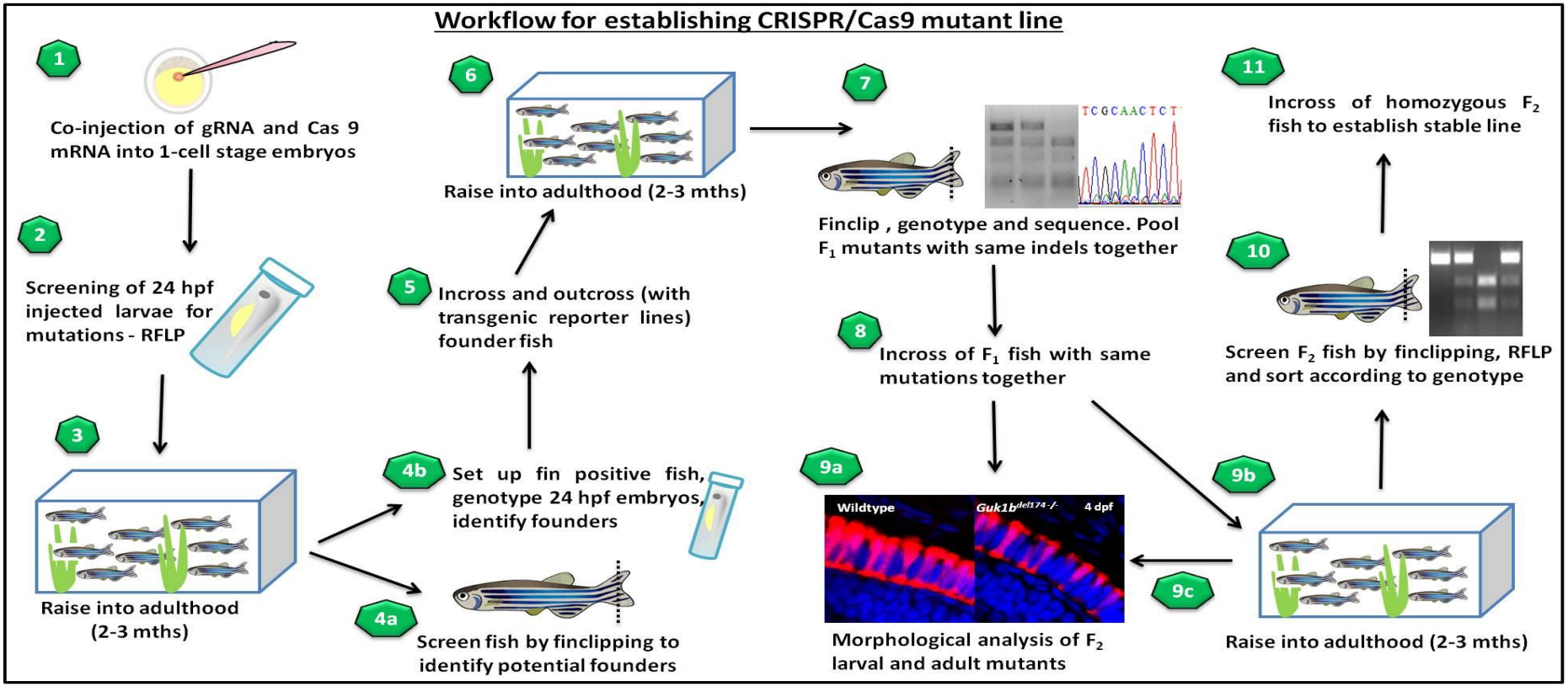

Figure 9: Schematic diagram depicting the workflow for establishment of CRISPR/Cas9 induced mutant lines. CRISPR gRNA was designed and co-injected with Cas9 mRNA into one-cell stage zebrafish embryos (1). The injected larvae were screened at 24 hpf through RFLP assay for presence of indel mutations (2). Multiple rounds of injected larvae were successively raised into adulthood (3) and finclipped to identify fin positive 'potential founders' (4a). These 'potential founders' were incrossed and the F_1 progeny genotyped to identify true founder (F_0) pairs (4b). The F_0 were then incrossed or outcrossed to transgenic reporter lines and the F_1 raised into adults (5, 6). These adult fish were genotyped via finclipping, sequenced to determine the mutation allele and fish with same mutation allele types were segregated together (7). F_1 heterozygous mutant fish harbouring the same mutation allele were incrossed and the F_2 progeny raised (8, 9). The F_2 larvae and adult mutants were subjected to morphological analysis (9a, 9c). F_2 adults were screened and sorted out according to their genotype and the homozygous mutants were incrossed to establish a stable mutant line (10, 11).

2.14. Sample processing for immunostaining and imaging

2.14.1. Cryo-sectioning of zebrafish retinas

Zebrafish larval heads or adult retinas were PFA fixed and then washed three times with 1x PBST, for 5 mins each, using a horizontal shaker. Samples were transferred and orientated into liquid 1.5% low melting agarose (LMA) with 5% sucrose solution prepared in 1x PBST. The samples were then allowed to solidify at RT for 5 to 10 mins before being placed at 4^0C for an additional 10 mins. Afterwards, samples were cut into small blocks and transferred into 2 ml tubes containing 1 ml of 30% sucrose/1x PBST solution and kept at 4^0C until sample blocks completely absorbed the sucrose solution and sunk to the bottom of the tube (approximately 2 days). Sample blocks to be cryo-sectioned were placed into a sample holder, covered with tissue freezing medium, followed by snap freezing in liquid nitrogen. These mounted samples were allowed to settle for 1 hr to the desired temperature for sectioning. The cryostat (Leica CM1850) was set and cooled down to -25^0C prior to sample mounting. 16 µm thick sections were cut and collected onto alternating Superfrost Excell poly-lysine coated slides (Fisher Scientific). Slides were placed into a slide box and stored at -20^0C.

2.14.2. Immunostaining on cryo-sections

Slides after cryo-sectioning were dried at 37^0C for 30 mins to 1 hr, and sections were outlined with a hydrophobic marker (PAP pen, Sigma) to contain the reagents added during the following steps. Samples were rehydrated in 1x PBST for 5 mins at RT in a wet box (all incubations took place in a wet box from here onwards). The slides were incubated with selected primary antibodies (Table 4) for 2 hrs and then washed five times with 1x PBST in a Coplin jar for 7 mins each. Subsequently, the samples were incubated with Alexa Fluor secondary antibodies (Life Technologies, Table 4) for 2 hrs at RT. The samples were again washed with 1x PBST as mentioned previously. Selected samples were additionally labelled with Bodipy TR ceramide

complexed to BSA (Life Technologies) to outline cell membranes, for 1 hr at 37^{0}C. The nuclei in the sections were stained with DAPI for 15 mins at RT before washing for four times with 1x PBST for 5 mins each. The slides were mounted with 20 µl of MOWIOL and covered with a Fisherfinest Superslip coverslip (Fisher Scientific). Prepared samples were stored at 4^{0}C till imaging with a LSM 510 confocal microscope.

2.14.3. Fluorescence TUNEL staining on cryo-sections

As before, slides were dried at 37^{0}C for 30 mins and areas with samples were circled with a hydrophobic marker to contain the reagents used. The samples were then rehydrated with 1x PBST before addition of 150 µl of equilibration buffer. Slides were incubated for 10 mins at RT. Afterwards, the equilibration buffer was replaced with 150 µl TdT enzyme solution in reaction buffer (3:7 ratio) and incubated at 37^{0}C for 2 hrs. The reaction was stopped by addition of 200 µl STOP buffer (prepared with 10 µl STOP solution in 430 µl MQ water) for 10 mins after an initial rinse with STOP buffer. Samples were washed thrice with 1x PBST for 1 min each, before incubating with 300 µl of anti-digoxigenin antibody (1:50 dilution), overnight at 4^{0}C. The following day, samples were washed five times with 1x PBST for 7 mins each and then incubated with secondary antibody (refer to Table 4), for 2 hrs at RT. Subsequently, samples were washed as previously described and the nuclei stained with DAPI (see section 2.14.2.). Finally, the samples were mounted for imaging with MOWIOL, covered with a coverslip and stored at 4^{0}C. Reagents used for the TUNEL assay were from the ApopTag Peroxidase In Situ Apoptosis Detection Kit (Millipore).

2.14.4. Whole mount in situ hybridization (WISH)

Larval samples stored in 100% methanol were rehydrated sequentially with 75%, 50% and 25% MeOH and 1x PBST thrice, with each wash lasting for 5 mins on an orbital shaker. Afterwards, samples were permeabilized with 500 µl of 5 µg/ml Proteinase K (Fermentas)/1x PBST with

treatment times ranging from 1 to 15 mins based on the developmental stage. Proteinase K treatment was stopped by addition of 1 ml of 1x glycine/PBST (100 µl of 0.1 g/ml glycine stock solution in 5 ml of 1x PBST) solution and washed twice. The samples were re-fixed with 2 ml of 4% PFA/PBST for 30 mins on a shaker at RT, following which samples were washed with 1x PBST thrice for 5 mins each, on a shaker (refer to Table 17 for buffer and reagent preparation).

Table 17: Table detailing the preparation of reagents used for WISH.

10x PBS stock	**Total Volume (1 L)**
NaCl	58.44 g
KCl	1.45 g
Na_2HPO_4	8.37 g
KH_2PO_4	1.50 g
MQ water	Top up to 1 L

1x PBST	**Total Volume (1 L)**
10x PBS	100 ml
20% Tween-20	5 ml
MQ water	Top up to 1 L

0.5 M $MgCl_2$	**Total Volume (250 mL)**
$MgCl_2$ $6H_2O$	25.41g
MQ water	Top up to 250 ml

SSCT buffer I	**Total volume (50 ml)**
Formamide	25 ml
20x SSC	5 ml
20% Tween-20	250 µl
MQ water	Top up to 50ml

SSCT buffer II	**Total volume (50 ml)**
20x SSC	5 ml
20% Tween-20	250 µl
MQ water	Top up to 50ml

SSCT buffer III	**Total volume (50 ml)**
20x SSC	500 µl
20% Tween-20	250 µl
MQ water	Top up to 50ml

Hybridization Mix	**Total Volume (50 mL)**
Formamide	25 ml
20x SSC buffer	12.5 ml
50 mg/ml Heparin	150 µl
Torula RNA	250 mg
20% Tween-20	250 µl
MQ water	Top up to 50 ml

5 M NaCl	**Total Volume (250 mL)**
NaCl	73.05 g
MQ water	Top up to 250 ml

50x Glycine	**Total Volume (10 mL)**
Glycine	1 g
1x PBST	10 ml

Pre staining buffer	**Total volume (50 ml)**
5 M NaCl	1 ml
0.5 M $MgCl_2$	5 ml
1 M Tris-HCl, pH 9.5	5 ml
20% Tween-20	250 µl
MQ water	add up to 50 ml

NBT staining	**Total volume (10 ml)**
5M NaCl	200 µl
1M Tris-HCl pH9.5	1 ml
20% Tween	50 µl
NBT (with MgCl2)	200 µl
MQ water	add up to 10 ml
*Reagent volume prepared varies according to sample size	

500 µl pre-hybridization solution (Hybmix) was added to the samples, and samples were incubated in a 65^0C water bath (GFL) for 2 hrs. The pre-hybridization solution was removed and 500 µl probe solution was added and incubated overnight at 65^0C. The sense and antisense

gnb3b probes (1:100 working solution) were denatured for 10 mins at 80^0C and cooled on ice before being added to the samples.

The next day, the probe solution was recollected and a series of stringency washes were performed, starting with SSCT buffer I wash, twice at 65^0C for 30 mins. The wash buffer was changed to SSCT buffer II (once), followed by SSCT buffer III (twice). All washes were carried out in a 65^0C water bath and samples were incubated for 30 mins each. After the last washing step, the samples were recalibrated with 1x PBST and incubated with 500 µl of blocking solution (5% sheep serum (Sigma)/PBST) for 1 hr at RT on a shaker, to block unspecific antibody binding sites.

Next, the blocking solution was replaced with 500 µl of anti-DIG antibodies conjugated to alkaline phosphatase (1:2000 dilution, Roche) and incubated for 2 hrs on a shaker at RT. The samples were then thoroughly washed with 1x PBST for 20 mins, for a total of six times, with one of the washes occurring overnight at 4^0C. The samples were then incubated with 2 ml of pre-staining buffer (see Table 17) for 5 mins twice at RT. The pre-staining buffer was removed and 500 µl of NBT staining solution was added to the samples. Samples were incubated in the dark, till adequate staining was achieved. Once the desired staining level was reached, the reaction was stopped via washing with 1x PBST. The samples were kept in 4^0C till imaging was performed, and sectioned when necessary.

2.14.5. Whole mount in situ apoptosis detection

The ApopTag Peroxidase In Situ Apoptosis Detection Kit (Millipore) was used to analyse programmed cell death in the morphant zebrafish. Embryos stored in 100% MeOH were rehydrated sequentially (see section 2.14.4.) and endogenous peroxidases were quenched using 1 ml of 3% hydrogen peroxidase (VWR) in 1x PBST for 10 mins. Following quenching, samples were washed twice with 1x PBST for 1 min and then incubated in 50 µl equilibration buffer for 1 hr 30 mins at RT. The equilibration buffer was removed and replaced with 50 µl of TdT enzyme in reaction buffer (3:7 ratio), and incubated at 37^0C for 1 hr. This solution was then removed and

220 µl STOP buffer was added and incubated for 10 mins at RT. The samples were then washed three times with 1x PBST for 1 min. Next, 100 µl of anti-digoxigenin antibody conjugated with peroxidase was added to the samples, incubated at RT for 1 hr before placing the samples for overnight incubation at 4^0C. The following day, samples were washed thrice with 1x PBST for 5 mins each, and then incubated with 500 µl of DAB solution (1 DAB tablet dissolved in 5 ml of MQ water) for 30 mins at RT, on an orbital shaker. The DAB solution was removed and samples were stained with 500 µl of DAB/Urea/H_2O_2 (1 DAB tablet and 1 Urea/H_2O_2 tablet mixed in 5 ml of MQ water) solution at RT. The staining reaction was stopped with MQ water once sufficient staining was obtained. The samples were subjected to 1x PBST wash for 5 mins, three times and stored at 4^0C until imaging.

2.14.6. Retina sample preparation for transmission electron microscopy

Adult fish retinas were dissected out and prefixed in 2 ml of 2% PFA/2.5% glutaraldehyde (Agar Scientific) fixative (containing 600 µl of 50% PFA, 1.5 ml of 25% glutaraldehyde and 12.9 ml of Sorenson's buffer) for 2 hrs at RT, followed by overnight fixation at 4^0C. The following day, prefixed retinas were washed with Sorenson's buffer 5 times and samples were postfixed with 1% osmium tetroxide (Agar Scientific)/Sorenson's buffer for 4 to 5 hrs on a shaker at RT. Samples were rewashed with Sorenson's buffer 5 times, and then dehydrated with 30%, 50%, 70%, 80%, 90%, 95% and 100% of EtOH/MQ water for 10 mins each on a shaker at RT. The 95% and 100% EtOH wash was carried out twice each. The dehydrated samples were then infiltrated with a 1:1 ratio of 100% EtOH/propylene oxide (Fluka) for 30 mins on a shaker at RT. After this, the solution was replaced twice with 100% propylene oxide for 30 mins each on a shaker. The samples were then incubated with epoxy resin/propylene oxide in a 1:1 ratio for approximately 5 hrs. After this, samples were replaced with a 3:1 ratio of epoxy resin/propylene oxide and incubated overnight on a shaker at RT. Next, samples were infiltrated with two changes of 100% epoxy resin for 4 hrs each, as before. Subsequently, samples were embedded in a silicon mould

with fresh resin and were left to polymerize in a 60^{0}C Isotemp Vacuum oven (Fisher Scientific), overnight. Sorenson's buffer and epoxy resin preparation details are given in Table 18.

Table 18: Table describing reagents required for preparation of Sorenson's buffer and Epoxy resin.

Sorenson's buffer		
	Reagents	**Volume (µl)**
Solution A	Na_2HPO_4	4.37 g
	MQ water	500 ml
Solution B	KH_2PO_4	3.17 g
	MQ water	350 ml
Buffer-to-use	Sol. A	363 ml
	Sol. B	137 ml
	Total Volume:	**500 ml**

Epoxy resin		
	Reagents	**Volume (µl)**
SpiChem	ERL 4206	5 g
SpiChem	DER 736	3 g
Sigma	NSA	13 g
SpiChem	S-1	0.2 g
	Total Volume:	**21.2 g/ml**
1. Stir all reagents together with magnetic beads till solution is evenly mixed. 2. Use a vacuum pump to remove air bubbles. Store at -20^{0}C.		

Ultrathin sections (90 nm) were cut using a Leica EM UC7 Ultramicrotome with a diamond knife, and collected onto 100 mesh copper grids (EMS). The samples were stained with 5% uranyl acetate/water (EMS) for 2 mins followed by Reynold's lead citrate (Nacalai Tesque, Inc.) for 2 mins. Sample grids were washed with MQ water in between the stainings, four times each. Staining solutions were kindly provided by Ms. Keshma from the Singhealth Advanced Bioimaging Core Facility. Samples were stored in a grid box at RT, till imaging.

2.15. Imaging of samples using low and high end microscopy

2.15.1. Compound/stereomicroscopy

WISH and in situ apoptosis stained samples were first washed in 1x PBST and then transferred into 70% glycerol (AppliChem) for 5 to 10 mins, followed by 100% glycerol. Individual whole mount larvae were aligned onto microscope slides (Continental Lab Products) with 100% glycerol and overview images were acquired using a Stereomicroscope (Nikon SMZ1000). For higher magnification images of the retina, the retina was dissected out and images were captured using a Compound Microscope (Nikon Eclipse 90i). Both microscopes utilize the NIS element basic software for image acquisition and analysis.

2.15.2. Confocal microscopy

Fluorescent samples were imaged with a Zeiss LSM 510 Meta Confocal Microscope, using the Zen 2009 software. Single plane images of approximately 1 to 2 µM thick confocal slices were acquired by either directly imaging for transgenic reporter EGFP expression, and/or after immunostaining, using the 405 nM, 488 nM and 633 nM laser lines. Images were taken using 10X and 20X water immersion objective lenses or a 63X oil immersion objective lens with manual zoom applied. Image analysis was performed using the Zeiss LSM Image Browser 4.2.0.121 software.

2.15.3. Transmission electron microscopy

Samples were imaged with a JEOL-2100 Transmission Electron Microscope, connected to a WA Orius 833 camera (Singhealth Advanced Bioimaging Core Facility). Images were taken at 8,000X and 25,000X magnifications with a 0.5 sec exposure. Images were stitched together using Adobe Photoshop CS5 and analyzed.

2.16. Measurement of cGMP levels in adult retinas by competitive ELISA

cGMP levels in adult fish retinas were quantified using the Cyclic GMP XP Assay kit (Cell Signaling Technology) following the manufacturer's protocol, with modified sample preparation. All steps involved in sample preparation were performed on ice. Individual adult fish retinas were dissected (refer to section 2.4.2.) and both retinas were added into 25 µl of 1x cell lysis buffer consisting of 410 µl 10x cell lysis buffer, 410 µl 10 mM PMSF, 410 µl 10 mM IBMX and 2.87 ml MQ water. The retina samples were homogenized with a pestle. The volume was topped up to 500 µl with 1x cell lysis buffer. The samples were then subjected to sonication (Sonics & Materials Inc.), at 50% amplitude, 5 sec on/off for a total of three cycles with pulse 2. The samples were incubated on ice for 10 mins and then centrifuged at 4^0C for 30 mins at 14,800 rpm. The supernatant was transferred to new tubes and was vortexed. Then samples were

added to microwells coated with cGMP antibody. The cGMP standards used in this assay were prepared via serial dilution according to the supplier's protocol. Briefly, 50 µl of cGMP-HRP conjugate was added first into the coated microwells, followed by either 50 µl of cGMP standard controls or retina sample preps into the respective antibody coated wells. The wells were incubated for at least 3 hrs on an orbital shaker at RT. The wells were then washed four times with 200 µl of 1x wash buffer. Addition of 100 µl of TMB substrate and incubation for 15 mins allowed for the chemical reaction to proceed and color development to occur. The reaction was stopped by adding 100 µl STOP solution. The total 200 µl reaction mix was then transferred into a 96 well flat bottom plate (Greiner Bio-One). The absorbance was measured using a microplate reader (Tecan) at 450 nM wavelength and the standard curve was plotted using the four-parameter logistic equation with GraphPad Prism 6.0 software. Absolute concentrations of cGMP in retinal samples were then calculated using the derived values.

2.17. Bioinformatics tools

Sequence of target genes were retrieved from Ensembl (McLaren et al., 2010) for design of primers, MOs, TALEN pair target sites and CRISPR gRNA target sites. Selected sequences were used as queries in BLASTN searches (Altschul et al., 1990) to ensure absence of any off-target binding sites. Nucleotide and protein sequence alignments were carried out with MultAlign software (Corpet, 1988). The ExPASy-Translate tool (Gasteiger et al., 2003) was used for conversion of nucleotide sequences into amino acid sequences and for analysis of introduced indel mutations into the zebrafish genome. 3-Dimensional (3D) protein models for *gnb3b* and *guk1b* mutant protein sequences were rendered using SWISS-MODEL (Biasini et al., 2014). Swiss-PdbViewer v4.1.0 was used for analyzing derived 3D protein model (Guex et al., 2009). ImageJ 1.49v was utilized for quantification of expression levels of RT-PCR amplicons (Schneider et al., 2012).

3. Results

Transcriptome analysis in retinas of *prpf8* and *prpf31* morphant larvae provided the basis for my doctoral project. From the list of differentially regulated transcripts, two genes were selected for functional characterization. *gnb3b* and *guk1b* were found to be strongly down-regulated upon knock-down of *prpf8/31*. Not much is known about the roles played by these genes in photoreceptors. In order to understand their function, gene knock-down by splice-site MOs and knock-out by TALEN and CRISPR/Cas9 approaches were used for *in vivo* analysis using zebrafish as the model organism. Morphological analysis of the photoreceptors was conducted using transgenic reporter lines and immunostaining at different stages of development and in adults, as well as transmission electron microscopy and biochemical assays.

3.1. Spatio-temporal expression of *gnb3b* in zebrafish

It was previously reported that *gnb3* is expressed in the mouse, monkey and bovine retina, specifically in cone photoreceptors and possibly also bipolar cells, and that this pattern is conserved across various other vertebrates (Larhammar et al., 2009; Ritchey et al., 2010). In my project, *gnb3b* expression was analyzed in one to four days old zebrafish larvae by whole mount in situ hybridization (WISH, Fig. 10). Initially, *gnb3b* expression was restricted to the epiphysis at 24 hpf (Fig. 10A), followed by expression in a small patch in the ventral retina (Fig. 10B), as described earlier (Howe et al., 2013). Later, expression expanded dorsally and by 72 hpf, half of the retina expressed *gnb3b* (Fig. 10C). By 96 hpf, the retina appeared to be almost completely stained, especially in the photoreceptor layer (Fig. 10D-D'''). Interestingly, the ventral region of the retina where *gnb3b* expression initially started from, appeared to be devoid of any expression (Fig. 10D'', red arrow). In addition, *gnb3b* expression was observed in the epiphysis of 24 - 72 hpf larvae (data not shown).

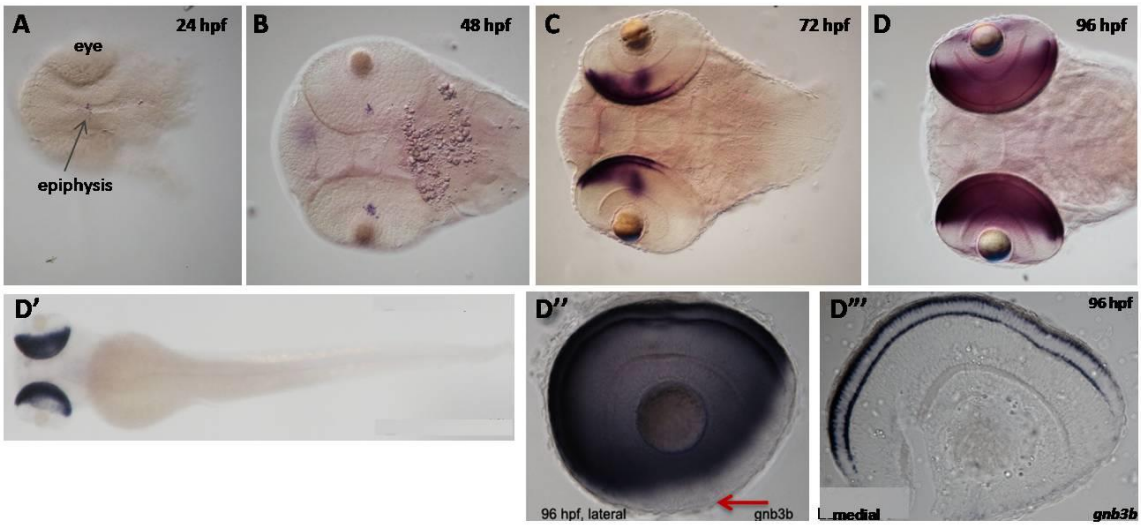

Figure 10: *gnb3b* expression pattern analysis in 1 - 4 dpf larvae using WISH staining. A: Weak expression is observed in the epiphysis (arrow) of 24 hpf embryos. B: At 48 hpf, a few cells in the ventral most region of the retina expresses *gnb3b*. C: *gnb3b* expression expands to cover almost half of the retina by 72 hpf. D: At 96 hpf, *gnb3b* is expressed throughout the retina. D': Overview dorsal image of whole larvae with *gnb3b* expression restricted to the retina. D'': The eyes were dissected out and imaged at higher magnification. *gnb3b* expression covered almost the entire retina, except for the ventral-most region (red arrow). D''': After WISH, the eyes were cryo-sectioned and it was revealed that *gnb3b* expression is restricted to the photoreceptor layer. Sense probe staining showed that the signal obtained was specific (data not shown).

3.2. Morpholino mediated knock-down of *gnb3b* expression

In order to understand the involvement of *gnb3b* in photoreceptor formation and function, morpholino based knock-down experiments were performed. *gnb3b* was knocked-down using splice-site specific MOs that were designed to target the exon-intron junctions 4 and 5 of *gnb3b* (Fig. 11A). The experimental dosage of the used MOs (*gnb3bupMO2* and *gnb3bdownMO2*) was optimized by co-injecting varying concentrations. A high MO concentration of 4.0 or 6.25 mg/ml resulted in overall severely deformed embryos with developmental defects such as small eyes, heart and abdominal edema, and an inability to hatch at 96 hpf, with a high rate of larval death. In contrast, embryos injected with MO at a reduced dosage of 3.1 mg/ml had an overall normal morphology, with slightly smaller eyes. From here onwards, all knock-down experiments were performed with a MO concentration of 3.1 mg/ml. The efficiency of the used splice-site MOs in knocking-down *gnb3b* was determined using semi-quantitative reverse transcriptase-PCR (RT-PCR). Upon injection of splice blocking MOs, the splice-sites of the target intronic sequences get

bound and therefore introns get retained. This results in the disruption of the coding sequence and/or NMD of the mRNA, reducing the amount of transcripts available for translation into functional protein.

RNA isolated from control and MO injected embryos at 96 hpf (n = 3 independent experiments) was reverse transcribed into cDNA and amplified using exon 4 - exon 5 (E4-E5) and intron 4 - exon 5 (I4-E5) primers, flanking the target region.

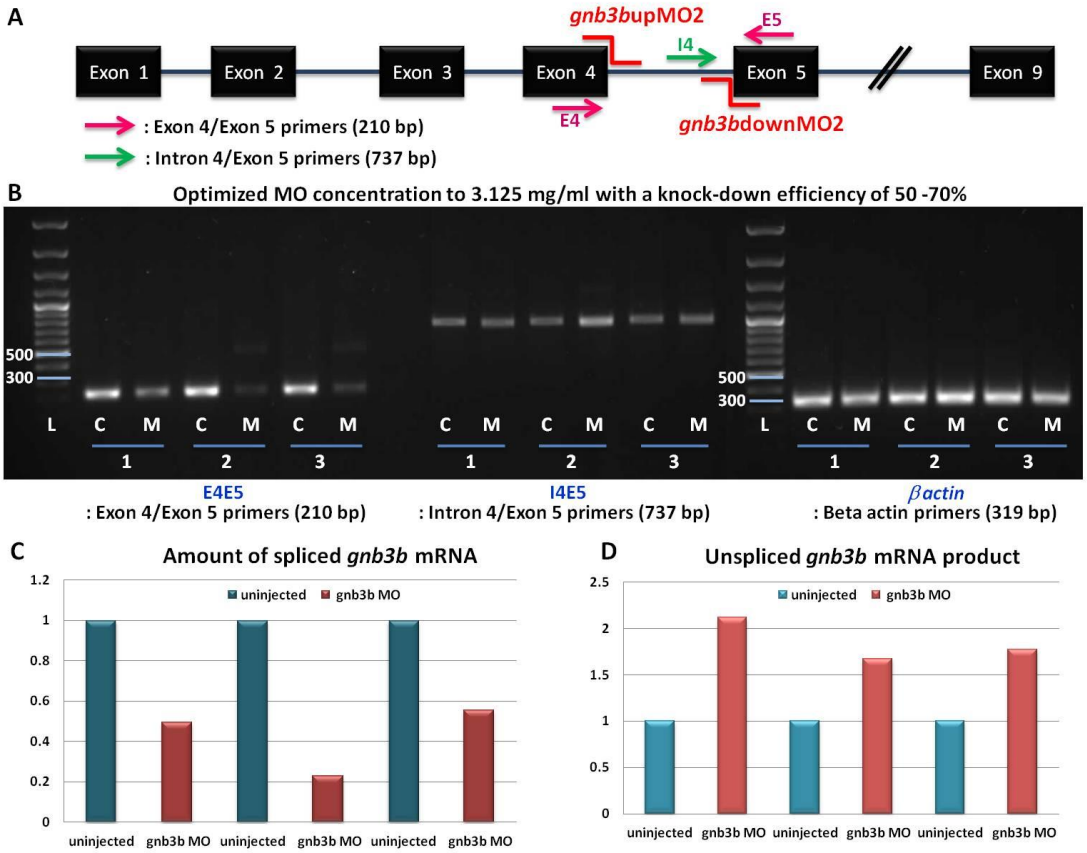

Figure 11: *gnb3b* MO target sites and analysis of *gnb3b* knock-down efficiency in four days old larvae. A: The *gnb3b* splice-site MOs were designed to target the junctions between exon 4 (*gnb3bupMO2*) and exon 5 (*gnb3bdownMO2*) as shown in the diagram. Primers E4-E5 and I4-E5 were used for subsequent RT-PCR analysis. B: Following optimization of MO concentration, the efficiency of *gnb3b* knock-down was determined. The gel image depicts the knock-down of *gnb3b* and retention of intron 4 in the morphants, performed in three independent experiments. Image on the left panel, E4-E5, shows a reduction in the amount of spliced products with an increase in the retention of intron 4 in morphants (I4-I5, centre). On the right are amplicons of *β-actin*, used as loading control for normalization. C: Injection of MOs at a concentration of 3.1 mg/ml resulted in a knock-down efficiency of 57% on average, following baseline correction. D: The morphants had a 1.85 fold increase in the amount of retained intronic products after baseline correction. C, wildtype uninjected control sample; MO, morpholino injected sample.

Figure 11B shows the gel image of the amplified transcripts of *gnb3b*, with a reduction in E4-E5 amplicons and an increase in intron 4 retention in morphants. Statistical analysis using ImageJ showed that *gnb3b* transcripts were knocked-down with an efficiency of 57% (Fig. 11C) and had a 1.85 fold increase (Fig. 11D) in the amount of retained intronic products in the morphants. Notably, also in control embryos not all introns were spliced out. *β-actin* was used as loading control and for baseline correction in the assay. Next, morphological analysis was carried out on the morphant retinas to determine the effect of *gnb3b* knock-down on photoreceptors.

3.2.1. Knock-down of *gnb3b* results in cone photoreceptor abnormalities

Retinas of *gnb3b* morphants at 4 dpf were sectioned and immunostained to label different photoreceptor types: the antibody 1D4 detects outer segments of red cone photoreceptors, zpr-1 stains double cone pair (red/green photoreceptors), and zpr-3 labels outer segments of rod and double cone pair photoreceptors (Fig. 12).

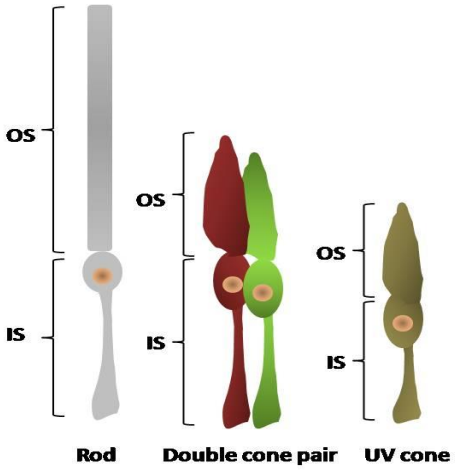

Figure 12: Schematic diagram of rod and cone photoreceptors. The outer segments (OS) of rod, double cone pair (red and green cones) and UV cones are shown. The inner segments (IS) of the rod and cone photoreceptors are connected to the outer segments via a connecting cilium. Rods have an elongated columnar OS, double cones form a conical shaped outer segment and are placed in close proximity to one another. The OS of green cone is shorter than the red cone OS. UV cones are the shortest cone cell type identified in the zebrafish retina, with a short cone shaped OS.

Morphants labelled with zpr-1 and 1D4 showed an overall reduction in signal strength with aberrant outer segment morphology of the cone cells (Fig. 13A', B'). In control retinas, the cone photoreceptors were organized in a well-defined array with distinct outer and inner segments (Fig. 13A, B). Morphant retinas on the other hand, had regions within the retina that were lacking outer segments with the elongated inner segments of double cones appearing slightly shorter (Fig. 13A', yellow arrows). In morphants, however, it was also observed that some

regions were well organized and packed with developed photoreceptors, albeit missing outer segments (Fig. 13A', blue arrow). This could be due to either a mosaic distribution of the injected MOs or to an efficient regeneration of damaged photoreceptors. The outer segments of red cone cells were evidently anomalous, with either gaps in the retina or poorly defined structures and had weakly stained cells in comparison to controls (Fig. 13B, B', yellow arrows).

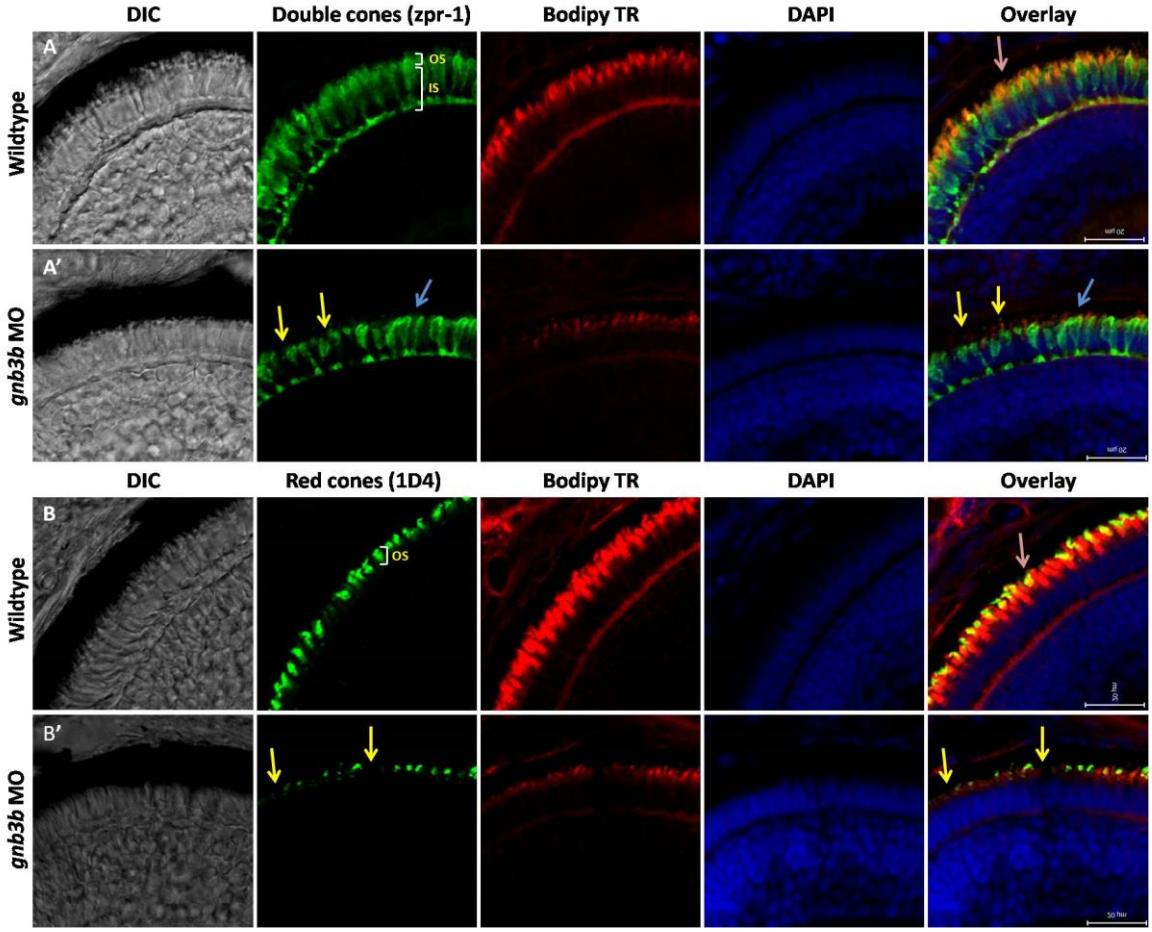

Figure 13: Cone photoreceptor morphology in *gnb3b* morphant larvae at 4 dpf with missing outer segments and aberrant cell morphology. Images shown in panels A and B are of uninjected controls, and panels A' and B' are of *gnb3b* MO injected larvae. A: In wildtype larvae, double cones labelled by zpr-1 are arranged in a regular array with clearly distinct outer segments on an elongated cell body. A': Morphant photoreceptors lack outer segments, and there is weak Bodipy TR membrane staining observed (yellow and pink arrows). The inner segments are still intact in most cells, though some cells are seen with shorter cell bodies. B: Outer segments of wildtype red cones labelled by 1D4 appear regularly organized with distinct morphology and co-localization with Bodipy TR. B': In morphant larvae, the red cone outer segments are weakly stained and a large proportion of the outer segments are missing (yellow arrows). The 1D4 staining does not co-localize with membrane staining. OS: outer segment, IS: inner segment; Scale bar = 20 µm.

The observed cone photoreceptor phenotypes in morphants could be a result of under-developed cells or ongoing degeneration of photoreceptors to various degrees.

On the other hand, there was no obvious distinguishable difference in rod photoreceptor morphology between wildtype controls and morphants (Fig. 14A-B'). The rod cells generally appeared intact with comparable staining intensity (Fig. 14A-B', yellow arrows). Therefore, knock-down of *gnb3b* did not seem to adversely affect rod photoreceptors structure. This is not surprising as it has been shown that *gnb3b* is expressed in cone photoreceptors but not in rods (Lagman et al., 2015).

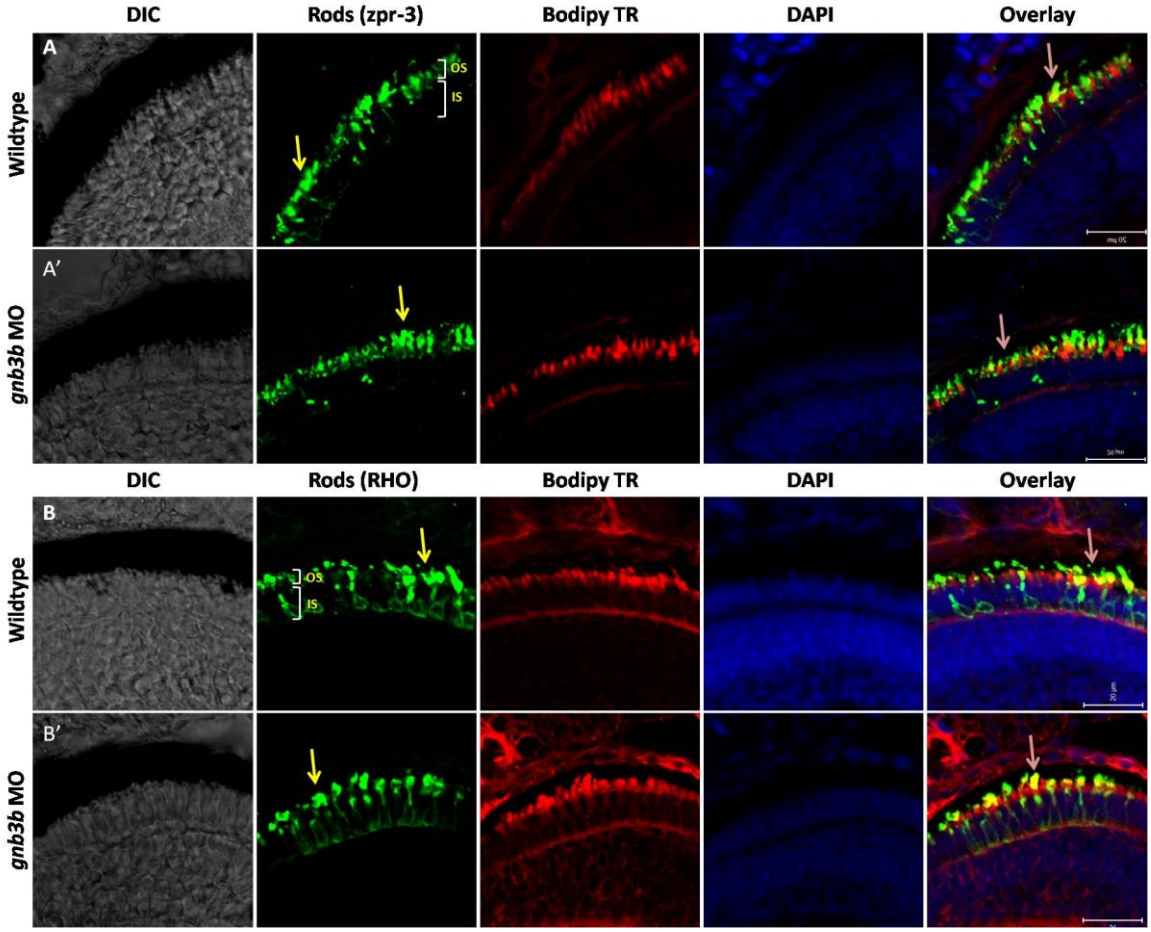

Figure 14: Rod photoreceptors appear unaffected in *gnb3b* morphants at 4 dpf. A, B: Rod outer segments labelled by zpr-3 immunostaining and rod cells labelled by EGFP in *Tg (Rho:EGFP)* in transgenic zebrafish, respectively. Rod cells are organized and arranged in a regular pattern in the wildtype with outer segments starting to develop (yellow arrows). A', B': In *gnb3b* morphants, the rod photoreceptor structure appears comparable to that of the wildtype, with outer segments co-localizing with Bodipy TR membrane staining (yellow and pink arrows). OS: outer segment, IS: inner segment; Scale bar = 20 µm.

In addition to immunostaining, the sections were also stained with Bodipy TR, which labels cell membranes. Bodipy TR labelling gave an overview of the morphology of all rod and cone photoreceptor cells in the retina. Following Bodipy TR labelling, it was obvious that in the morphants a knock-down of *gnb3b* led to a reduction in the number of photoreceptors as well as atypical photoreceptor structures (Figs. 13, 14). In the retina of control larvae, photoreceptors were densely packed with regular arrangement and consistent morphology. Co-localization of membrane stain together with cell type specific markers revealed an intact and well defined outer segment morphology of photoreceptor cells (Figs. 13, 14, pink arrows). Morphants, on the other hand, depicted cone photoreceptors with various shapes and sizes, and minimal co-localization of membrane staining with zpr-1 and 1D4 (Fig. 13A', B'). The observed diverse morphologies could indicate that cells are undergoing various stages of degeneration. Zpr-3 staining and Bodipy TR staining appeared to co-localize in rods, suggesting that rod cell morphology is not as severely affected (Fig. 14A', B'). In addition, live imaging of *gnb3b* morphants in a *Tg (SWS1:EGFP*) reporter background, revealed that in morphants the EGFP signal was significantly reduced with irregularly shaped UV cones (Supplementary Fig. 1).

Taken together, these data suggest that *gnb3b* is required for the maintenance of structural integrity of cone photoreceptors but not necessarily for rods. However, this does not eliminate the possibility that rod cells may be affected secondarily over time due to a 'bystander effect' (Lewis et al., 2010a).

3.2.2. Analysis of apoptosis in *gnb3b* morphants

The observed morphological defects in the retinas of *gnb3b* morphants suggest a possible ongoing degeneration of photoreceptors. Therefore, terminal deoxynucleotidyl transferase dUTP nick end labelling (TUNEL) staining was performed to detect apoptotic cells in embryos at 24 hpf. Surprisingly, extensive numbers of apoptotic cells were detected throughout the entire *gnb3b* morphant embryos (Fig. 15B, red arrows), especially in the retina and posterior trunk. In

comparison, uninjected control larvae had sparsely distributed apoptotic cells with slightly increased numbers of apoptotic cells in the trunk region (Fig. 15A). To test the specificity of the MO induced defects, embryos were co-injected with *gnb3b* and p53 MOs, to inhibit the apoptosis pathway. This resulted in a dramatic reduction in the number of apoptotic cells in retina and trunk tissues (Fig. 15C). Hence, the observed increase in the number of apoptotic cells in *gnb3b* morphants is likely due to the unspecific off-target effects elicited by the *gnb3b* MOs.

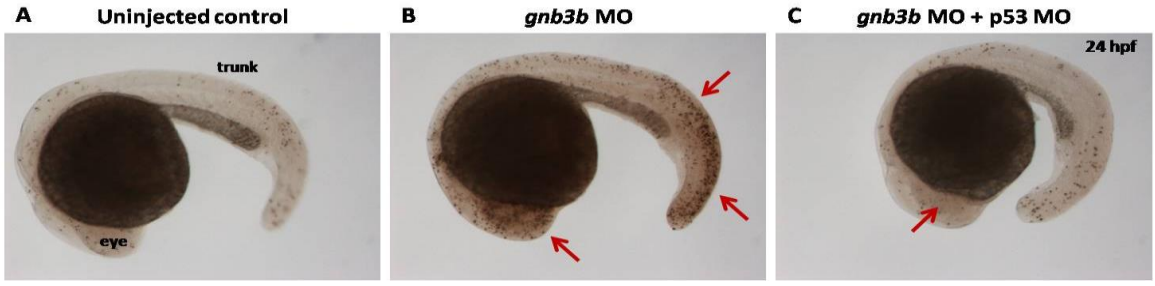

Figure 15: Whole mount TUNEL staining of 24 hpf embryos. A: Few apoptotic cells were observed in uninjected embryos with single clusters of dying cells in the retina and trunk. B: *gnb3b* MO injected embryos with extensive cell death throughout the larvae. Particularly, large numbers of apoptotic cells occurred in the forebrain, eyes and posterior trunk (red arrows). C: In embryos co-injected with *gnb3b* and *p53* MOs, numbers of apoptotic cells were reduced, even in the eyes and trunk. N = 15 per sample type, performed in duplicate.

In addition, to determine whether *gnb3b* could have a possible function outside the retina, WISH staining time was extended to approximately 16 -18 hrs and then analysed. Even after extended staining time, the signals were restricted to the retina and not detected in the larval trunk (Fig. 16A). Therefore, semi-quantitative RT-PCR was utilized to identify presence of *gnb3b* transcripts in other tissues. Uninjected control, standard MO injected and *gnb3b* MO injected larvae at 4 dpf were dissected between the head and trunk region. RNA was isolated separately from eyes and trunk samples, and reverse transcribed into cDNA. PCR amplification using the E4-E5 and I4-E5 primers revealed that *gnb3b* transcripts were present in the trunks of 4 dpf larvae, albeit weakly (Fig. 16B, left panel). Retention of unspliced *gnb3b* products in the trunk could not be detected, probably due to the low amount of transcripts, below detection limit at this stage (Fig. 16B, middle panel). *β-actin* was used as loading control (Fig. 16B, right panel). Presence of

gnb3b transcripts in the trunk raises the possibility that the observed extensive cell death in the trunks of *gnb3b* morphants could be attributed to a knock-down of *gnb3b* in these tissues. However, this does not eliminate the possibility that cell death occurring in the trunk results from MO mediated off-target effects.

Taken together, the preliminary MO knock-down study highlighted the importance of *gnb3b* for structural integrity of cone photoreceptors but not for rods, in four days old larvae.

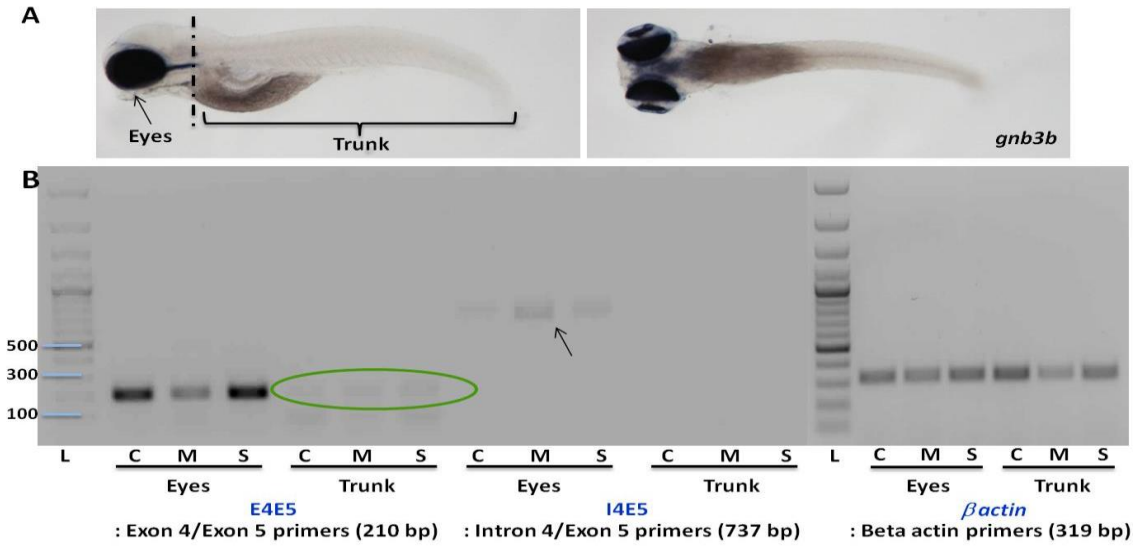

Figure 16: WISH and RT-PCR analysis of *gnb3b* expression in head and trunk at 4 dpf. A: Dorsal and lateral views of embryos at 4 dpf after prolonged WISH staining using a *gnb3b* probe. *gnb3b* expression is restricted to the eyes and the ventral-most brain structures. Broken line in A depicts the level of dissection used for subsequent RNA isolation from head and trunk tissue. B: Gel image showing amplified products after PCR with E4-E5 and I4-E5 primers, *β-actin* was used as loading control (image far right) for eye and trunk samples. In the retina, *gnb3b* transcripts were identified in all samples, with morphants showing an increase in the amount of *gnb3b* transcripts with retained intron 4. C: Controls, M: *gnb3b* morphants, S: standard control morphants; n = 150 per sample set, 3 technical replicates.

As the long term consequence of *gnb3b* deficiency remains to be determined, together with potential off-target effects introduced by the MO and also a failure of the morphants to survive into adulthood, I proceeded with creating *gnb3b* knock-out mutants using the TALEN technology.

3.3. Design of TALENs and generation of *gnb3b* mutants

Two TALEN pairs were designed using the software TAL Effector Nucleotide Targeter 2.0, one pair targeting exon 3 and the second exon 7 (Fig. 17A) (Doyle et al., 2012). The target sites were selected based on the criteria that 1) the Tal effector target sites are preceded by a T at the 5' end, 2) the spacer length spans 15 - 24 bases, and 3) that each repeat variable contained di-residue units of 15 - 20 bases (Cermak et al., 2011). The selected target sequences were used as queries in a BLASTN search to ensure the absence of off-target binding sites. The schematic diagram in Figure 16B provides a brief summary of the steps taken towards the generation of TALEN pairs. The detailed protocol is provided in the Materials and Methods section (refer to section 2.13.1.). The 'unit assembly' protocol was used to generate the desired TALEN expression vectors, with modular combination of TALE repeat units (kindly provided by Dr Sampath's lab, Temasek Life Science Laboratories) (Huang et al., 2011).

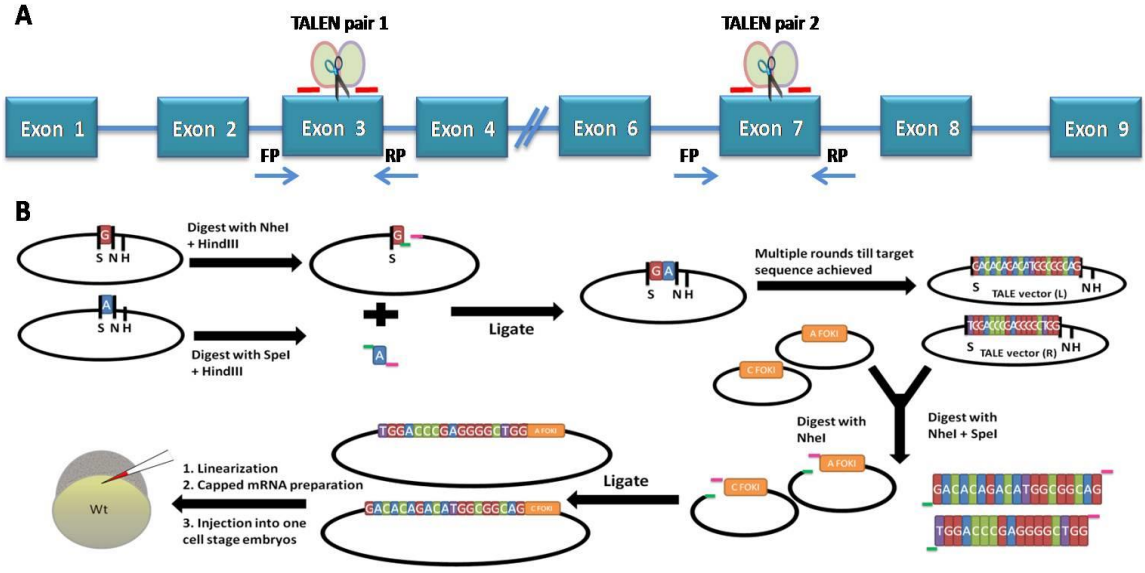

Figure 17: Schematic diagram illustrating target sites and the design and process of generating a TALEN pair. A: Regions within exon 3 and exon 7 were selected for genome modification by TALEN. For each target site, two flanking TALEN arms were designed. For screening of introduced mutations, primers were designed in the introns, flanking exons 3 and 7, each with a unique restriction enzyme site. B: The desired TALE arm sequences were cloned into a vector by sequentially combining the TALE repeat units via the 'unit assembly' method. Once the sequence of interest was fully assembled, the sequence was sub-cloned into another vector containing monomeric FokI nuclease. These TALEN expression vectors were *in vitro* transcribed and the mRNA from both the left and right arm was co-injected into one-cell stage embryos. FP: forward primer, RP: reverse primer.

TALE repeat units were sequentially combined via cloning into a backbone vector to form the desired TALE arm sequences. The fully assembled individual TALE arm sequence of interest was then sub-cloned into another vector containing monomeric FokI nuclease. Once the TALEN expression vectors were created, the plasmids were sequenced, linearized and *in vitro* transcribed to generate capped mRNA. Either mRNAs for a single TALEN pair or two TALEN pairs were co-injected into one-cell stage zebrafish embryos, with varying concentrations ranging from 50 ng/µl to 300 ng/µl. One to two days old injected embryos were tested for the introduction of insertion or deletion (indel) mutations by screening for alterations in selected unique restriction sites at the target regions. TALEN pair 1 and pair 2 were screened independently with restriction enzymes MwoI and PciI, respectively, through a restriction fragment length polymorphism (RFLP) assay. For samples that were co-injected with both TALEN pairs, primers designed could not amplify the entire length between exon 3 and exon 7 specifically. Therefore, these embryos were screened at individual exons for introduced mutations.

A total of 157 and 93 individual embryos were screened after TALEN pair 1 and TALEN pair 2 injection, respectively, without identifying any positive mutants (Fig. 18A, B).

A

TALEN pair 1 (E3)_ MwoI		
Embryos	Positive	Negative
Injected	0	157

B

TALEN pair 2 (E7)_ PciI		
Embryos	Positive	Negative
Injected	0	93

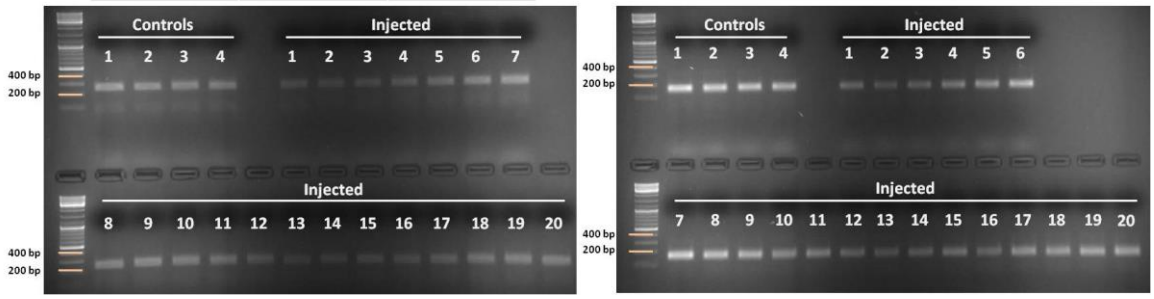

Figure 18: Representative gel image depicting PCR amplicons after enzymatic digestion, for identification of introduced mutations in injected larvae. A: MwoI was used as restriction enzyme for RFLP screening of TALEN pair I injected samples. A total of 157 single larvae were screened and all were negative for introduction of mutations at the MwoI site. B: Samples injected with TALEN pair 2 were screened with PciI and a total of 93 individual larvae were tested and none of them were positive for mutations.

Due to the difficulties experienced with TALEN in successfully generating F_0 mutants, and the concomitant technological advancement of more efficient CRISPR/Cas9 protocols (Hwang et al., 2013), I decided to use a CRISPR/Cas9 approach to generate mutant lines for *gnb3b*.

3.4. Generation of *gnb3b* mutants using the CRISPR/Cas9 system

CRISPR/Cas9 target sites for *gnb3b* were designed using the program ZiFit Targeter version 4.2 (Sander et al., 2010; Hwang et al., 2013). A single target site was chosen using the following criteria: the target site needs to have a GG dinucleotide at the 5' terminal and end with a 'NGG' protospacer adjacent motif (PAM), giving a sequence structure of GG-$(N)_{18}$-NGG (called guide RNA, gRNA). A BLASTN search was carried out to ensure minimal off-target hits upon selection of target sequences. The ZiFit program provides a sequence of the target site, and two oligo sequences that are required for gRNA preparation. The workflow undertaken towards the generation of a stable *gnb3b* mutant line is shown in Figure 9 (Material and Methods section).
The gRNA was selected to target exon 5 of *gnb3b* (Fig. 19A, left panel). The designed gRNA oligos were annealed, phosphorylated and cloned into the pDR274 vector. Selected clones were sequenced and then *in vitro* transcribed prior to injection. In parallel, Cas9 nuclease mRNA was prepared by linearization of the pMLM3613 Cas9 expression vector, *in vitro* transcription and polyadenylation of the transcript (Fig. 19B, right panel). The gRNA and Cas9 mRNAs were co-injected into one-cell stage embryos at a concentration of 50 ng/µl and 300 ng/µl, respectively. To screen for successful introduction of mutations, a unique restriction site close to the 3' end of the gRNA sequence was selected. The rationale behind this screening method is that upon introduction of indels by the Cas9 nuclease at the region of interest, the restriction site gets disrupted and the PCR amplicons will remain undigested while samples from controls and unaffected injected siblings will be completely digested (Fig. 19C). For *gnb3b*, HaeIII was used to screen for mutations.

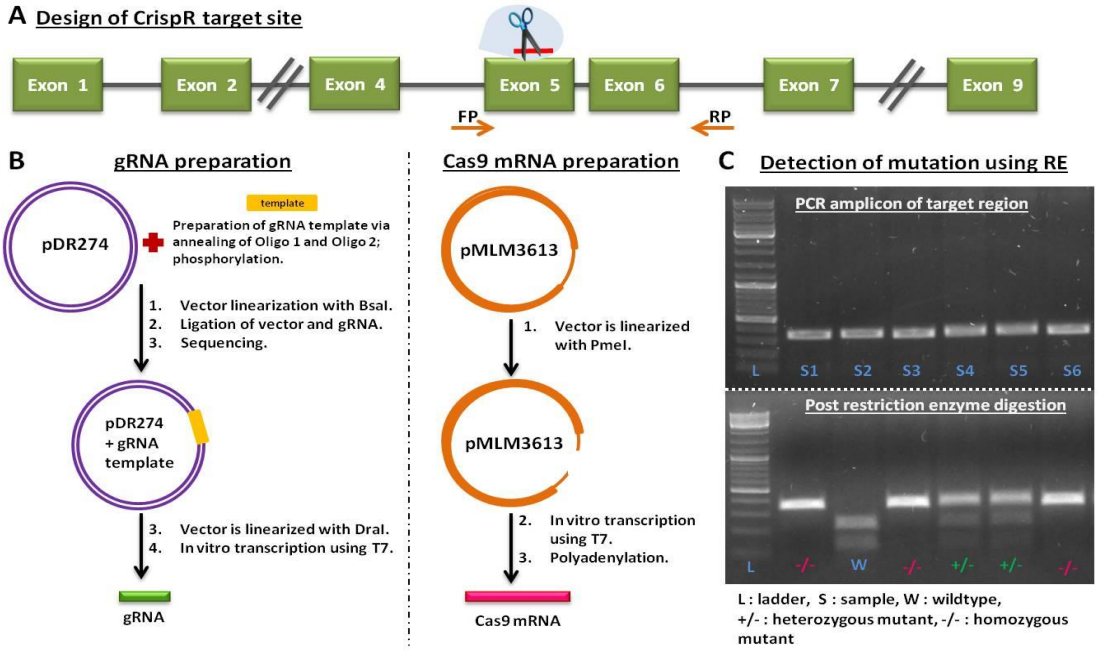

Figure 19: Schematic diagrams illustrating the process of design, generation of CRISPR/Cas9 mRNA and screening for mutations. A: *gnb3b* has nine exons, with the coding region starting from exon 2. The guide RNA was designed to target exon 5, primers for screening of mutants were designed in intron 4 and intron 6. B: The left panel shows the preparation of gRNA, whereby the template sequence for gRNA was produced via annealing and phosphorylation of two oligos prior to being cloned into the linearized pDR274 vector. The newly cloned plasmid was linearized and *in vitro* transcribed to produce gRNA for injection. In the right panel, the process for Cas9 mRNA production is shown. The pMLM3613 plasmid encoding Cas9 transcript was linearized, *in vitro* transcribed and polyadenylated before injection. Both gRNA and Cas9 mRNA were co-injected into one-cell stage embryos. C: Gel image representing the screening for CRISPR/Cas9 induced mutations. Embryos co-injected with gRNA and Cas9 mRNA were screened using RFLP assay that recognizes a unique restriction enzyme (RE) site. Top panel of gel image shows the PCR amplification of target region. PCR amplicons were subjected to RE digestion. Wildtype samples (W) will show complete digestion, while samples with mutations will lead to a partially and/or incompletely digested product due to the loss of the restriction site. FP: forward primer, RP: reverse primer.

Embryos injected with CRISPR/Cas9 were tested at 24 hpf for the presence of mutations. In a primary screen, digested PCR amplicons were sequenced to determine the type of induced mutations (Fig. 20A). A variety of mutations were identified with deletion mutations most commonly seen. The deletion mutations ranged from 4 to 25 bases long with particular types of seven base pair deletions recurring often (Fig. 19A, Mut_8.21 and Mut_9.21). The injected larvae were raised into adulthood, screened for founders and the efficiency of *gnb3b* CRISPR/Cas9 was determined (Fig. 20B). Injected adult fish were set up in pairs and incrossed. The obtained F_1

progeny were pre-screened for introduced mutations using a RFLP assay. Incrossed parents which produced F_1 embryos with mutations were labelled as founders (F_0) and re-set up on a regular basis to raise the progeny into adults. 11 out of 15 potential founder pairs screened were positive for germline transmission of mutations, giving a high efficiency rate of 73.3%. Screening of F_1 embryos revealed that 21.1% of embryos were carriers of mutations suggesting germ line mosaicism. F_1 progeny from 9 out of the 11 F_0 fish pairs screened, carried a particular type of 7 base deletion (hereafter known as *gnb3b*^{del114}) while 5 of the 11 pairs in parallel carried a different type of 7 base deletion sequence (hereafter *gnb3b*^{del112}). F_1 progeny with three different mutation alleles namely, *gnb3b*^{del112}, *gnb3b*^{del114} and *gnb3b*^{del107}, were selected and incrossed to produce F_2 for establishment of stable *gnb3b* mutant lines.

A

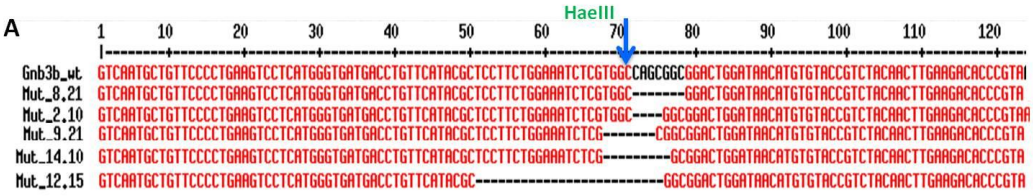

B

No. of potential F_0 pairs screened	No. of F_0 pairs identified	Rate of Transmission	No. of F_1 larvae screened	No. of positive F_1 identified	Rate of Transmission
15	11	73.3 %	350	74	21.1 %

C

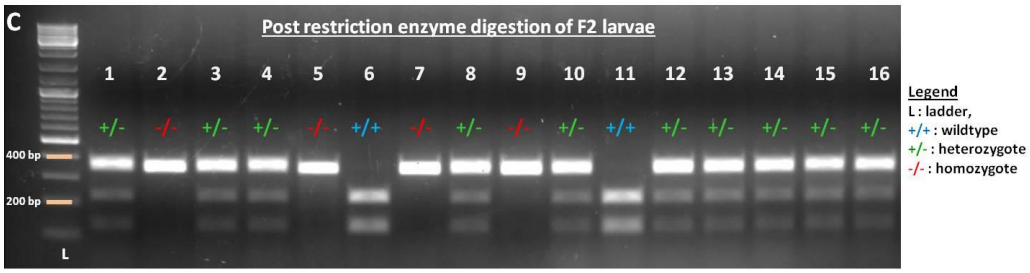

Figure 20: Overview of types of induced mutations and knock-out efficiency of *gnb3b* by CRISPR/Cas9. A: Sequencing results of individual clones revealed that deletion mutations were most commonly introduced by CRISPR/Cas9. The deletions ranged from 4 to 25 bases, with a commonly recurring seven base deletion sequences (as shown in Mut_8.21 and Mut_9.21). B: Efficiency of *gnb3b* CRISPR/Cas9 in introducing mutations in F_0 and F_1. A total of fifteen potential founder pairs were incrossed and eleven of them were identified to transmit mutations to the next generation. This gave an F_0 germline transmission efficiency of 73.3%. The F_1 larvae from these eleven pairs were screened at 24 hpf. Out of 350 larvae analysed, 74 were positive for harbouring mutations, giving a mutation rate of 21.1%. C: A representative RFLP analysis of 4 dpf F_2 larvae (HaeIII site is shown in A, blue arrow). Wildtype larvae had the PCR amplicon completely digested (two bands), heterozygous amplicons were partially digested (three bands) and homozygous mutants retained an undigested PCR amplicon (one band). FP: forward primers, RP: reverse primers.

The F_2 progeny were used for genotyping and morphological analysis at larval and adult stages. PCR amplification of the target region amplified an amplicon of 360 bases. Upon enzymatic digestion with HaeIII, two bands of 226 bp (base pairs) and 134 bp were obtained in control samples. In heterozygous mutants, the PCR amplicon was only partially digested revealing three bands, one undigested and two digested bands. In homozygous mutants, the PCR amplicons remained completely undigested as the unique restriction site had been disrupted in both alleles. A representative gel image for genotyping of F_2 progeny is shown in Figure 20C. Generally, the inheritance in the F_2 population followed the Mendel's laws of inheritance, whereby 25% of larvae were wildtype, 50% were heterozygous for a mutation in *gnb3b* and the remaining 25% were homozygous mutants. Trunks of larval samples and fins of adult fish were used for screening, to sort out and separate the fish in accordance to their genotype. The retina from individual genotypes was used for further functional characterization.

Mutant carriers from the three different alleles selected were maintained for establishment of mutant lines and their protein sequences were analyzed. Two of the lines have two different 7 base deletions and the third line has a 25 base deletion. All three mutant alleles are predicted to result in truncated proteins with the introduction of a premature stop codon. The *gnb3b*^{del112} and *gnb3b*^{del114} deletion alleles have their amino acid sequence in sync with wildtype Gnb3b protein for up to the first 111 and 113 amino acids, respectively, before a few amino acid sequence changes occur and a stop codon is introduced at amino acid position 124 (Fig. 21A). The third line, *gnb3b*^{del107} has its amino acid sequence in alignment up to position 106, after which the amino acid sequence is expected to be altered with a stop codon introduced at position 118. The full length Gnb3b is 338 amino acids long, hence in all three lines only approximately one third of the protein is expected to be present. The schematic diagram in Figure 21B shows the deduced domain structure of the full length wildtype Gnb3b protein and the region of truncation occurring in the mutant protein at amino acid position 124. G protein beta (Gβ) subunit is predicted to be made up of seven WD 40 domains which folds into a seven-

bladed β-propeller structure with an enclosed channel (Fig. 21C, left panel) that mediates protein-protein interaction with the G protein gamma (Gγ) and G protein alpha (Gα) subunits. Each blade in the β-propeller is made up of four β-sheets. The N-terminus of Gβ forms an α-helix and interacts with the N-terminus of Gγ subunit, and the fifth and sixth WD40 domains bind to the C-terminus of Gγ (Oldham and Hamm, 2008).

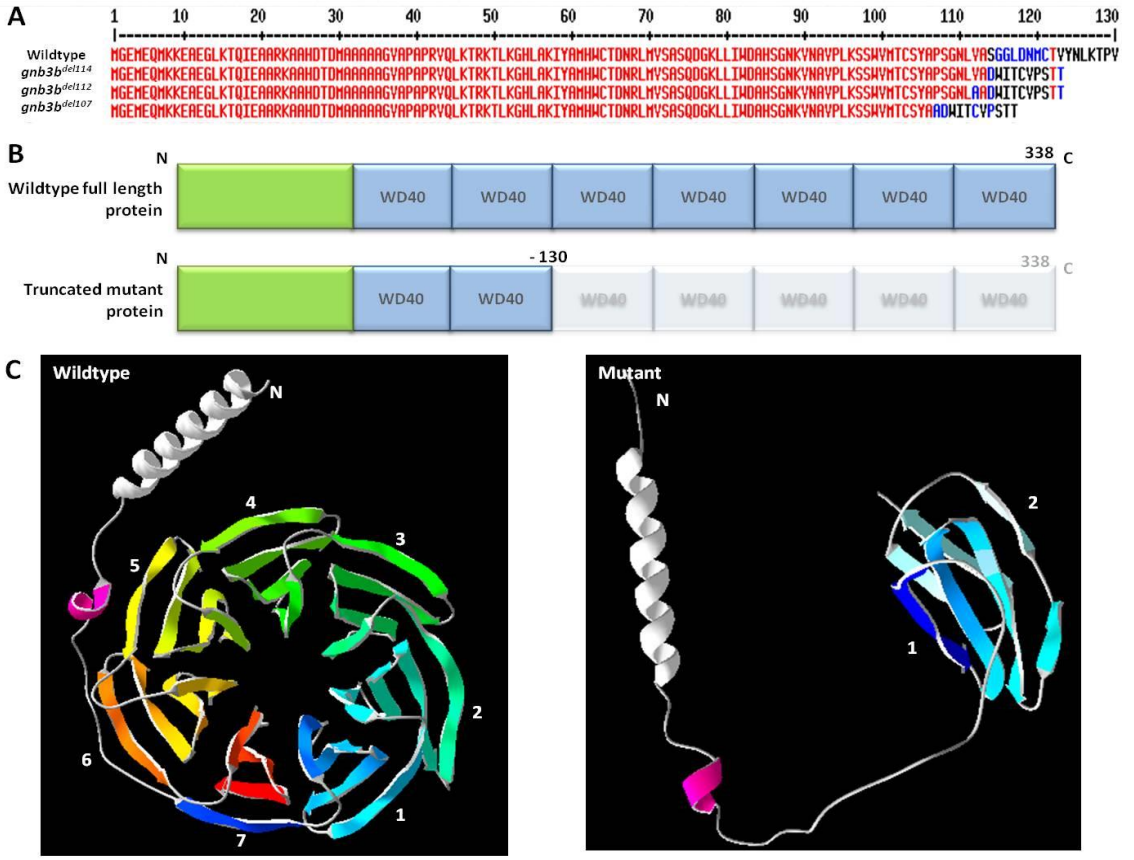

Figure 21: Modelling of *gnb3b* mutant proteins using bioinformatics tools. A: Three different alleles were selected for protein modelling, two of them have a 7 bp deletion and the third line has a 25 bp deletion. In one line, *gnb3b*^{del114}, the introduced mutation leads to the amino acid sequence being in frame up to position 113, and in the other line, *gnb3b*^{del112}, up till position 111. In both cases, the protein sequence gets truncated at amino acid position 124. The third line with a 25 bp deletion, *gnb3b*^{del107}, has a stop codon introduced at position 118. B: Schematic diagram that shows full length and predicted mutant Gnb3b domain organization. Wildtype Gnb3b protein is 338 amino acids long while mutant *gnb3b*^{del114} protein is 124 amino acids long. The wildtype Gnb3b has seven WD40 domains while in mutants only the first two WD40 domains are retained. C: 3D structural rendering of wildtype and mutant Gnb3b protein using SWISS-MODEL. The image on the left shows that the N-terminus is composed of a α-helix and a seven-bladed β-propeller. In contrast, the mutant Gnb3b protein only has an intact N-terminal α-helix but lacks the seven-bladed β-propeller structure. N: N-terminus; 1-7 labels the individual WD40 domains folded into the seven-bladed β-propeller structure in order.

The N-terminus of the Gα subunit forms contact points with the first and seventh blade as well as at the narrow end of the β-propeller channel (Wall et al., 1995). 3D modelling of the wildtype and mutant protein sequence using SWISS-MODEL and Swiss PdbViewer (Guex et al., 2009) showed that the predicted *gnb3b*^{del114} mutant protein structure was vastly different from that of the wildtype Gnb3b protein (Fig. 21C, right panel).

The *gnb3b*^{del114} mutant protein is predicted to lack the characteristic seven-bladed β-propeller structure with only the N-terminal α-helix still intact and folded properly. This can potentially result in improper *gnb3b*^{del114} protein folding and in turn affect subsequent protein-protein interactions and the signal transduction cascade.

3.4.1. Cone photoreceptors show aberrant morphology in *gnb3b*^{del114} mutant larvae

After the mutant lines had been established, the photoreceptor morphology of *gnb3b*^{del114} mutant larvae at 10 dpf was analysed. Mutant carriers were outcrossed to *Tg (SWS1:EGFP)*, in which UV cone photoreceptors express EGFP under control of a *SWS1* promoter (Yin et al., 2012). The UV photoreceptors were directly imaged for EGFP expression following cryo-sectioning and sample processing.

Wildtype UV cone photoreceptors are arranged in a continuous array of tightly packed cells in the retina, and have a distinct triangular shaped outer segment with a slender concaved inner segment (Fig. 22A, B). In heterozygous *gnb3b*$^{del114+/-}$ carriers, the cell arrangement appears to be regular with slightly shorter UV cones. Some of the UV cone cells had the tip of the outer segment missing and their inner segment body appeared more parallel than concaved (Fig. 22A, C, boxed). A couple of cells also lacked a defined outer segment. In the homozygous *gnb3b*$^{del114-/-}$ mutants, UV cone cells were relatively regularly arranged but had a shorter and far thinner and parallel cell body and almost all cells lacked about half of their outer segment (Fig. 22A, D,

boxed). Regions with missing cells (blue arrow) as well as cells with indistinct structure (yellow arrows) were also identified.

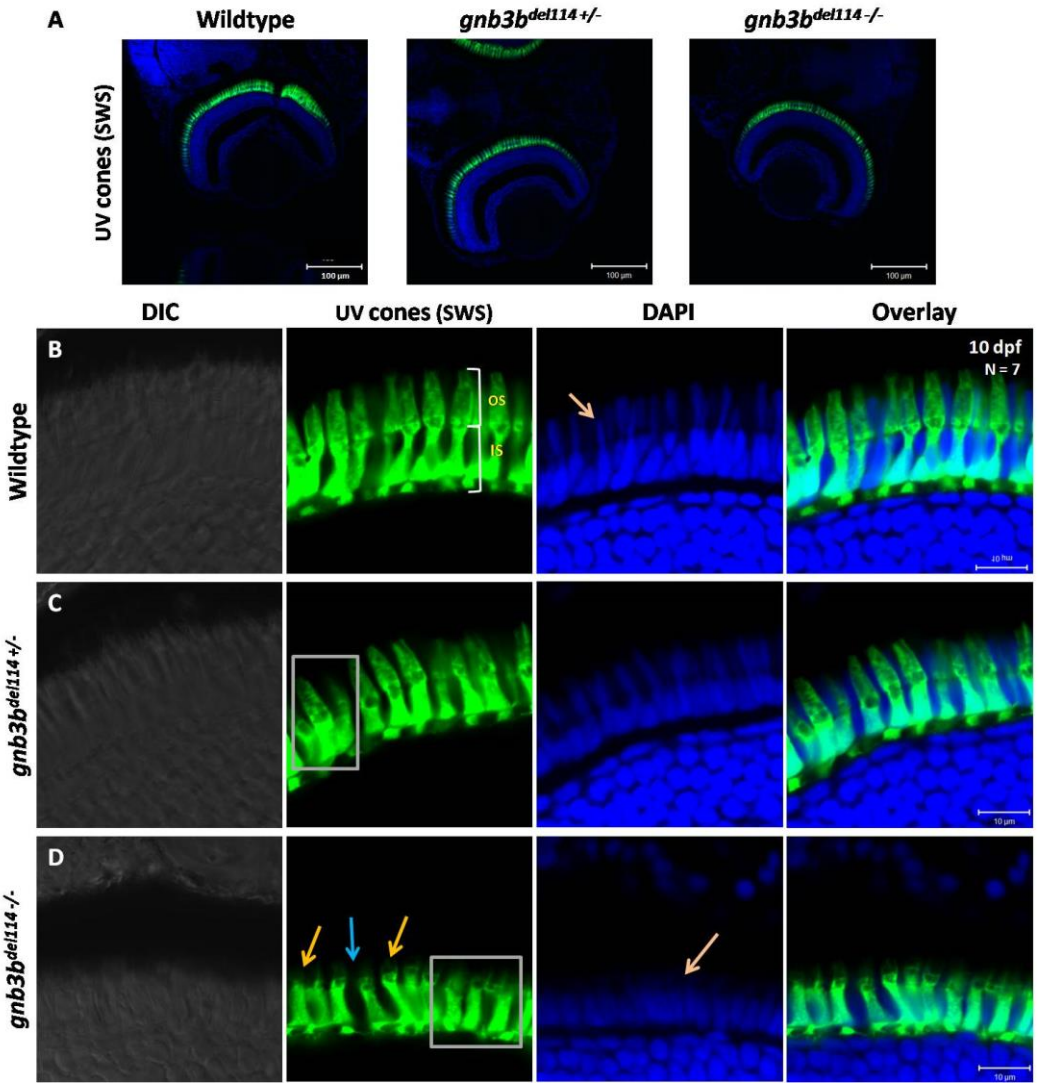

Figure 22: Morphological analysis of UV cones in 10 days old larvae, following cryo-sectioning and confocal imaging of EGFP expression. A: Overview image depicting the organization of UV cones in wildtype and mutant larval retina. B: The UV cones are formed with a conical outer segment and an extended inner segment in wildtype larvae. C: The heterozygous *gnb3b*$^{del114+/-}$ carriers have an overall similar UV cone morphology compared to controls, although the cells look slightly shorter. Some cells were missing the tip of the outer segment and had lost the concaved inner segment appearance (boxed). D: Homozygous *gnb3b*$^{del114-/-}$ mutants have thin, short UV cone cell bodies with almost all of the outer segments missing (yellow arrows). The distinct concaved inner segment body structure was altered and appeared more parallel (boxed). The cells were not as regularly arranged and regions with missing cells were visible (blue arrow). OS: outer segment, IS: inner segment; n = 7; Scale bar = 100 µm for overview images and 10 µm for B-D.

In wildtype siblings, double cones, which are stained with zpr-1, have a small circular outer segment and an elongated cell body with a slight constriction towards the base of the cell (Fig. 23A, B). The typical circular feature of the outer segment (outlined in Fig. 23B) could not be clearly identified in heterozygous and homozygous mutants (Fig. 23C, D). In *gnb3b*$^{del114+/-}$ carriers, the elongated inner segment was still visible albeit weakly stained.

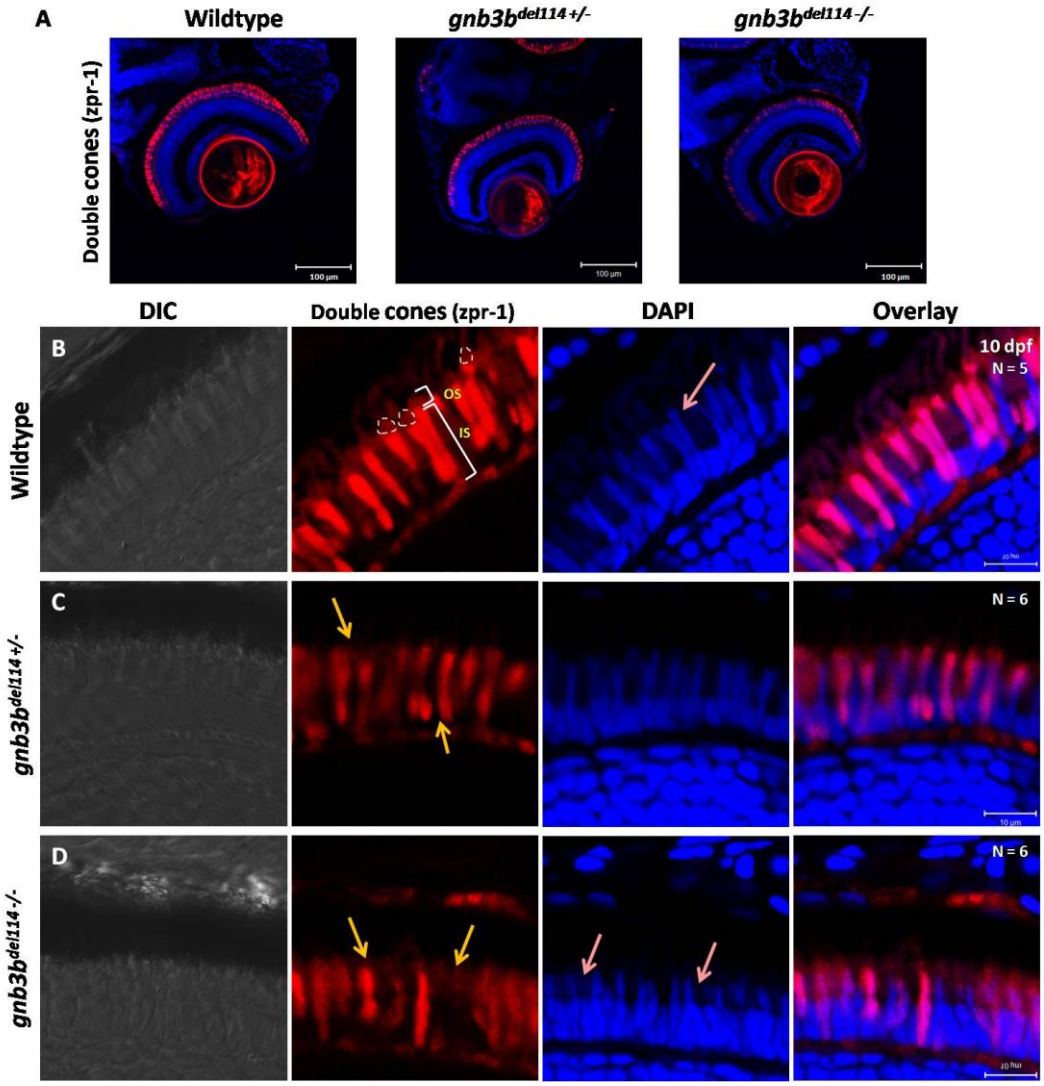

Figure 23: Double cones of 10 dpf larvae immunostained with zpr-1. A: Overview images of the larval retina reveal that double cones are aberrantly formed in the homozygous mutant. B: The wildtype double cones are characterized by a circular outer segment (outlined) with an elongated cell body. The nuclei of double cones are extended. C: In *gnb3b*$^{del114+/-}$ carriers, the circular outer segments are often missing and the cell body appears thinner and more weakly stained (yellow arrows). D: The *gnb3b*$^{del114-/-}$ mutants lack the typical double cone morphology. The cells have shorter inner segments of various shapes and sizes, with deficient outer segments (yellow arrows). Some regions in the retina were completely devoid of any double cone cells. Double cones were also weakly stained in the mutants. The characteristic extension of nuclei found in the cell body of double cones is shorter. OS: outer segment, IS: inner segment; n = 5 for controls and 6 for mutants; Scale bar = 100 µm for overview images and 10 µm for B-D.

The cell bodies of some of the double cones lacked the defined structures found in wildtype (Fig. 23C, yellow arrows). None of the double cones in *gnb3b*$^{del114-/-}$ mutants showed a properly formed cell body and cells were sparsely labelled. The mutant double cones exhibited various shapes and sizes without any distinct outer or inner segments (Fig. 23D, yellow arrows). There were gaps present in between the cell arrangement, indicating missing double cones.

Another interesting feature noticed in *gnb3b*$^{del114-/-}$ mutants was that the nuclei were generally shorter and not normally developed (Figs. 22, 23, pink arrows). The distinct extension of nuclei, belonging to the double cones inner segment, seen in wildtype and heterozygous carriers, were disrupted and the nuclei at the base of the outer nuclear layer appeared to be stacked on top of one another in the homozygous mutants. The nuclei of wildtype and heterozygous larvae were of comparable shape and length.

3.4.2. Rod photoreceptors are underdeveloped in *gnb3b* mutants

Low magnification overview images of zpr-3 stained 10 dpf control and heterozygous larvae showed clearly labelled rod photoreceptor outer segments, with strong staining observed at the periphery, while in the *gnb3b*$^{del114-/-}$ mutants these were weakly stained (Fig. 24A, green arrows). At this stage, the outer segments of rod photoreceptors have yet to develop a defined structure. Higher magnification of the outer segments showed that the outer segments of rod photoreceptors were developed and fanned out (Fig. 24B). Comparable staining intensity and outer segment pattern was also observed in heterozygous *gnb3b*$^{del114+/-}$ carriers (Fig. 24C). In contrast, there was a clear reduction in zpr-3 staining intensity in *gnb3b*$^{del114-/-}$ mutants, suggesting that rod photoreceptors were not properly developed (Fig. 24D). Rod outer segments were shorter in homozygous mutants (yellow arrows) and regions without rod outer segment staining were evident in the mutant retinas. This reduction in rod outer segments suggests a possible degeneration of rod photoreceptors or alternatively a developmental delay in rod formation.

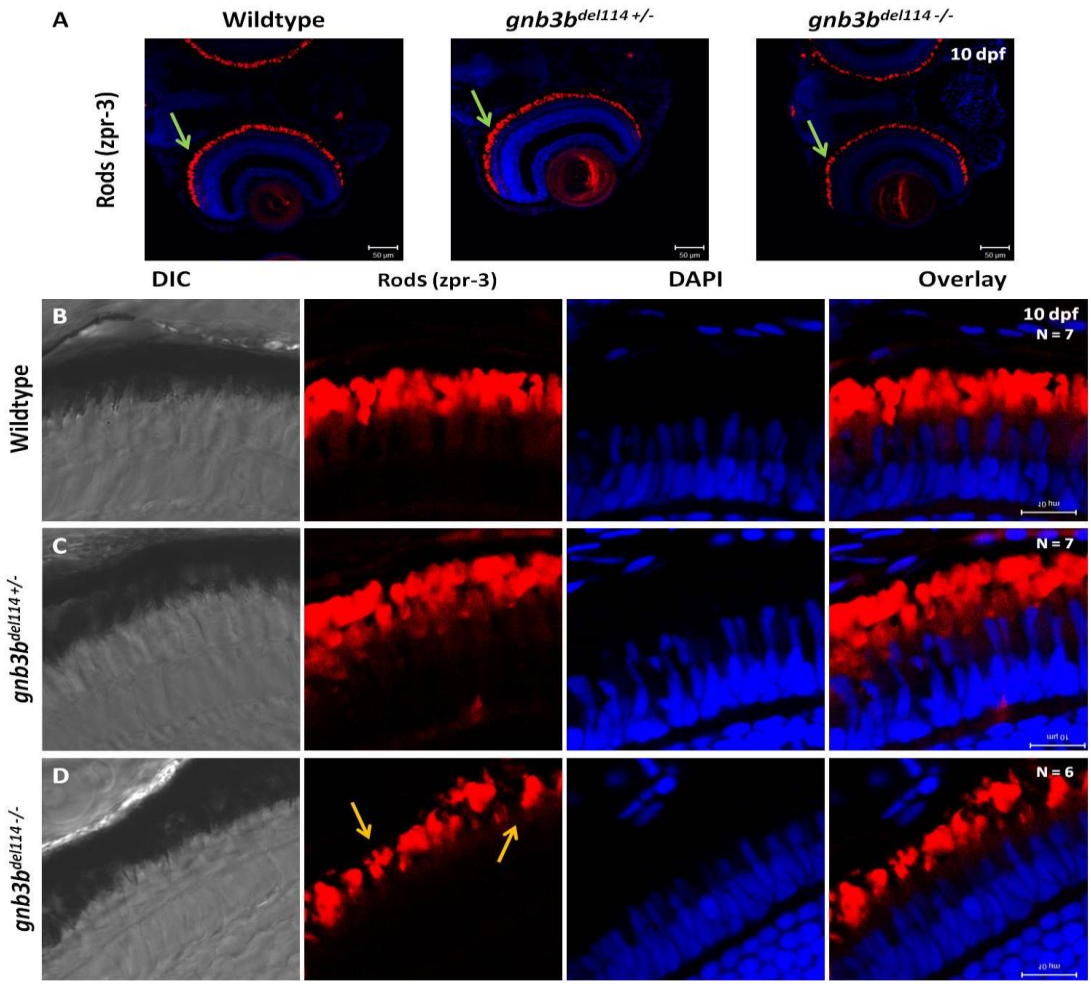

Figure 24: Immunostaining of rod photoreceptor outer segments with zpr-3 in 10 dpf larvae. A: The outer segments of rod photoreceptors in wildtype controls and heterozygous carriers were well developed in the entire retina with strong staining observed towards the periphery (green arrows). B: The rod outer segments were observed to extend out in the controls. C: Rod outer segment morphology in heterozygous carriers appeared comparable to controls. D: In *gnb3b*$^{del114-/-}$ mutants, zpr-3 staining intensity was slightly reduced and the rod outer segments were shorter and deformed (yellow arrows). Some regions within the retina had gaps devoid of rod cells. OS: outer segment, IS: inner segment; n = 7 for controls and heterozygous carriers, and 6 for homozygous mutants; Scale bar = 50 µm for overview images and 10 µm for B - D.

3.4.3. *gnb3b* mutants do not survive into adulthood

Surprisingly, no adult homozygous mutants were identified for any of the three different alleles when genotyping was performed at approximately four months of age (Fig. 25A). A total of 93 adult fish were genotyped and 28 of them were wildtype and the remaining 65 were heterozygous carriers. The ratio of wildtype and heterozygous fish in the absence of

homozygous mutants followed the Mendelian rules. This suggested that all homozygous *gnb3b* mutants had died between 10 dpf and four months of age.

To understand when and why death of homozygous mutants occurs, a batch of *gnb3b*^{del114} F_2 larvae were tracked over a period of one month from the date of birth. A total of 284 larvae were monitored over time and larvae showing signs of weakness, such as minimal movement or abnormal posture were euthanized and genotyped. Between 6 to 20 dpf, a total of 83 homozygous mutant larvae were identified out of the 284, as weak and dying, which reflected approximately 25% of the entire F_2 population analyzed (Fig. 25B). On days 6, 13 and 17, there was a particularly high number of larval death in homozygous mutants while on other days the numbers ranged from two to seven per day (Fig. 25B). Notably, there is an inherent batch to batch variation on the observed numbers for larval death and the time frame at which the homozygous mutants die.

A

Genotype	Type of deletion	Wildtype	Heterozygous	Homozygous
gnb3b^{del114}	7 bp del (CAG)	14	36	-
gnb3b^{del112}	7 bp del (TGG)	9	19	-
gnb3b^{del107}	25 bp del	5	10	-

B

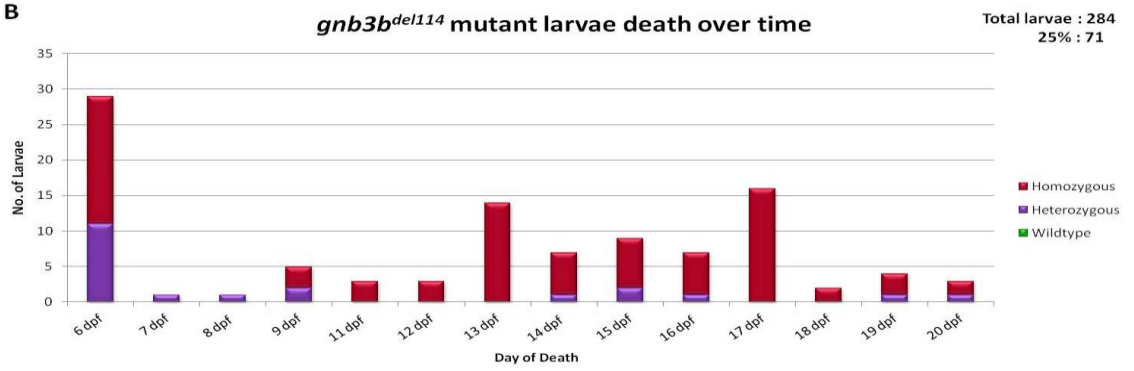

	6 dpf	7 dpf	8 dpf	9 dpf	11 dpf	12 dpf	13 dpf	14 dpf	15 dpf	16 dpf	17 dpf	18 dpf	19 dpf	20 dpf	Total
Wt	0	0	0	0	0	0	0	0	0	0	0	0	0	0	0
+/-	11	1	1	2	0	0	0	1	2	1	0	0	1	1	21
-/-	18	0	0	3	3	3	14	6	7	6	16	2	3	2	83
Total :	29	1	1	5	3	3	14	7	9	7	16	2	4	3	104

Figure 25: Absence of adult homozygous mutants in F_2 generation. A: F_2 adult fish genotyped from all three mutant alleles showed absence of homozygous mutants. B: A batch of 284 *gnb3b*^{del114} F_2 larvae was tracked over a period of one month. Weak and dying larvae were selected and genotyped; progressive death of homozygous mutants occurred over a period of one month. The graph shows the trend in which homozygous larval death progresses over time. The table below the graph provides with the absolute number of larvae genotyped within the F_2 batch.

Over the tracking period, all wildtype larvae developed normally, while some heterozygous carriers were weak on day 6 and one or two larval deaths occurred irregularly. From the data obtained, the homozygous mutants appear to be only capable of surviving for a period of one month. This raised the question whether the large scale death of homozygous *gnb3b*^{del114} mutants was due to a progressive deterioration of vision. This could result in the larvae being unable to scavenge for food, thereby making them weak and consequently lead to their death. To address whether the mutant larvae were visually impaired, a morphological analysis of the mutant retina was carried out.

3.4.3.1. Morphological analysis of *gnb3b* mutant larvae

Cone and rod photoreceptor morphology was analysed in selected *gnb3b*^{del114} homozygous mutant larvae at 20 dpf with overall weak health status. In these larvae, double cone cells were still present and organized in a relatively regular array, comparable to the situation in wildtype siblings (Fig. 26A, B). However, these double cones were much shorter, appeared stunted and lacked properly formed outer segments (Fig. 26B, C', green arrow).

Wildtype double cones normally extended from the pedicle by a ciliary stalk and pan out to form an oval-shaped inner segment with circular outer segment (Fig. 26C). The zpr-1 staining was also concentrated in certain regions, such as the outer segment and the foot pedicle in the wildtype siblings. In contrast, the mutant double cones had a slightly elongated inner segment that formed close to the pedicle foot (Fig. 26C', blue arrow), without a clearly distinguishable outer segment (Fig. 26B, C', yellow and green arrows). The zpr-1 staining was weaker and appeared more diffused throughout the retina.

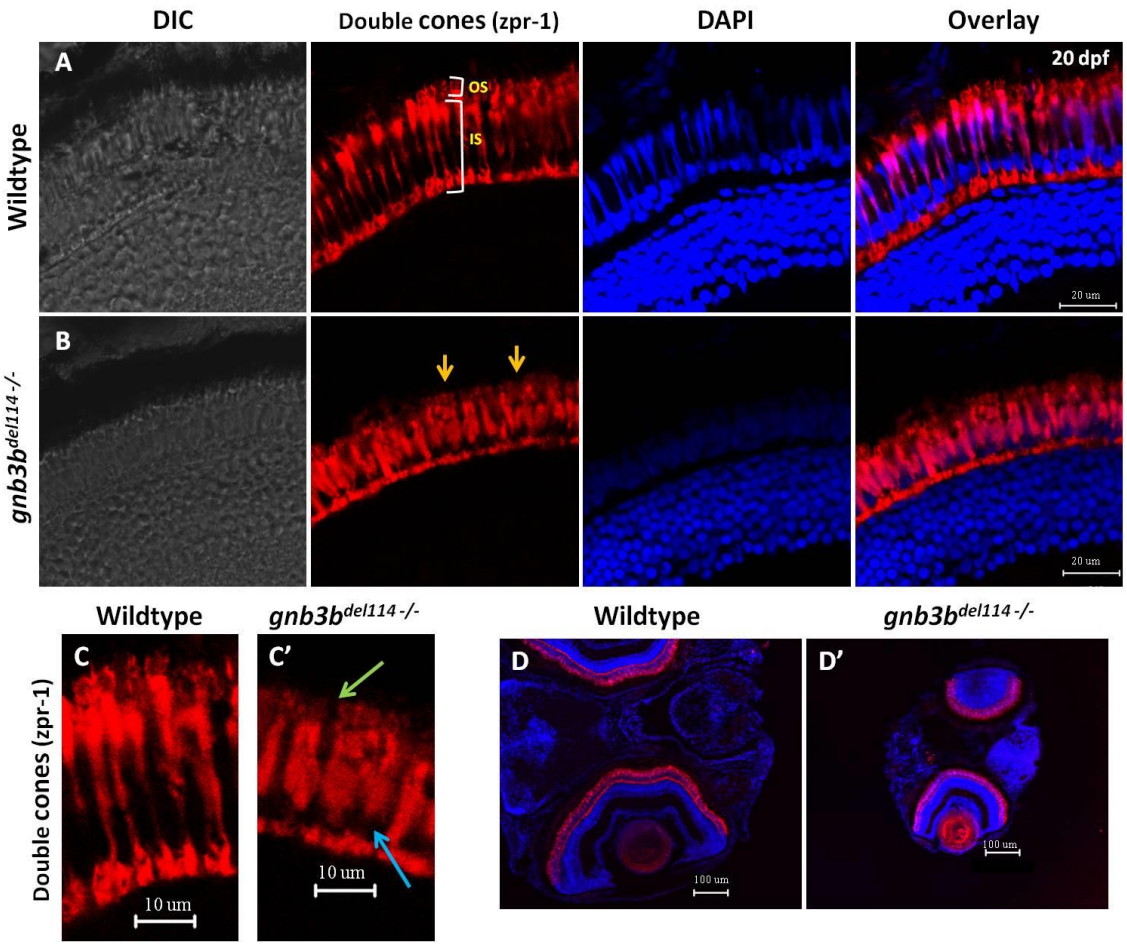

Figure 26: Double cone morphology in 20 dpf *gnb3b*$^{del114-/-}$ mutants. A: Wildtype double cones are elongated with a well structured cell body, organized in a regular array. The inner segment forms a thin stalk from the pedicle which extends out into an oval shaped cell body and a circular outer segment. B: In *gnb3b*$^{del114-/-}$ mutants, double cones are arranged in a regular pattern but appear much smaller and shorter in size. The outer segment is not clearly defined (yellow and green arrows), and zpr-1 staining is weak and more diffused. C and C': A closer view of individual double cone photoreceptors of control and mutant. The inner segment of the mutant forms close to the pedicle and lacks the thin stalk as seen in the wildtype (blue arrow). D and D': Overview image of wildtype and *gnb3b*$^{del114-/-}$ mutant larvae. The mutant retina shows an overall reduction in size when compared to wildtype. Zpr-1 staining is detected consistently throughout the mutant retina.

In addition, the structure of rod photoreceptors was analyzed. Wildtype rod photoreceptors had a distinct outer segment that fanned out above the nuclear layer (Fig. 27A), with weak staining observed in the inner segments (Fig. 27C, blue arrow).

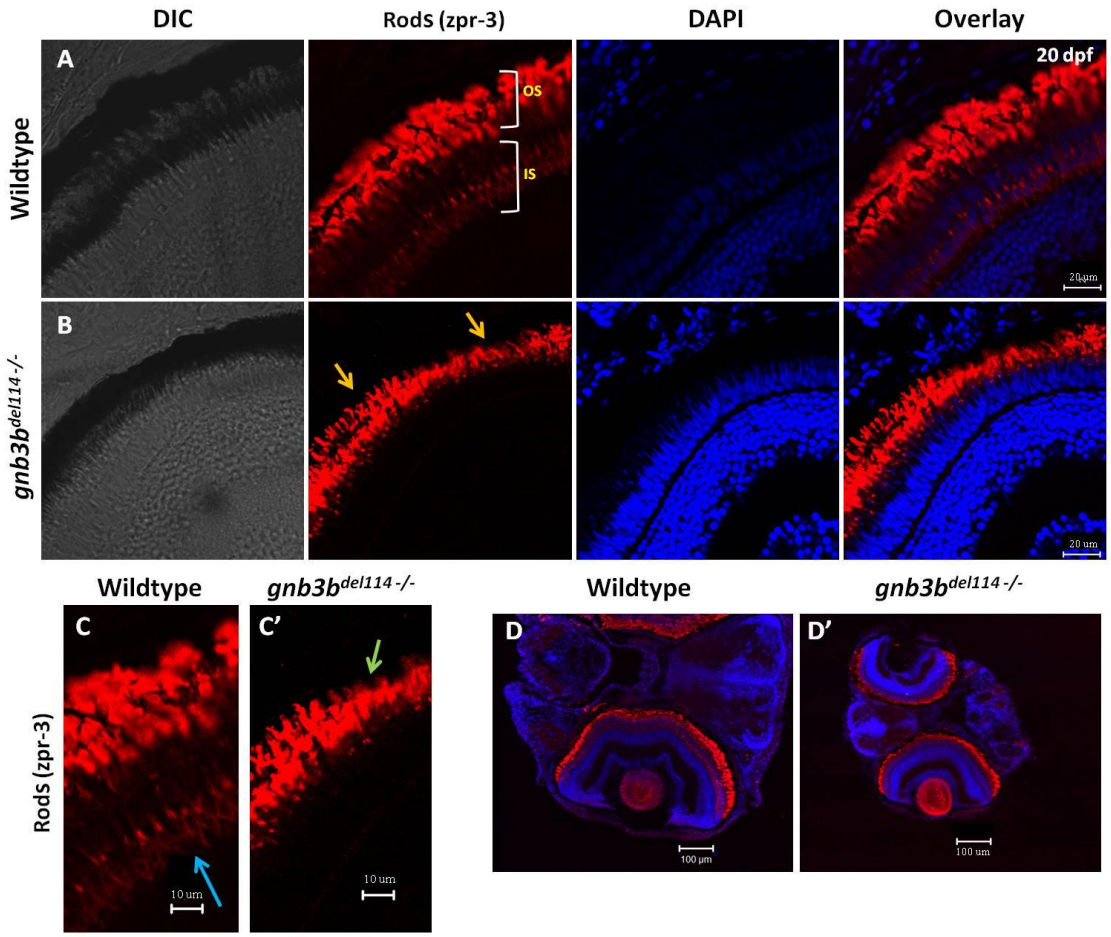

Figure 27: Rods are underdeveloped in *gnb3b*$^{del114-/-}$ mutants at 20 dpf. A: Wildtype rod cells are well developed with a distinctly occurring outer segment that fans out above the inner segment. B: In mutants, the rod outer segments are shorter and do not fan out as widely (yellow arrow). C and C': A closer view of individual rod photoreceptors of control and mutant larvae. In the control, the zpr-1 staining demarcates the inner segment (blue arrow) which is absent in mutants. Additionally, certain regions of the outer segment are shorter and thinner in the mutant (green arrow). D and D': Overview image of wildtype and *gnb3b*$^{del114-/-}$ mutant larvae shows that overall development of the mutant larvae is delayed. Nevertheless, rod photoreceptors, albeit malformed, are formed throughout the mutant retina.

In the mutant, the rod outer segments were shorter and did not fan out as widely and continuously as in control siblings (Fig. 27B, yellow arrows). Zpr-3 staining could not be detected in the inner segment of mutant rods as well (Fig. 27C').

Moreover, the nuclei of both cones and rods were shorter, consistent with the reduced photoreceptor length observed in mutants. The morphology of the mutant double cones and rods is suggestive of either an arrested development of photoreceptors, or to cells possibly undergoing extensive degeneration. Furthermore, an overview image of the larvae showed that

not only the retina, but overall development of the larvae was delayed, as the size of the mutant larval head was at least two times smaller than that of the control (Figs. 26D, D', 27D, D').

As photoreceptors were able to develop in the first ten days (Figs. 22-24), this raised the possibility of an early functional compensation in the homozygous mutants, which could not be maintained at later stages.

3.4.4. Possible gene compensation in *gnb3b*^{del114} mutants by its co-ortholog *gnb3a*

A recent paper by Lagman et al. reports that *gnb3a* is expressed in 3 dpf larvae and adult retinas, albeit at extremely low levels (Lagman et al., 2015). This led the authors to conclude that sub-functionalization of duplicated *gnb3* genes occurred in the retina. Based on their data, I speculate that upon *gnb3b* deficiency, *gnb3a* could potentially compensate for a loss of *gnb3b* function.

To test this hypothesis, RNAs from homozygous *gnb3b*^{del114} mutants and wildtype siblings were isolated at 3 dpf and reverse transcribed into cDNA (performed in three biological and technical replicates with six larval heads each, per sample type). The *gnb3a* expression levels were determined by PCR and quantified using ImageJ with *β-actin* used as loading control (Fig. 28A).

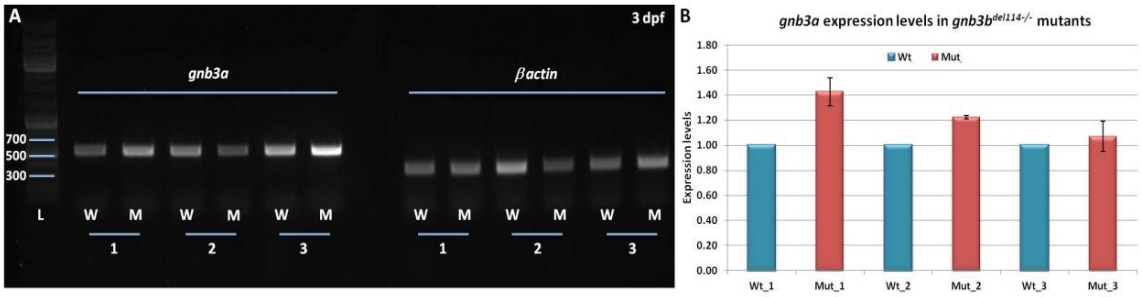

Figure 28: Expression analysis of *gnb3a* in *gnb3b* mutants at 3 dpf using semi-quantitative RT-PCR. A: Representative gel image depicting PCR amplicons of three independent sample sets. *β-actin* was used as loading control and for normalization. B: Average expression levels of *gnb3a* in *gnb3b*^{del114} mutants, quantified by ImageJ. On average, homozygous mutants expressed 20% more *gnb3a* transcripts than controls. N = 18.

In homozygous mutants, *gnb3a* expression was increased by approximately 20% on average when compared to wildtype, though this increase was not found to be statistically significant (Fig. 28B). The observed difference suggests a possible compensation by *gnb3a* early in mutant larvae. However, this increase in *gnb3a* appears to be not sufficient for the survival of *gnb3b*^{del114} mutant larvae into adults.

3.4.5. Adult *gnb3b* heterozygous mutant photoreceptors show irregularities and reduced cGMP concentration

The morphology of photoreceptors of 6 months old *gnb3b* heterozygous carriers was analyzed. This was to determine whether the minor larval morphological deficits observed in heterozygous carriers were still present at later stages. The double cones in adults form a characteristic 'V' shaped body with a circular outer segment that has extending filaments (Fig. 29A). As they develop, they tend to be positioned in close proximity to neighbouring cells to form the typical double cone pair structure with its characteristic morphology (Branchek and Bremiller, 1984). A thin stalk connects the cell body to the foot pedicle. In heterozygous carriers, the double cone organization appeared comparable to wildtype (Fig. 29A'). Additionally, some cells were seen to be missing parts of their outer segment, and in some cases there was a slight aberrance in the cell body (Fig. 29A', yellow arrows). The heterozygous rod cells did not show a distinguishable difference when compared to wildtype (Fig. 29B, B'). In both, the outer segments spanned out above the inner segments and were well developed. As zpr-3 staining does not label the cell body, it was not clear if there was any difference in rod cell numbers and length of the outer segment between carriers and wildtype.

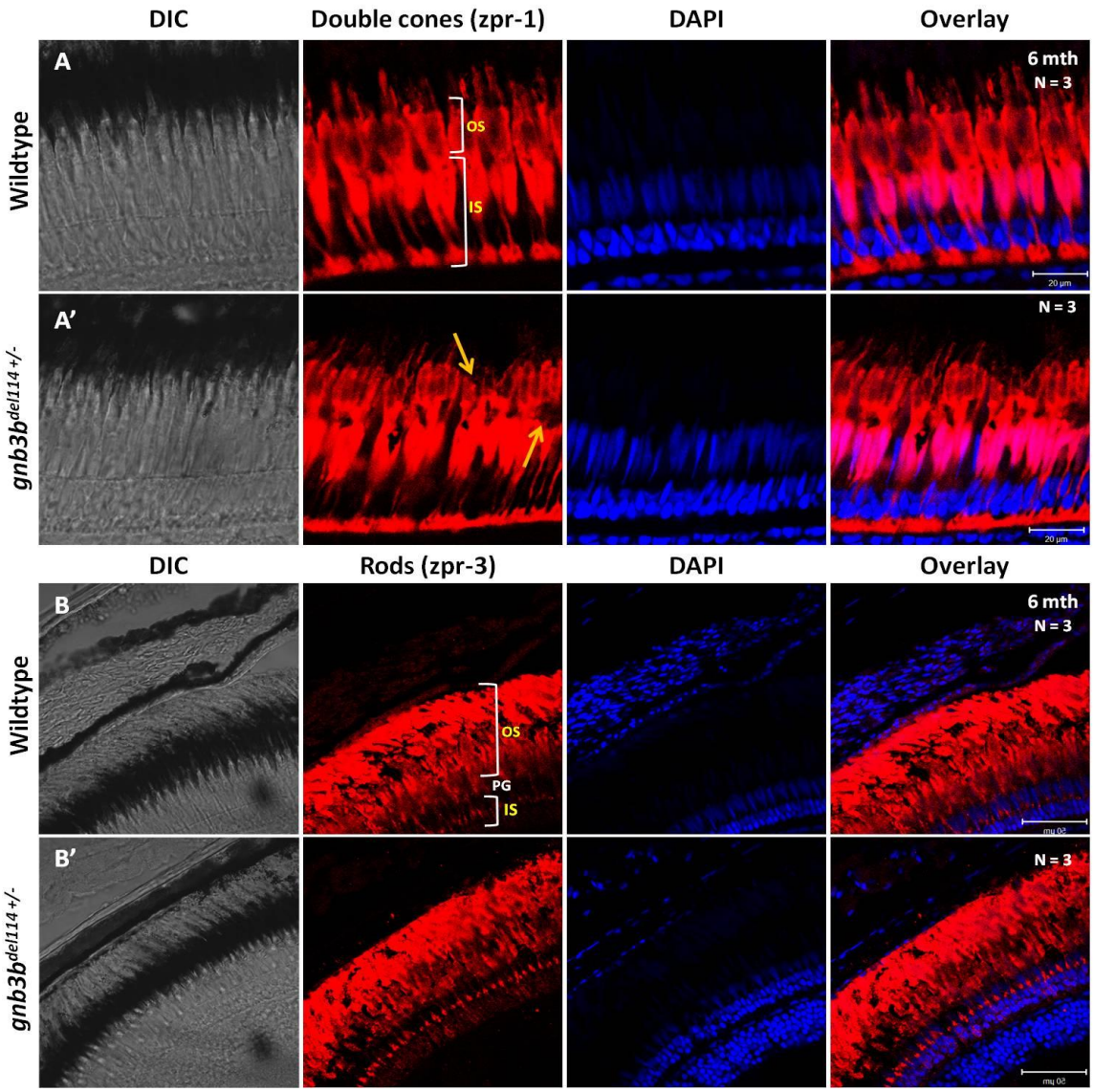

Figure 29: Morphological analysis of double cones and rods in heterozygous adult *gnb3b*$^{del114+/-}$ carriers. A: The wildtype double cones have a circular outer segment with filament-like extensions and a characteristic 'V' shaped inner segment. A thin stalk connects the cell body to the foot pedicle. A': The heterozygous double cones are organized similarly to the controls, although some cells partially lack their outer segments and have slight distortions of the inner segments (yellow arrows). B, B': No obvious difference in rod cell outer segment morphology is visible in *gnb3b*$^{del114+/-}$ carriers and controls. OS: outer segment, IS: inner segment, PG: pigment granules; n = 3 for controls and 3 for mutants; Scale bar = 20 µm for double cones and 50 µm for rods.

Additionally, the retina from 7 months old heterozygous carriers was used for determining cGMP concentrations. This assay was performed to gain insight into whether the anomalous photoreceptors were still functional. Retinas from four independent fish were isolated and extracts were prepared. The cGMP concentration was quantified using a competitive ELISA

assay. Each experiment was performed with two fish (per genotype) at a time, and the cGMP levels were measured in duplicates. cGMP extracted from samples 1 and 2 were prepared with the addition of a phospho-diesterase inhibitor, 3-isobutyl-1-methylxanthine (IBMX). This inhibitor was not added to samples 3 and 4 for comparison.

Using the given cGMP standard provided by the kit, a standard curve was plotted with the four-parameter logistic equation, and the cGMP concentration in the samples was calculated using the Hill equation (Fig. 30A). The table describes the average absorbance and the calculated cGMP concentrations, the ratio between controls and heterozygous carriers was determined (Fig. 30B).

A

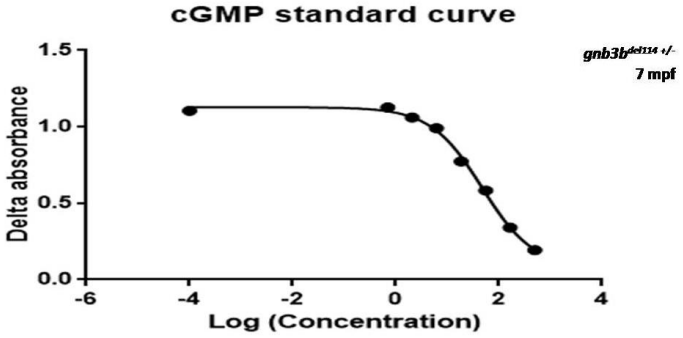

B

Genotype	Wt 1	Wt 2	+/- 1	+/- 2	Wt 3	Wt 4	+/- 3	+/- 4
Avg. Absorbance	0.745	0.773	0.811	0.877	1.130	1.095	1.157	1.197
cGMP Conc. (ug/ml)	24.923	21.782	17.965	12.433	6.121	7.009	5.489	4.620
Ratio between expt. sets	1 : 0.65				1 : 0.77			

* Sample 1 and 2 – prepared with IBMX, Sample 3 and 4 – prepared without IBMX

Figure 30: Quantification of cGMP concentrations in retinas of 7 months old *gnb3b* heterozygous carriers. Four independent fish per genotype were used for quantification of cGMP levels. A: Standard curve plotted using the four-parameter logistic equation with absorbance values from prepared cGMP standards. B: The absolute cGMP concentrations of experimental samples were calculated using the Hill equation. Values for average absorbance and concentration measured for four individual wildtype and heterozygous samples are shown. Heterozygous carriers had a 23 - 35% reduction in the level of cGMP compared to wildtype. P value calculated using unpaired t-test = 0.44. IBMX (3-isobutyl-1-methylxanthine): phospho-diesterase inhibitor.

Due to a partial loss of *gnb3b*, it was postulated that the overall phototransduction activity will be compromised in the heterozygous carriers and thus, a reduction in cGMP levels was expected. The eight fish tested had varying amounts of cGMP concentrations, but showed an average of 23 - 35% reduction in cGMP levels in the heterozygous carriers. A student T-test

analysis revealed that the observed difference was not statistically significant given a p value of > 0.05.

3.4.6. Summary of the functional analysis for *gnb3b*

Morphological analysis of *gnb3b* morphant retinas at 4 dpf revealed that double cone and red cone photoreceptors were severely affected. Cone outer segments were improperly formed and showed irregular sizes and shapes. Some double cone cells also showed defects in the inner segments and some cone cells were completely missing. On the other hand, the rod photoreceptor morphology appeared unaffected and comparable to that of wildtype controls.

In CRISPR/Cas9 generated *gnb3b*^{del114} mutants, I could show that homozygous mutants do not survive into adulthood, with larvae progressively dying over a period of one month from the date of birth. Histological analysis of homozygous mutant larval retinas at 10 dpf revealed that UV and double cones were aberrantly formed, with largely missing outer segments and shorter inner segments. Rod photoreceptors appeared to have a developmental delay, showing reduced expansion of the outer segments. Expression analysis of its co-ortholog *gnb3a* revealed a slight up-regulation in larval *gnb3b* homozygous mutants suggesting a potential functional compensation.

In adult heterozygous carriers, double cones showed minor morphological anomalies in their outer segments, while no discernible differences were detected in rods. Determining cGMP levels revealed a reduction in the retinas of heterozygous carriers, albeit below significance thresholds.

3.5. A functional analysis of *guk1b* in the zebrafish retina

A previous study using MO knock-down had shown that down-regulation of *guk1b* leads to rod photoreceptor degeneration and disintegration of the pigment epithelium resulting in intra-retinal pigment deposition (Brocher et al., unpublished). Both features are typical hallmarks of a human RP phenotype suggesting that *guk1b* is a potentially interesting RP candidate gene. Therefore, I generated *guk1b* mutant zebrafish for a more detailed functional characterization.

3.5.1. Establishment of *guk1b* mutant zebrafish using the CRISPR/Cas9 system

A similar methodology as described above was used to generate *guk1b* mutant zebrafish lines. Briefly, the target site was selected to be in exon 7 using the ZiFit Targeter version 4.2 program (Fig. 31A). Following annealing and phosphorylation of guide oligos, they were cloned into the vector pDR274, sequenced and the gRNA was *in vitro* transcribed. gRNA and Cas9 mRNA were co-injected at a concentration of 50 ng/µl and 300 ng/µl, respectively, into one-cell stage embryos. Injected embryos were initially screened by RFLP assay for introduced mutations using the BsrI restriction enzyme. At 24 hpf, individual embryos were screened, and selected PCR amplicons were cloned and sequenced. This showed that the majority of mutations were deletions ranging from 3 to 21 bp in length (Fig. 31B). Once it was confirmed that the designed gRNA was effective in introducing mutations, multiple rounds of injections were performed and injected embryos were raised. At 3 months of age, the injected fish were genotyped by fin-clipping. Fin positive fish were considered as potential founders and incrossed. A total of 65 injected adult fish were genotyped and 25 of them were fin positive for mutations. Initially, six pairs of potential founders were incrossed and F_1 larvae were analysed for germline transmission of mutations. All six pairs were identified to transmit the mutation to the next generation, yielding a 100% germline transmission rate. A total of 238 F_1 embryos from all six F_0 pairs were screened and 42 individual embryos were identified to be positive for mutations (Fig. 31C). This gives an F_1 efficacy rate of 17.6%.

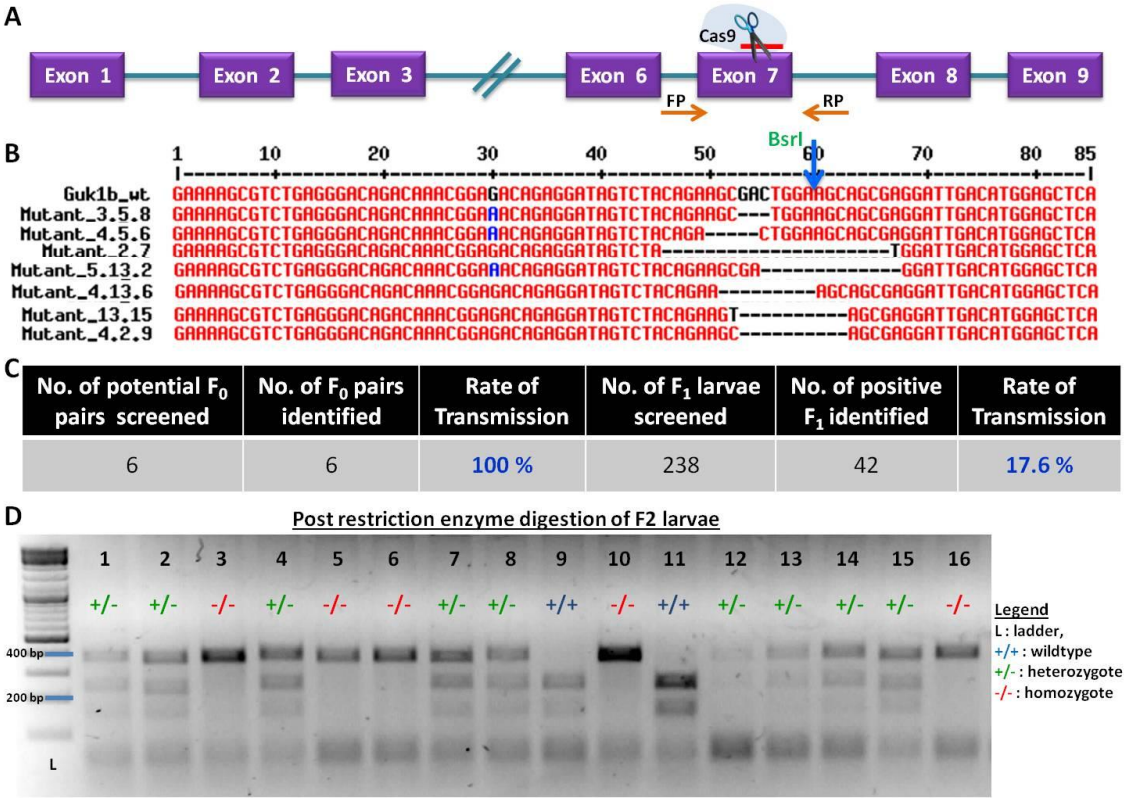

Figure 31: Schematic diagram depicting the exon selected for introduction of mutations and quantification of CRISPR/Cas9 efficacy. A: *guk1b* has a total of nine exons with eight coding exons. Based on the suitability and requirements for efficient CRISPR/Cas9 gRNA, a target site in exon 7 was chosen. Primers were designed to flank exon 7 for screening of mutants. B: Sequencing of F_0 clones revealed deletion mutations as the most commonly introduced type of changes in *guk1b*. The deletions ranged from 3 to 21 bp with a 10 and 13 bp deletion (as shown in Mutant_4.2.9, 5.13.2) occurring repetitively. C: The efficiency of mutagenesis was determined at the F_0 and F_1 level. Six potential founder pairs were incrossed and all six of them had germline transmission yielding 100% efficiency. Of the 238 F_1 larvae screened from all six founders, 42 of them had mutations, thereby giving an F_1 efficacy of 17.6%. D: Representative gel image of 4 dpf F_2 larval RFLP screen using BsrI (cutting site is shown by blue arrow in A). The *guk1b* PCR amplicon of wildtype larvae was completely digested. Heterozygous carriers were identified by partially digested PCR products (three bands) and homozygous mutants had one undigested band. FP: forward primers, RP: reverse primers.

Of the various types of deletions, a 10 and 13 bp deletion occurred rather frequently. F_1 progeny from 5 out of the 6 F_0 pairs screened carried the 10 bp deletion (hereafter *guk1b*^{del174}) while two of the founders carried the 13 bp deletion (hereafter *guk1b*^{del175}). In parallel, some embryos from these founders also carried other types of deletions but at lower frequency. F_1 fish carrying these two alleles were selected for establishment of stable *guk1b* mutant lines.

F_1 larvae were subsequently raised into adulthood, screened for mutations and segregated according to their genotype. F_1 fish carrying the same 10 and 13 bp deletions were incrossed respectively, to produce F_2 progeny with wildtype, heterozygous and homozygous *guk1b* background. The designed *guk1b* PCR amplicon was 398 bp long and spanned the target region. Upon complete digestion of the PCR amplicon with BsrI, the product will be fragmented into two bands of 148 and 250 bp, respectively. Wildtype larvae will show these two bands while heterozygous *guk1b* carriers will only be partially digested and have three bands (undigested full length band and two digested fragments). The PCR product of homozygous mutants remained undigested (Fig. 31D). Screening of F_2 larvae showed that the inheritance of the mutations occurred in accordance to Mendel's laws, with 25% of the larvae being wildtype or homozygous mutants and the remaining 50% being heterozygous for the mutation in *guk1b*.

Having selected two different alleles for the generation of stable *guk1b* mutant lines, the protein sequence was analyzed. In the case of the 10 bp deletion (*guk1b*^{del174}), the protein sequence was in sync with wildtype sequence up to amino acid 173. The 13 bp deletion line (*guk1b*^{del175}) was in frame up to 174 amino acids (Fig. 32A). Both lines had altered amino acid sequences beyond these points and the proteins were deduced to be truncated at position 190 for *guk1b*^{del174} and 189 for *guk1b*^{del175}, with the introduction of a premature stop codon. The diagram in Figure 32B portrays the full length and presumed mutant Guk1b protein structure. The full length Guk1b protein is 223 amino acids long with the conserved guanylate kinase domain spanning from amino acid position 3 to 215. In mutants, the amino acid sequence is expected to be intact only for the first 174 amino acids, resulting in the partial loss of the guanylate kinase domain.

The 3D structures of wildtype and mutant Guk1b protein were modelled using SWISS-MODEL and Swiss PdbViewer (Fig. 32C). Based on the available mouse guanylate kinase structure, the Guk1 protein is folded into three distinct parts: the CORE, the NMP-binding region and the LID domain (Sekulic et al., 2002). When ATP and GMP bind to guanylate kinase, structural

conformational changes lead to the LID and NMP binding-regions to come into close proximity to the CORE region, forming a compact structure. This assists in the catalytic activation and production of ADP and GDP.

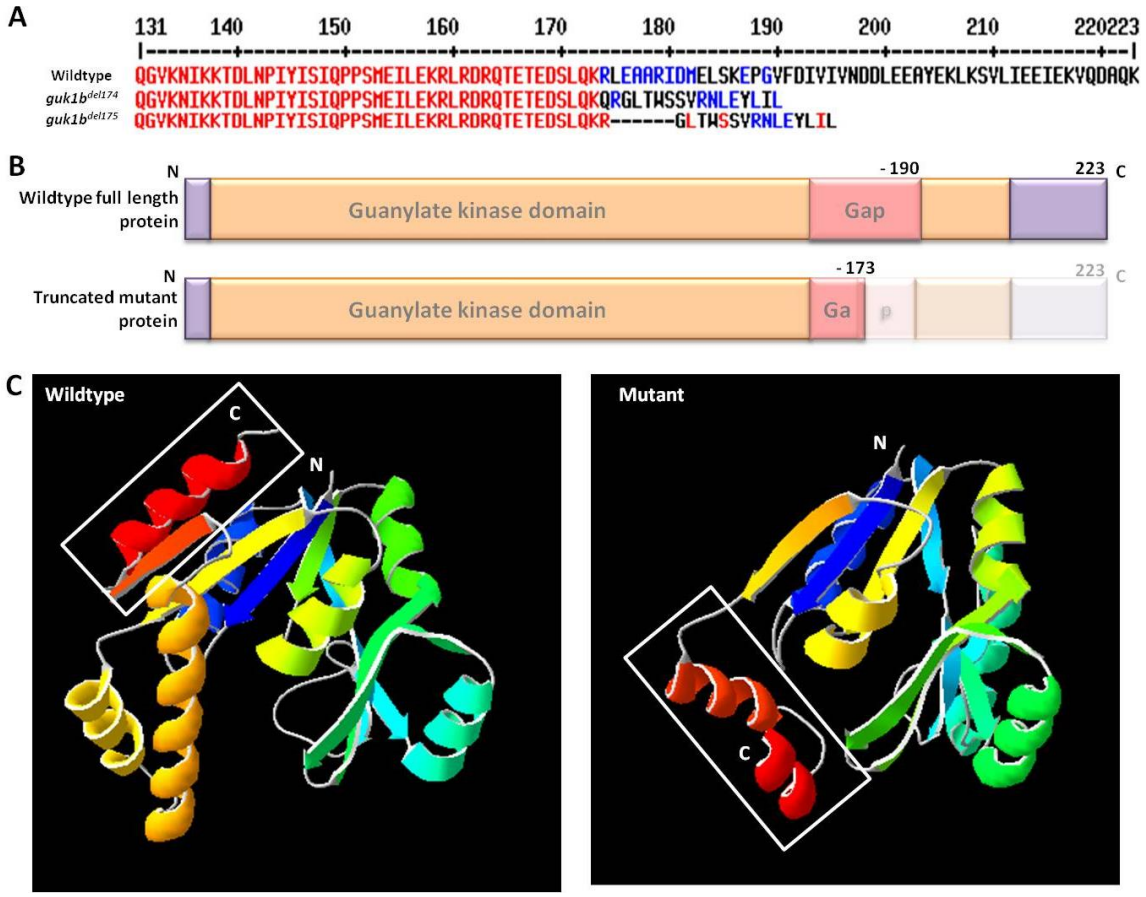

Figure 32: Protein sequence analysis and 3D modelling of the deduced mutant Guk1b protein. A: Two different alleles were selected for establishing stable mutant lines for *guk1b*. One carried a 10 bp deletion and the other a 13 bp deletion, which lead to a premature stop of translation and hence protein truncation. The first 173 amino acids are retained in the *guk1b*^{del174} mutant protein after which the sequence gets altered and truncates at amino acid position 190. The second *guk1b*^{del175} line has 174 amino acids in frame after which the sequence is shortly altered and gets truncated at position 189. B: Schematic diagram depicting domains in full length and mutant Guk1b protein. The wildtype protein is 223 amino acids long and introduction of mutation is expected to result in a truncated protein of about 190 amino acids. The conserved guanylate kinase domain extends from the N-terminus to the C-terminus. Therefore in the *guk1b* mutants, part of the functional domain is predicted to be lost. C: Modelling of wildtype (left) and mutant Guk1b protein (right) using SWISS-MODEL. As the mutation occurs towards the end of the protein, a partial loss of the β-sheet or conversion of the terminal β-sheet to an α-helix near the C-terminus appears likely (white rectangle). N: N-terminus, C: C-terminus.

Based on the predicted 3D protein structure, it is possible that in the mutants, when compared to wildtype protein structure, either the β-sheet near the C-terminus is lost or the β-sheet is

converted into an α-helix due to the frameshift that altered the amino acid sequence (Fig. 32C, white rectangle). In both cases, a significant conformational change is expected to occur in the mutated Guk1b protein. In *guk1b* mutants, the alteration in the amino acid sequence occurs within the predicted CORE region of the guanylate kinase domain. The photoreceptor morphology was therefore analysed, to determine the effect of the introduced mutations.

3.5.2. Aberrant cone and rod morphology in *guk1b* mutants

Once the mutant lines were established, a morphological analysis was carried out at larval (4 dpf) and adult (between 6 to 7 months) stages. Morphological data were obtained from mutants with a 10 bp deletion (*guk1b*$^{del174-/-}$). All samples were cryo-sectioned prior to immunohistochemistry or directly imaged for fluorescence.

3.5.2.1. UV cones are disrupted in *guk1b*$^{del174-/-}$ mutants

First, UV cone photoreceptors were analysed by direct imaging in transgenic reporter lines where EGFP expression is driven by the *SWS1* promoter. This line was established by outcrossing the mutant founders with the transgenic reporter line *Tg (SWS1:EGFP)*.

The UV cone cells of *guk1b*$^{del174-/-}$ larval mutants exhibited various morphologies. In controls, UV cones are tightly packed and arranged in a continuous array (Fig. 33A, B). In mutants in contrast, the UV cells were more loosely arranged, and sometimes cells appeared to be missing (Fig. 33A, C, pink arrow). They lacked the typical structure of UV cells, which is a triangular shaped outer segment and an hour-glass shaped inner segment, as seen in control cells (Fig. 33B). Most UV cones did not have a properly formed outer segment and had a rectangular cell body (Fig. 33C, yellow arrow). There were also UV cones, which were strongly reduced in size with almost half of the cell missing. On the other hand, there were some UV cones in mutants that looked comparable to those in controls. The level of EGFP expression was slightly reduced in mutants as well suggesting reduced *SWS1* reporter activity.

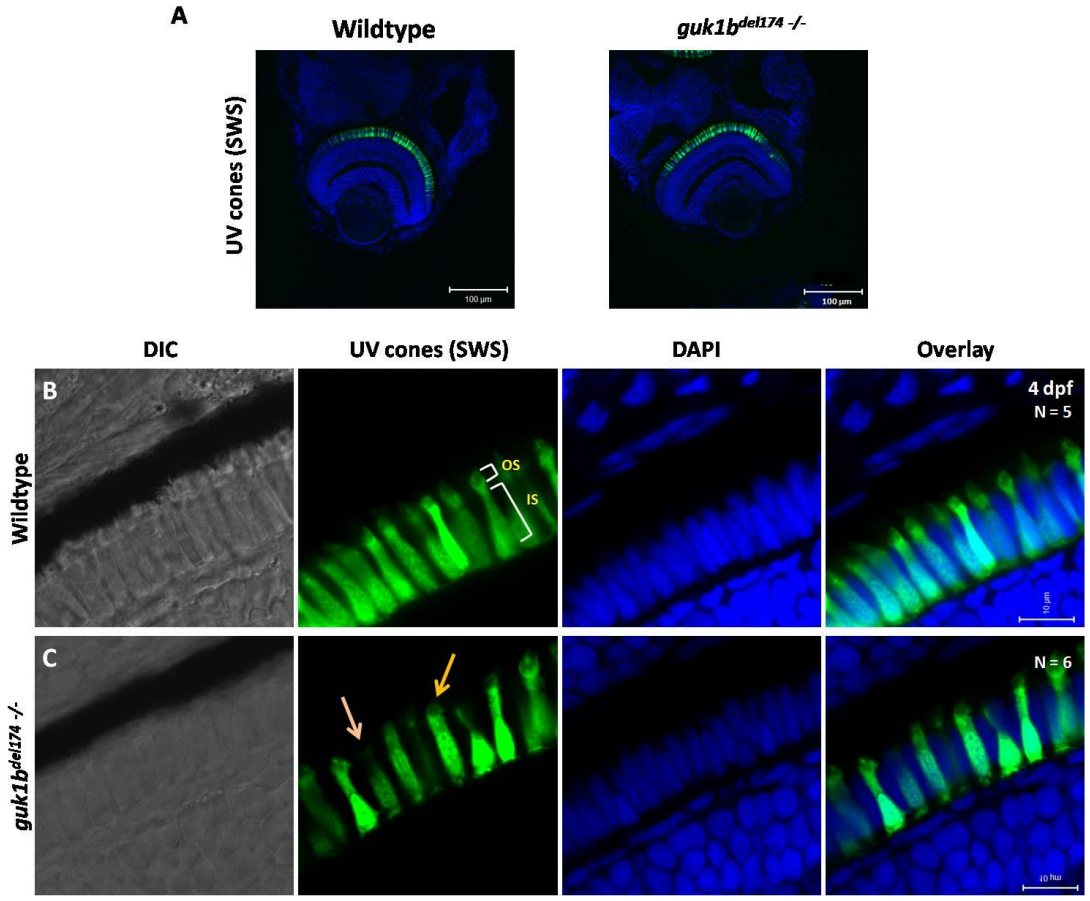

Figure 33: Aberrant UV cone photoreceptor morphology in *guk1b*$^{del174-/-}$ mutants at 4 dpf. A: Overview images of the wildtype and mutant larval retina. B: Control larval retina with UV cone structure defined as 'triangular' cone outer segment and elongated 'jug-shaped' inner segment, arranged in a regular array. C: Typical UV cone features were found to be disrupted in *guk1b*$^{del174-/-}$ mutants. Most cells lacked a clear outer segment (yellow arrow) and the cell bodies appeared rectangular instead of curved. In addition, the UV cones were more loosely arranged with gaps (pink arrow). OS: outer segment, IS: inner segment; n = 5 for wildtype and 6 for mutant; Scale bar = 100 µm for overview images and 10 µm for B-C.

Next, the morphology of the retina was analysed in adult mutants. In controls, the outer and inner segments of UV cones had a defined oblong shape with a thin stalk extending to form a pedicle at the base, on top of the inner nuclear layer (Fig. 34A). *guk1b*$^{del174-/-}$ mutants, on the other hand, appeared to have an irregular arrangement of outer and inner segments (Fig. 34B). The expression of EGFP was also slightly reduced in adult *guk1b*$^{del174-/-}$ mutants, which allowed for the distinct constriction in the middle of UV cells to be seen. This constriction is not obvious in controls. Therefore, the mutant UV cones appeared with a more triangular outer segment and a circular or triangular cell body (Fig. 34B). The extending stalks and pedicles at the base of UV

cells were intact in mutants. There were some UV cells which were shorter and thinner with parts of the outer segment absent (Fig. 34B, yellow arrow). Gaps, indicating missing cells, were present in the adult mutant retina (pink arrow).

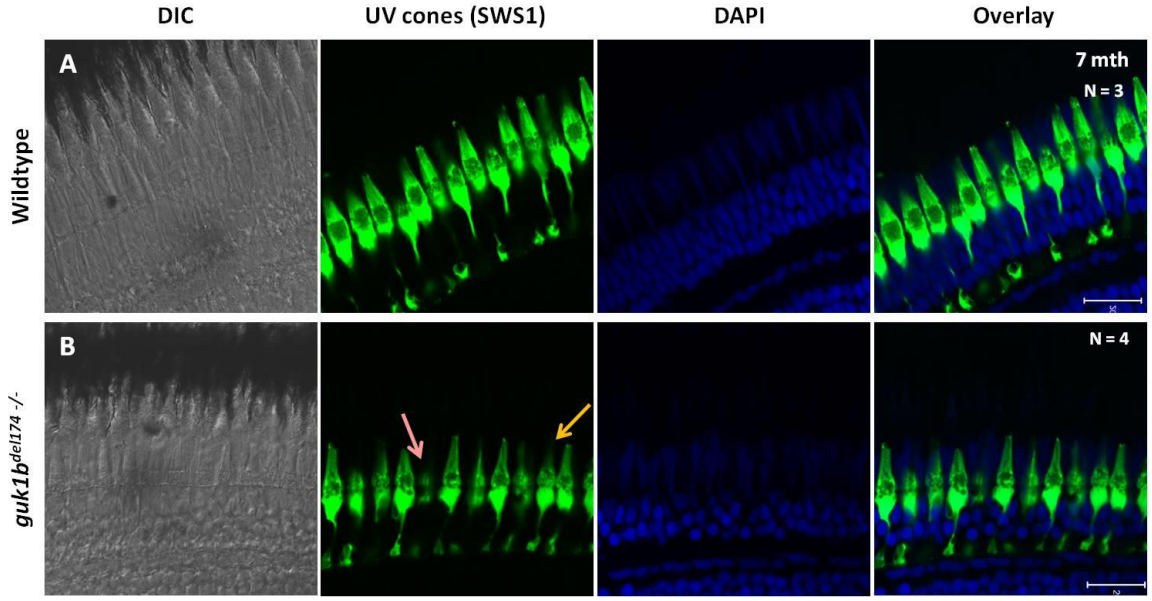

Figure 34: Abnormal morphology of UV cones in adult mutant retinas. A: Wildtype adult UV cones are seen with an oblong shaped cell body with a thin stalk connecting to the pedicle base organized in a regular array. B: *guk1b*$^{del174-/-}$ mutant UV cones partially mimicked the wildtype morphology. In the middle of the UV cone cell body, a defined constriction was observed due to weaker EGFP signal that reveals a thin narrow 'triangular' outer segment and a 'triangle' shaped lower half in the mutant. Some EGFP positive cells were missing the outer segment tip (yellow arrow) and had a more curved lower half. Areas lacking UV cones were also evident in mutants (pink arrow). N = 3 for wildtype and 4 for mutant; Scale bar = 20 µm.

3.5.2.2. Double cone cells are malformed in *guk1b*$^{del174-/-}$ mutants

Double cones of wildtype and mutant retinas were labelled by zpr-1 antibody staining. Four days old control larvae showed a regular array of cells with a short outer segment and an elongated cell body, though individual cells had slight variations in their morphology. The general morphology observed was an oval shaped cell body that constricted closer to the basal end before panning out to form a pedicle base (Fig. 35A, B).

Double cones of *guk1b*$^{del174-/-}$ mutants generally lacked an outer segment and some cells were shorter than their neighbours (Fig. 35A, C, yellow arrow). Most of the mutant cells followed a

structure of a rectangular cell body with a less discernible constriction at the posterior end (Fig. 35C, green arrow). The pedicle foot at the base, however, was still intact (Fig. 35C, blue arrow). In wildtype controls, the double cone cells were slightly spaced apart rather than tightly packed. In mutants, this spacing was even wider and several double cones were only weakly stained (Fig. 35A, right panel).

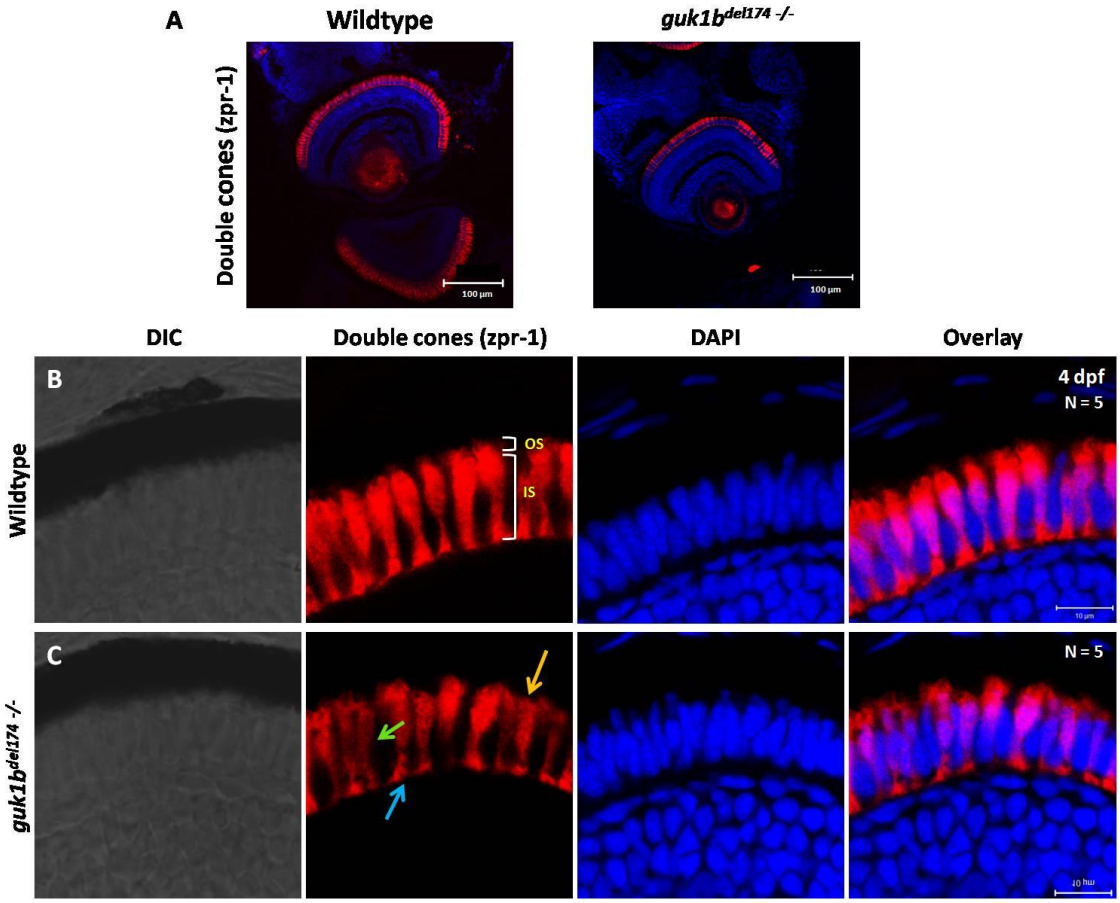

Figure 35: Four days old *guk1b*$^{del174-/-}$ mutant larvae have irregularly shaped double cones. A: The overview image of the larval retina shows that double cones are not properly formed. B: In wildtype controls, double cones have a short outer segment and a long inner segment with a constriction towards the base of the cell. C: In *guk1b*$^{del174-/-}$ mutants, some cells were missing the outer segment (yellow) and the inner cell bodies appeared shorter and thinner than in controls (green arrow). The pedicle foot remained intact in all cells (blue arrow) but generally the zpr-1 staining throughout the double cone layers was weaker. OS: outer segment, IS: inner segment; n = 5; Scale bar = 100 µm for overview images and 10 µm for B-C.

The double cones of wildtype adult retinas are seen with an almost circular outer segment with filament-like protrusions and a 'V' shaped inner segment (Fig. 36A). Continuous to the cell body, a thin filament-like stalk connects the cell body to the foot pedicle. In contrast, *guk1b*$^{del174-/-}$

mutants are missing the distinct circular outer segment, and instead have a more elongated and oval-shaped outer segment (Fig. 36B, yellow arrow). The inner segment of the mutant cones have a wider top and a constricted bottom, which varied from cell to cell and differed from the typical 'V' shaped cell body observed in controls.

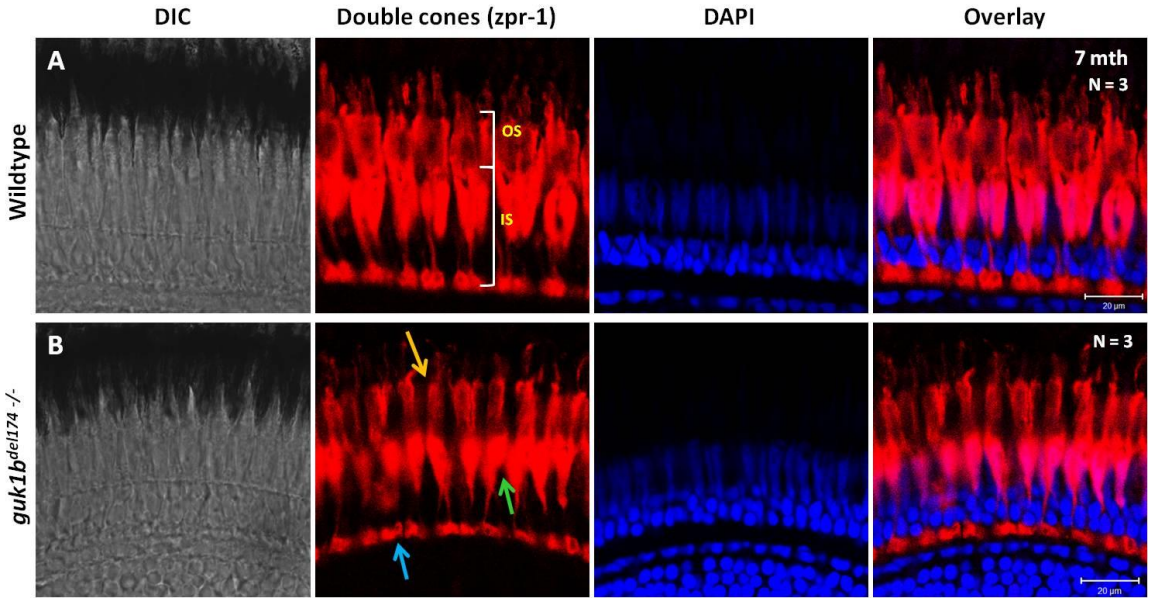

Figure 36: Double cones show structural anomalies in adult *guk1b*$^{del174-/-}$ mutants. A: Wildtype double cones have a circular outer segment with filament like projections. The inner segments form a 'V' shaped body with neighbouring cells in close proximity thus forming the characteristic double cone pair structure. A thin stalk connects the cell body to the foot of the cell. B: Mutant cones have a more elongated outer segment with intact filamentous projections (yellow arrow). The inner segments have varied and distorted shapes across the retina (green arrow). The pedicles of the double cones were thinner (blue arrow) than in wildtype. OS: outer segment, IS: inner segment; n = 3; Scale bar = 20 µm.

In *guk1b*$^{del174-/-}$ mutants, the neighbouring cells were spaced apart from one another, and this could be attributed to the more oval than 'V' shaped cell body (Fig. 36B, green arrow). Finally, the pedicles of two cells were not as closely positioned as in the wildtype, where this is a typical feature of double cones existing in pairs (Fig. 36A, B, blue arrow).

3.5.2.3. Analysis of rods cells in *guk1b*$^{del174-/-}$ mutants

Apart from cones, rod cell morphology was also examined by immunostaining with zpr-3, which labels rod and double cone outer segments. At larval stages, morphological changes were

indiscernible between controls and mutants (Fig. 37A). The outer segments were strongly stained and had an indistinguishable morphology across different cells (Fig. 37B, C, yellow arrows). A thin line of labelling was seen at the base of rod photoreceptors for both controls and mutants. Some cells had their inner segments and cell membranes labelled as well.

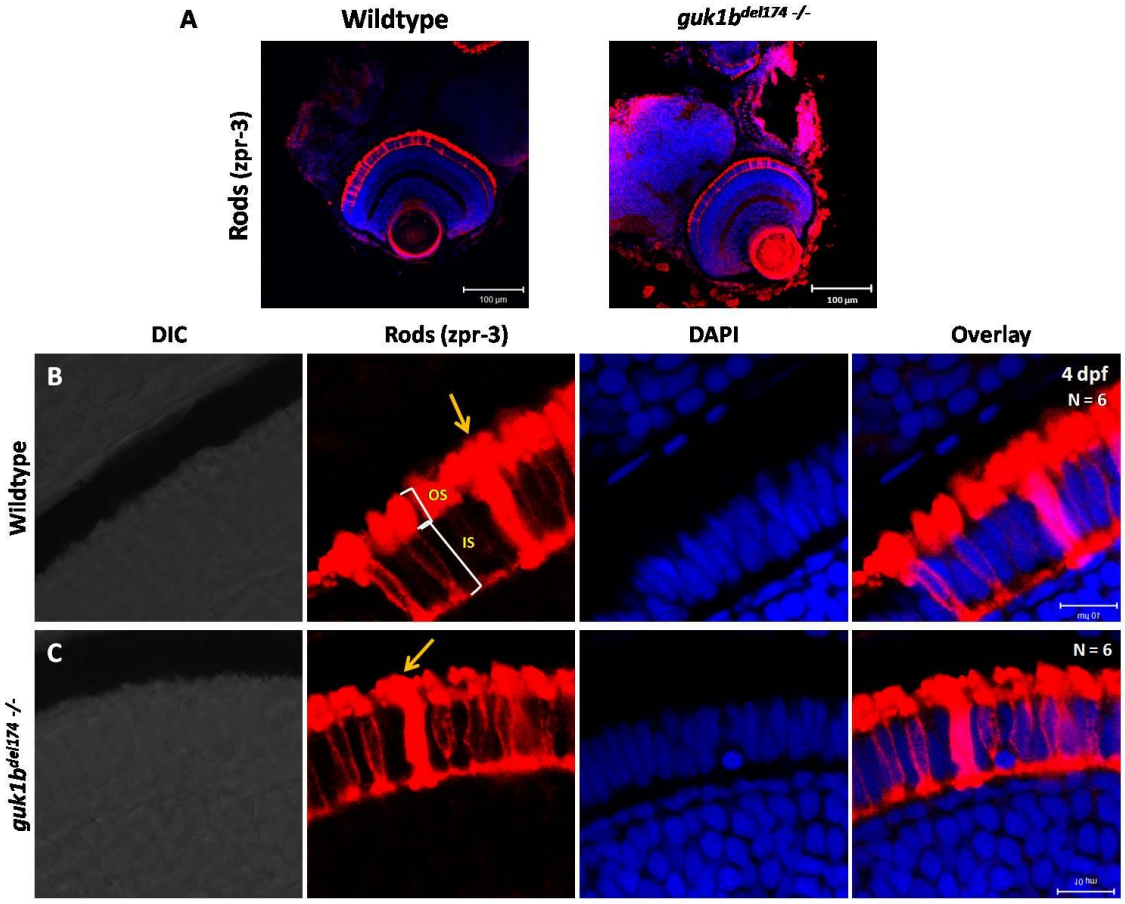

Figure 37: Rods of *guk1b*$^{del174-/-}$ mutant larvae have a comparable structure as in wildtype. A: Overview images of larval retina showed comparable rod morphology between wildtype and mutants. B: The zpr-3 antibody labels the outer segments of rods (and double cones) and demarcates the cell body with a thin outline. C: The *guk1b*$^{del174-/-}$ mutant rods are similarly labelled as in wildtype and appear unaffected. The outer segments are of equivalent size (yellow arrow) and labelled with similar intensity. OS: outer segment, IS: inner segment; n = 6; Scale bar = 100 µm for overview images and 10 µm for B-C.

When the adult retina was immunolabeled with zpr-3, no obvious differences in the morphology was detected between mutants and controls (Fig. 38A, B).

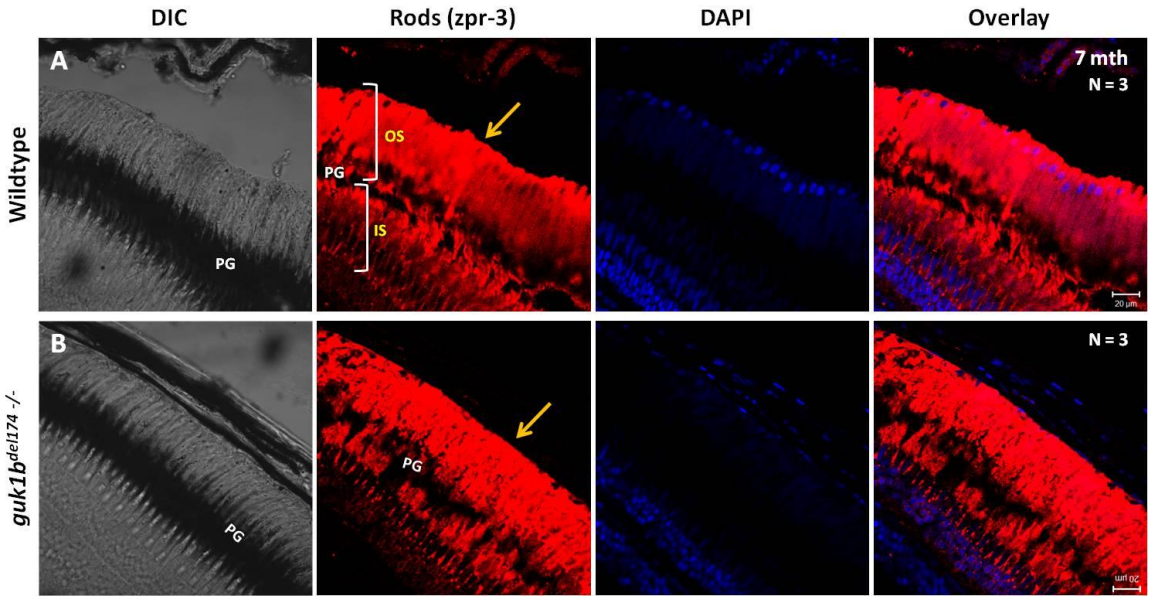

Figure 38: Rod morphology in the adult and *guk1b*$^{del174-/-}$ mutant retina after zpr-3 staining. A: The filamentous rod outer segments extended beyond the pigment granules (PG) layer of the retina and the inner segments are partially labelled by zpr-3. B: The rod outer segments in *guk1b*$^{del174-/-}$ mutants are of similar length to that of wildtype (yellow arrow). A clear difference in the rod cell morphology was not observed in the mutants. OS: outer segment, IS: inner segment; n = 3; Scale bar = 20 µm.

The outer segments of rod cells appeared filamentous and extended beyond the pigment granules (PG) layer with properly aligned inner cell bodies below the PG layer. The outer segments of *guk1b*$^{del174-/-}$ and control rods had approximately equal length and were stained with comparable intensity (Fig. 38, yellow arrows). The zpr-3 marker does not delineate individual cell bodies of rods and cones. Therefore, differences in cell numbers could not be detected. Hence, a mutant line in the background of *Tg (Rho:EGFP)* was used for further analysis of the adult retina. The mutant founders were outcrossed to the transgenic reporter line *Tg (Rho:EGFP)*. In this line, EGFP is expressed under control of the *Rho* promoter and labels individual rod cell bodies and outer segments. Due to a delay in EGFP expression in larvae, this line was only used for analysis of the rod morphology in adults.

In this reporter background, wildtype rod outer segments appeared well elongated and compactly packed, with the inner segments regularly arranged (Fig. 39A).

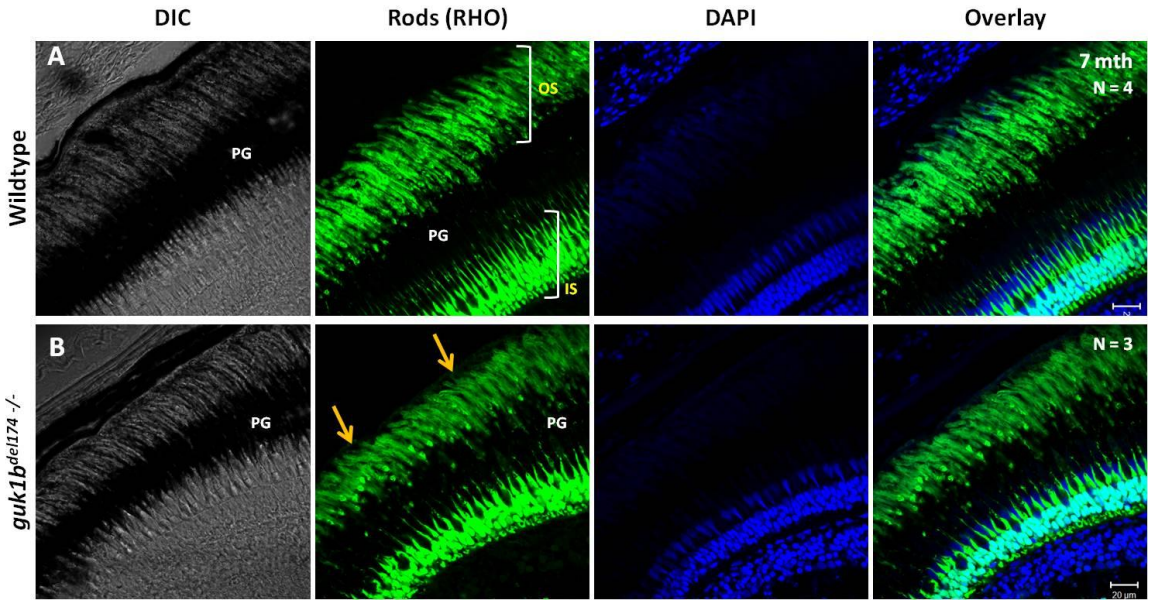

Figure 39: Rod photoreceptor outer segments appear shorter in *guk1b*$^{del174-/-}$ mutants. A: In the wildtype retina, rod outer segments are tightly packed and elongate beyond the PG layer in arrays. Strong EGFP signal is observed in cell bodies, overlapping with nuclei, and in the filament-like protrusions above the nuclei. B: Outer segments of the rod photoreceptors in *guk1b*$^{del174-/-}$ mutants overall appear normal, albeit, are slightly shorter in length (yellow arrows). The inner segments appear normal with possible minor disturbances in the cell bodies. EGFP expression is also weaker in the outer segments while EGFP expression in the cell bodies was comparable to that of the wildtype. OS: outer segment, IS: inner segment; PG: pigment granules; n = 4 for wildtype and 3 for mutant; Scale bar = 20 µm.

On the contrary, rod outer segments of *guk1b*$^{del174-/-}$ mutants were slightly shorter in length and had less EGFP expression suggesting reduced *Rho* promoter activity (Fig. 39B, yellow arrows). Other than that, the packing and regularity of the outer and inner segments of rods were comparable to that of wildtype, albeit with slight disturbances of the inner segments. This does not rule out the possibility that rod photoreceptors may develop defects at later stages.

To briefly summarize, the UV and double cone photoreceptors were observed with aberrant morphology, whereby their outer segments had deformities at both larval and adult stages. Some cone cells had inner segments that did not conform to the typical morphology seen in their wildtype siblings. Rods remained unaffected with only slight shortening of the outer segments observed in the adult mutants. Considering that photoreceptors were affected in *guk1b*$^{del174-/-}$ mutants, in particular the cone photoreceptors, this raised the question whether the lamellar disks in the outer segments of cones, which are essential for photoreception, were

properly formed in mutants. To address this, electron microscopy (EM) was used to analyse the ultrastructure of photoreceptors in the adult retina.

3.5.3. Analysis of photoreceptor lamellar disks in *guk1b*$^{del174-/-}$ mutants using EM

The immunostaining and fluorescence imaging of cryo-sections of *guk1b*$^{del174-/-}$ mutant retinas as described above revealed that outer segments of photoreceptors exhibited irregularities, especially in cone cells. It remained unknown, however, whether the lamellar disks, where phototransduction takes place, were formed properly. Using EM, information on the ultrastructure of photoreceptors, particularly their outer segments, was obtained. EM samples were prepared from retinas of seven months old *guk1b*$^{del174-/-}$ mutants and images were captured from three independent ultrathin sections using the JOEL 2100 transmission electron microscope.

Based on the morphology and size of cone photoreceptors seen in EM, cones that had a short outer segment and appeared as individual cells were deduced to be short single cones or otherwise known as UV cones. On the other hand, when two cones lay in close proximity to one another with their cell outer segment and inner segment in close contact, these were identified as double cones. Rod cells were identified based on their distinct elongated columnar outer segments.

Wildtype UV cones had a clear and distinct cone-shaped outer segment, in which the lamellar disks were regularly aligned and densely packed (Fig. 40A, A'). In contrast, UV cones of *guk1b*$^{del174-/-}$ mutants were distinctly shorter and had disrupted outer segment tips (Fig. 40B). In most cells, the mutant outer segments generally had a small, partially formed but intact cone structure, proximal to the inner segment. The outer segments were densely packed with regularly arranged lamellar disks (Fig. 40B). However, some cells did not have this tight packing in the outer segment (data not shown). The tips of the UV cone outer segments were unevenly formed with some cells having protrusions of lamellar disks (Fig. 40B', arrows, inset).

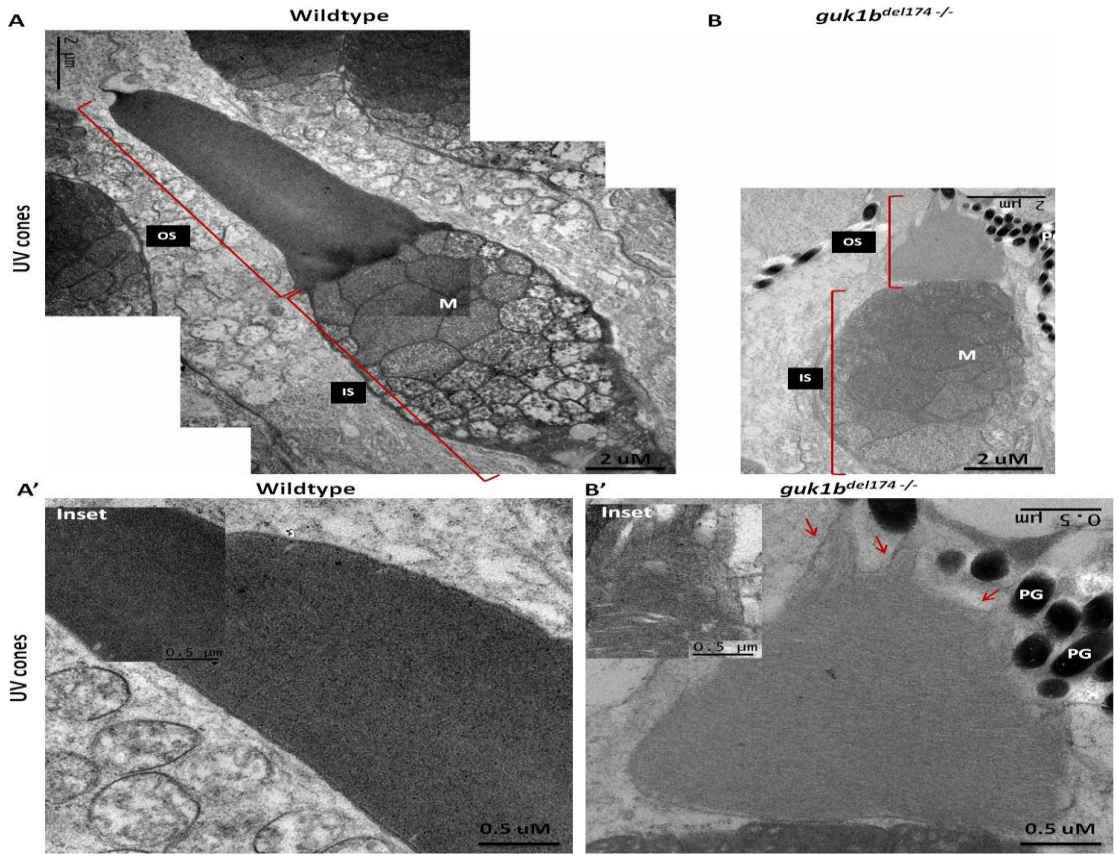

Figure 40: EM analysis of outer segments of UV cones in wildtype and *guk1b*$^{del174-/-}$ mutants. A: Wildtype UV cones are densely packed with lamellar disks and have a distinct outer segment (A', inset). B: In *guk1b*$^{del174-/-}$ mutants, the UV cone cells are smaller with only a partially formed outer segment. The lamellar disks are properly organised and folded in arrays. The tips of the outer segments are unevenly formed with protrusions made up of lamellar disks (B', arrows, inset). A' and B': Close up of the tips of UV cone outer segments. OS: outer segment, IS: inner segment, PG: pigment granules, M: megamitochondria. Scale bars are indicated in the bottom right corners.

This could be a possible consequence of ongoing degeneration of the outer segments or that the UV cones have failed to develop proper cell morphology. The inner segments of both wildtype and mutant photoreceptors developed properly and contained tightly packed megamitochondria. Megamitochondria are modified mitochondria that are uncommonly large. These are postulated to provide the required energy and to enhance spectral sensitivity of photoreceptors (Kim et al., 2005; Tarboush et al., 2012).

Wildtype double cone cells have a columnar outer segment that closes off towards the tip forming a more conical outer segment (Fig. 41A, A'). Together, the two cells form a circular-like outer segment as previously observed by zpr-1 immunostaining (Fig. 36A). The lamellar disks in

the double cones are more loosely packed and separations between infolding disk layers were evident (Fig. 41A', arrows). Double cones were shorter in *guk1b*$^{del174-/-}$ mutants with some cells having layers with slightly more densely packed lamellar disks (Fig. 41B, B').

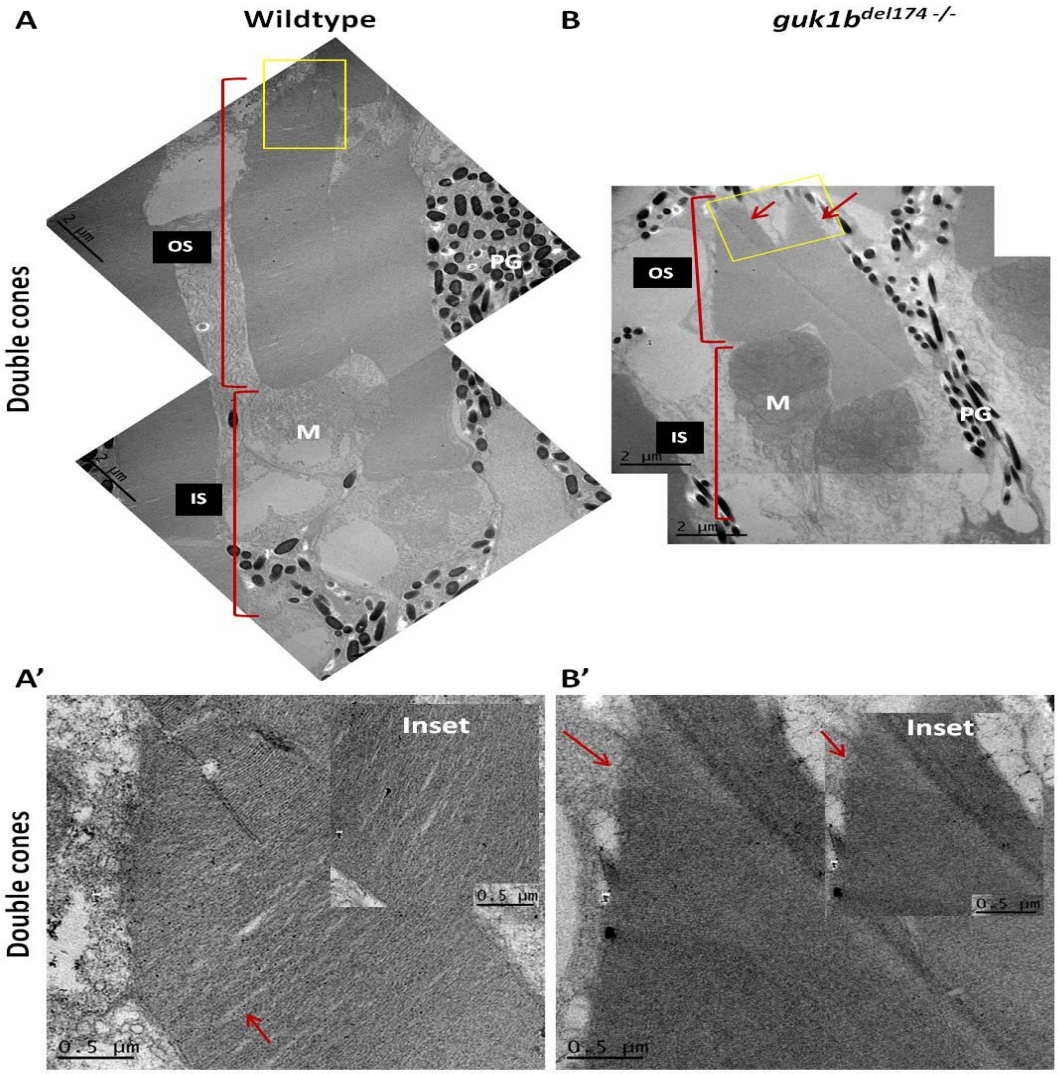

Figure 41: Double cone outer segments of *guk1b* mutants are irregularly formed. A: In the wildtype retina, the outer segments of double cones are elongated columnar structures that tether off at the tip to form a conical morphology. The lamellar disks are more loosely packed than in UV cones and gaps in between the layers were identified (A', arrow, inset). B: In *guk1b*$^{del174-/-}$ mutants, double cones are smaller in size and do not have an elongated columnar outer segment. Instead, the outer segments form an immediate cone structure. Most of the cone cells are densely packed with lamellar disks (B', arrow, inset). A' and B': Higher magnification views of the double cone outer segments (boxed region). OS: outer segment, IS: inner segment, PG: pigment granules, M: megamitochondria. Scale bars are indicated in the bottom left corners.

In these cells, the columnar portion of the outer segment was shorter and the cells displayed a sharp edged cone-shaped tip (Fig. 41B, arrow). The cone cells were also not as tightly juxtaposed

to one another. This arrangement is comparable to that observed after zpr-1 immunostaining, where the double cones appeared as single cells rather than as pairs, with distinct cell structures (Fig. 36B). Some mutant double cones were also seen with aberrantly formed outer segments while others were comparable to that of wildtype (data not shown). Different double cone cells of both wildtype and mutants were observed to have varied inner segment morphologies with varying numbers of megamitochondria (Fig. 41).

The overall morphology of rod photoreceptors was comparable between wildtype and mutant retinas, consistent with data obtained from the transgenic reporter line (Fig. 39).

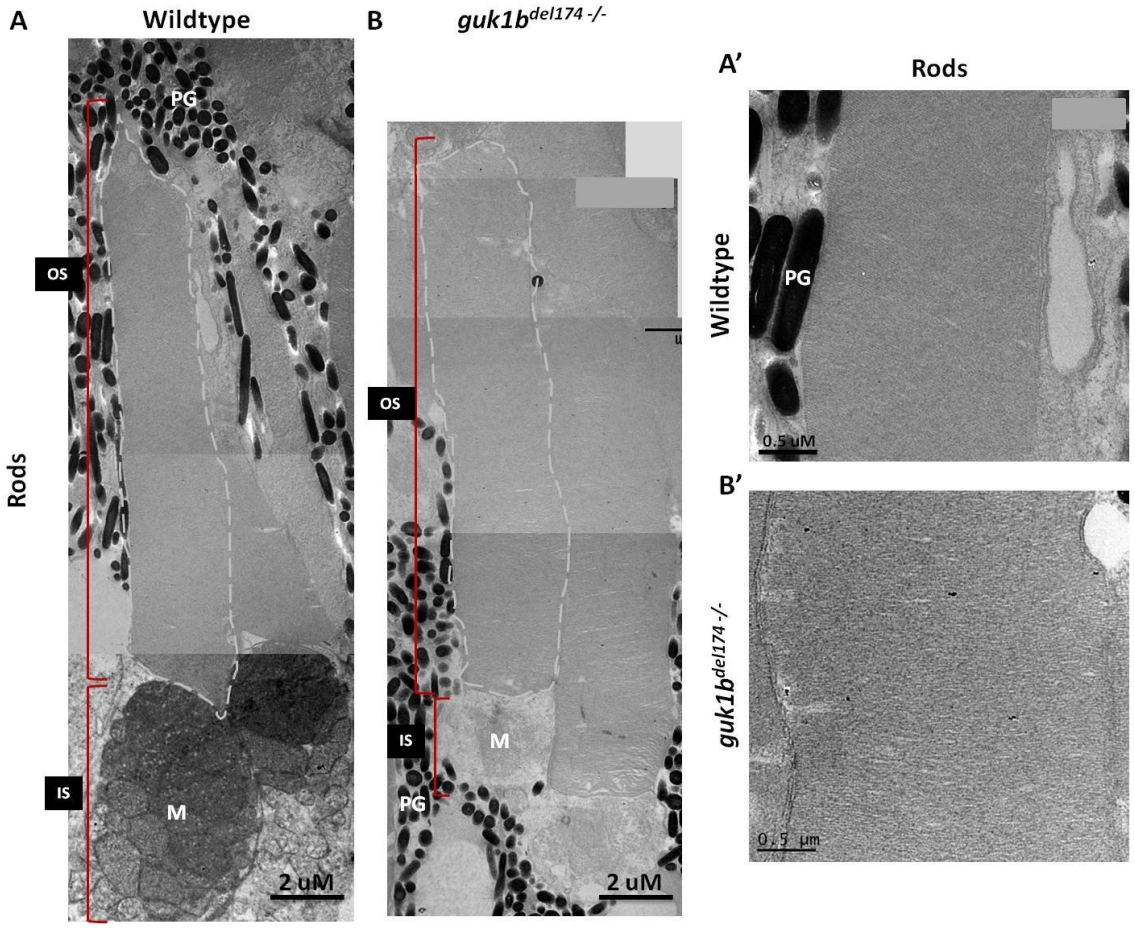

Figure 42: Ultrastructure of rod photoreceptors in wildtype and *guk1b*$^{del174-/-}$ mutants. A: In wildtype retinas, the outer segments of rod photoreceptors are elongated columnar structures with loosely packed lamellar disks. B: Outer segments of mutant rod cells appear slightly shorter but otherwise the morphological structure is comparable to that of the wildtype. In both wildtype and mutants, the width of the outer segments varied. A' and B': Enlarged views of lamellar disks in rod outer segment. OS: outer segment, IS: inner segment, PG: pigment granules, M: megamitochondria.

The rod cells were seen with a long elongated columnar outer segment (Fig. 42A, B, outlined), with the outer segment width varying across individual rod photoreceptors (Fig. 42A', B'). The rod outer segments were slightly shorter in the mutants but otherwise the formation of the lamellar disk layers and folding appeared normal.

3.5.4. Quantification of cGMP levels in *guk1b*$^{del174-/-}$ mutant retinas

The extensively shortened and aberrant outer segments of cone photoreceptors in *guk1b*$^{del174-/-}$ mutants suggested that the *guk1b* kinase activity could be impaired in mutants, thereby affecting the functionality of photoreceptors. In order to determine the phototransduction activity, cGMP levels were quantified in retina extracts using a competitive ELISA assay as described above.

In this assay, retinas from individual fish were dissected out and used for cGMP isolation and quantification. A total of six 10 months old *guk1b*^{del175} (13 bp deletion) mutant fish (F_2) were used. The experiments were performed in batches of two fish per genotype and experiment, with cGMP levels from samples 1 - 4 measured in duplicates and samples 5 - 6 measured in quadruplicates. A standard curve was plotted using the four-parameter logistic equation with the given cGMP standard from the kit (Fig. 43A).

The sample concentration was calculated using the Hill equation. In the table provided, the average absorbance and average calculated cGMP concentration is given (Fig. 43B). Based on the obtained data, the cGMP concentrations of all tested 11 fish were found to be highly variable. Mutant fish samples 1 - 4 showed approximately 20% - 50% lower amounts of cGMP than their tested wildtype siblings (2 – 4). In contrast, mutant fish 5 and 6 showed approximately 20% more cGMP in the retina than wildtype fish 5 and 6. Using a student T-test, the observed difference was quantified to be not significantly different, at a p value of > 0.05.

A

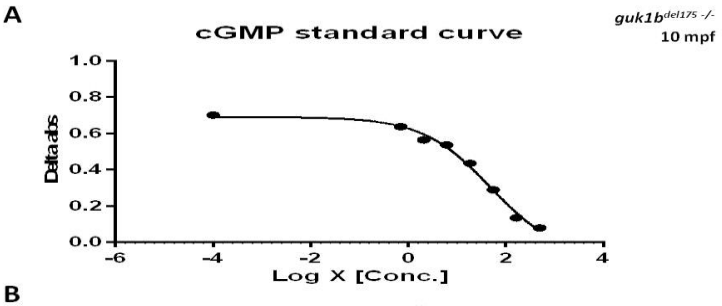

B

Genotype	Wt 1	Wt 2	-/- 1	-/- 2	Wt 3	Wt 4	-/- 3	-/- 4	Wt 5	Wt 6	-/- 5	-/- 6
Avg. Absorbance	-	0.329	0.388	0.405	0.444	0.403	0.467	0.412	0.505	0.454	0.481	0.432
cGMP Conc. (ug/ml)	-	41.41	19.91	15.78	14.38	20.95	11.48	19.42	18.47	26.10	22.44	30.15
Ratio between expt. sets		1 : 0.43				1 : 0.87				1 : 1.2		

Figure 43: Competitive ELISA assay to quantify the amount of cGMP in retinas of 10 months old wildtype and *guk1b*$^{del175-/-}$ mutants. A total of six individual fish per genotype was used for the isolation of cGMP (as six independent biological samples). A: Representative graph of the standard curve plotted using the four-parameter logistic equation, based on absorbance values obtained from prepared cGMP standards. B: The absolute cGMP concentration of experimental samples was calculated using the Hill equation. The average absorbance and concentration measured for the six individual wildtype and mutant samples are given. There was a 20 - 50% reduction in the amount of cGMP concentration in mutant fish 1 - 4. On the other hand, mutant fish 5 - 6 showed a 20% increase in cGMP levels when compared to wildtype. Calculated p value using unpaired t-test = 0.95.

Given that the photoreceptors in *guk1b*$^{del174-/-}$ mutants were highly anomalous, the possibility of these mutant photoreceptors undergoing continuous degeneration and regeneration was raised. Therefore, the number of degenerating and regenerating cells was quantified.

3.5.5. The *guk1b*$^{del174-/-}$ mutant retina is not undergoing significant apoptosis or proliferation

Based on the observation that cone cells had severe abnormalities especially in the outer segments suggested that the photoreceptors in mutants underwent extensive degeneration. To address this possibility, I carried out TUNEL assay on adult retinal sections. This assay works by binding of the TdT enzyme to the 3' hydroxyl group (3' OH) of fragmented DNA in apoptotic cells, which is then detected by fluorescence labelling.

The nuclei of wildtype and mutant photoreceptors appeared to be arranged in an intact pattern and signs of apoptotic bodies were not detected by DAPI stain (Fig. 44). The TUNEL assay

revealed that both wildtype and mutant retinas showed some extent of apoptotic photoreceptors (Fig. 44A, A', arrow). However, the mutants did not show an obvious increase in the number of apoptotic cells.

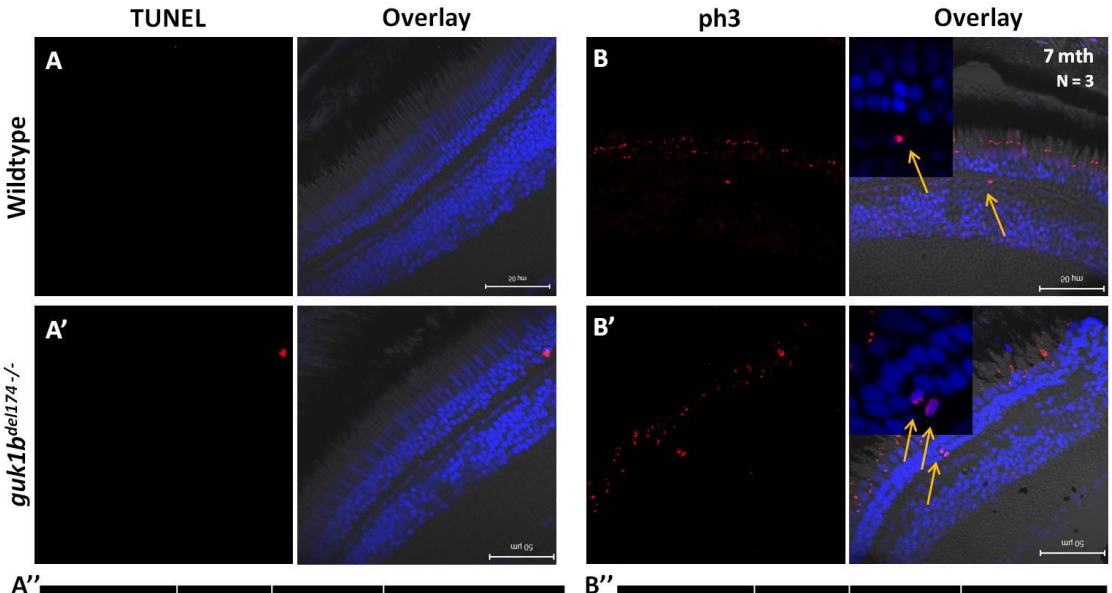

A''

guk1b^{del171}	Retina	Sections	TUNEL Positive
Wt	3	9	7
Homozygous	3	8	5

B''

guk1b^{del171}	Retina	Sections	ph3 Positive
Wt	3	9	5
Homozygous	3	9	6

Figure 44: TUNEL assay for detection of apoptotic cells and ph3 staining for detection of proliferating cells on adult retina sections. A, A': DAPI staining of photoreceptors in mutants reveal normally arranged nuclei comparable to that of the controls. Only few cells were identified to be apoptotic in both wildtype and *guk1b* mutant retinas. A'': Cell counts revealed no significant increase in the number of apoptotic cells between the two genotypes. Seven apoptotic cells were detected in wildtype and five apoptotic cells in *guk1b* mutant retinas. B: In wildtype samples, not many ph3 positive cells were detected, with only five mitotic cells identified (inset, yellow arrows). B': Similar to the wildtype, only six ph3 positive cells were counted in the mutant retinas (inset, yellow arrows). B'': Numbers of ph3 positive cells were tabulated from three independent retinas, nine sections each, from both wildtype and mutant samples. The mutant photoreceptors are not extensively regenerating. N = 3 for wildtype and mutant; Scale bar = 50 µm.

A total of three fish retinas was analysed, and only apoptotic cells found in the photoreceptor layers were counted, independently from nine wildtype and eight mutant sections, respectively. In wildtype, seven TUNEL positive cells were identified and in the *guk1b*$^{del174-/-}$ mutants a total of five TUNEL positive cells were counted (Fig. 44A''). This shows that the number of photoreceptors undergoing apoptosis in adult *guk1b*$^{del174-/-}$ mutants was not significantly different from that of control retinas. However, this does not eliminate the possibility that

photoreceptors are in the early stages of apoptosis or have completed apoptosis at an earlier stage.

In addition to the TUNEL assay, staining was also performed for phosphorylated-histone 3 (ph3) as a marker for detecting cells in M-phase. This was done in order to determine the number of proliferating cells, which is suggestive for regeneration to replace 'dying' photoreceptors in the mutant retina. Only a small number of cells were identified to be ph3 positive in both control and mutant retinas (Fig. 44B, B', arrow points to a mitotic cell in the inner cell nuclear layer). This is in contrast to the expectation of an increase in the number of mitotic cells in mutants undergoing extensive regeneration in order to replace degenerating photoreceptors.

In the adult retina, Müller-glia cells are responsible for regeneration of new photoreceptors. Hence, ph3-labelled nuclei in the inner nuclear cell layer, where Müller-glia cells reside, were counted as measure for the number of regenerating photoreceptors. Ph3-labelled cells from a total of three independent fish eyes, from nine sections each were imaged and counted. The control retina had five ph3 positive cells while six positive cells were detected in the *guk1b*$^{del174-/-}$ mutant retina (Fig. 44B''). Thus, there is no significant increase in the number of regenerating cells in the mutants.

3.5.6. Analysis of compensation by *guk1a* in *guk1b* mutants

The possibility of functional compensation in *guk1b*$^{del174-/-}$ mutants by its co-ortholog *guk1a* was tested by determining expression levels using semi-quantitative RT-PCR. An earlier reported WISH analysis of up to 2 days old zebrafish embryos had shown that *guk1a* expression is restricted to the cardiovascular system (Sprague et al., 2006). RNA was isolated from wildtype siblings and *guk1b*^{del174} F_2 homozygous mutants at 3 dpf and reverse transcribed into cDNA (three biological replicates with 15 larvae per sample). *guk1a* was PCR amplified from these samples (three technical replicates) and quantified using ImageJ (Fig. 45A, B).

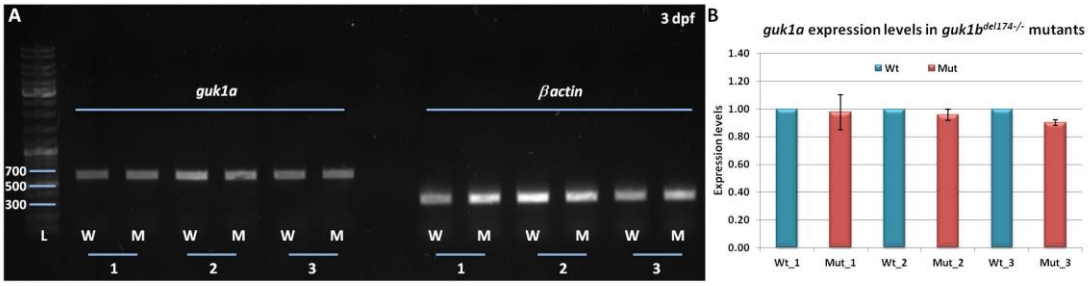

Figure 45: Analysis for gene compensation in *guk1b* mutants by its co-ortholog *guk1a*. A: Representative gel image depicting PCR bands for *guk1a* using cDNA prepared from 3 dpf *guk1b*^{del174} F_2 mutants (15 larvae per biological triplicate). *β-actin* was used as loading control and for quantification of *guk1a* expression. B: Graph depicting *guk1a* expression levels in *guk1b* mutants, quantified by ImageJ. On average, there is approximately 10% decrease in the expression levels of *guk1a* in the mutants.

Interestingly, *guk1a* expression levels in the mutants were reduced by approximately 10% on average. Therefore, a compensation by *guk1a* in the mutants appears unlikely.

3.5.7. Summary of *guk1b* function in zebrafish photoreceptors

Data collated from the *guk1b*^{del174} mutant line showed that homozygous mutants were able to survive into adulthood. Analysis of the photoreceptor morphology showed that UV and double cones had severe anomalies in the outer segments at both larval and adult stage. In contrast, rod photoreceptors were not as severely affected and only had slightly shorter outer segments. These mutant data are different from previously obtained MO knock-down data, where rods were observed to undergo extensive degeneration (Brocher et al., unpublished). Of the different photoreceptors analysed, UV cones were found to be the most severely affected in both larvae and adults. Ultrastructure analysis of the photoreceptors by electron microscopy revealed that in mutants the lamellar disks were formed properly and were mostly intact, but that the outer segments were strongly reduced in size. However, a biochemical assay used to quantify cGMP levels supported the idea that the phototransduction pathway was not disrupted in these mutants. Additionally, it was found that the co-ortholog *guk1a* is not up-regulated in the *guk1b*^{del174} mutant retina making a compensatory role unlikely.

4. Discussion

In adRP, almost 50% of patients suffering from this disease have an unknown molecular etiology (Hartong et al., 2006). For the remaining 50%, deficiencies in ubiquitously expressed pre-mRNA processing factors (Prpfs) have been identified as one of the causes for the inherited degeneration of photoreceptors (Vithana et al., 2001; Tanackovic et al., 2011). It remains to be understood how deficiencies in such ubiquitously expressed proteins lead to a retina specific disease. In the current study, two candidate genes, *gnb3b* and *guk1b*, which were strongly down-regulated upon *prpf8/31* knock-down in a zebrafish RP model, were selected for functional characterization.

Gnb3b and *guk1b* were selected based on their putative roles in the phototransduction cascade. In RP as well as various other retinal degenerative diseases, pathogenesis is caused by deficiencies in factors related to phototransduction. This includes rhodopsin, phosphodiesterase 6 subunits, the α-subunit of the G protein transducin and many more (Hartong et al., 2006; Ferrari et al., 2011; Veleri et al., 2015). Zebrafish Gnb3b and its mammalian ortholog GNB3 are highly conserved at the sequence and expression level across various vertebrates such as fish, frog, chicken, cow, mice and humans. In these species, its expression pattern is restricted to cone photoreceptors and in some cases bipolar cells (Ritchey et al., 2010; Dhingra et al., 2012). GNB3 is a member of the transducin family and is the β subunit of this heterotrimeric G protein. It therefore acts upstream in the phototransduction cascade and is proposed to be involved in the activation of cGMP specific PDEs. A tight regulation of cGMP levels is essential during phototransduction to ensure that photoreceptors are capable of undergoing repeated hyper- and depolarization. The cGMP levels are maintained by a constant recycling of GTPs. GUK1 catalyzes the conversion of GMP to GDP by addition of a phosphate group from ATP, for cGMP re-synthesis (Konrad, 1992; Sekulic et al., 2002). A study conducted in yeast GUK1 null mutants revealed that these mutants are not viable (Konrad, 1992). This hints at the importance of GUK1

for the production of GDP for survival. Based on its chromosomal localization, GUK1, the human ortholog of zebrafish *guk1b*, has been speculated to be involved in Usher Syndrome 2A (USH2A), which results in blindness and deafness (Fitzgibbon et al., 1996; Hamel, 2006). Importantly, however, no functional data are available at present that would directly link GUK1 to retinal diseases.

The exact roles played by *gnb3b* and *guk1b* in photoreceptors have yet to be determined. To address this, the present study was designed to functionally characterize *gnb3b* and *guk1b* in photoreceptors using a zebrafish model for the first time. Initial studies were conducted using morpholino based gene knock-down and later, mutants were created using genome editing by CRISPR/Cas9. The photoreceptor morphology was then analysed and compared in morphants and mutants.

4.1. Expression pattern analysis of *gnb3b*

Spatio-temporal expression analysis in zebrafish showed that *gnb3b* expression started in the epiphysis as early as 24 hpf. At 48 hpf, *gnb3b* expression was restricted to a small region in the ventral retina, which expanded over the next two days to cover all photoreceptors. Additionally, between 24 and 72 hpf, *gnb3b* expression was observed in the epiphysis as well. The observed expression pattern was consistent with recently reported findings in zebrafish (Lagman et al., 2015). In that study, it was demonstrated that *gnb3b* expression was limited to cone photoreceptors within the retina and not observed elsewhere in the retina. Existing expression data available for mammalian GNB3 suggest the expression of this gene to be retina related, with most studies conducted in the retina and not in other tissues across different species (Ritchey et al., 2010). RT-PCR performed in chick showed that *gnb3* is expressed in other tissues such as heart, brain, liver, kidney and others (Tummala et al., 2006). Likewise, semi-quantitative RT-PCR analysis performed in the present study revealed that *gnb3b* is weakly expressed in the

trunk of 4 dpf zebrafish larvae. Overall, these expression data suggest that *gnb3b* might have functions outside the retina as well.

4.1.1. Gnb3b and the phototransduction signalling cascade

The heterotrimeric G protein transducin is composed of Gα, Gβ and Gγ subunits. Missense mutations in the cone specific Gα subunit, GNAT2, are known to cause achromatopsia in humans. This is a retinal disease, where patients suffer from color blindness due to the loss of cone photoreceptor functions (Pang et al., 2010). Cone photoreceptors of mice carrying a naturally occurring single point mutation in *Gnat2* do not show any cone response in electroretinograms (ERGs) and undergo degeneration (Jobling et al., 2013). Over time a reduction in rod response was also observed. In these mice, the mutation was predicted to occur near the GDP binding site that is required for the exchange of GTP. The authors speculated that an altered transducin protein structure is the cause for the lack of cone cell function.

In another mouse model, a naturally occurred inversion of a region on chromosome 4 resulted in *Gnb1* not being expressed, and subsequently in homozygous lethality (Kitamura et al., 2006). *Gnb1* encodes for one of the Gβ subunits of transducin that is expressed in rod photoreceptors. Heterozygous carriers exhibited with extensive photoreceptor degeneration with diminished ERG response over time. These authors postulated that the role of *Gnb1* is in phototransduction and in the maintenance of photoreceptors, and causes retinal degeneration if mutated. Thus far, *Gnb1* has not been implicated in patients with retinal diseases (Baehr and Frederick, 2009). In a previous study, patients suffering from cone, cone-rod or macular dystrophies were screened for mutations in Gβ and Gγ subunits (Gao et al., 1998). As no carriers were identified, it was concluded that both subunits are unlikely to be causative for these diseases. However, based on the limited cohort size in their study, these authors notably did not rule out the possibility that these genes are involved in the pathogenesis of retinal diseases. Thus, it is possible that mutations in genes encoding for G protein subunits can result in eye diseases. *gnb3b* encodes

for a Gβ subunit which associates with Gα and Gγ to form the heterotrimeric G protein, and is expressed in cone photoreceptors (Oldham and Hamm, 2008; Lagman et al., 2015). I therefore hypothesized that a deficiency in *gnb3b* may lead to a dysregulation of the phototransduction pathway and photoreceptor deficiencies.

To address this hypothesis, I generated a *gnb3b*$^{del114-/-}$ mutant zebrafish, which harbours a 7 base pair deletion. A 3D computational model suggested that the predicted mutant Gnb3b protein lacked a seven-bladed β-propeller structure. This β-propeller structure is crucial for protein-protein interactions, forming important contact points between the Gβ, Gα and Gγ subunits (Oldham and Hamm, 2008). It can be hypothesized that the mutant protein will not be able to associate with Gα and Gγ subunits and therefore is non-functional. However, future biochemical and/or structural analysis need to confirm this hypothesis.

Without correct formation of the G protein complex, the phototransduction pathway in cone cells will be impaired, which is expected to result in constantly depolarized photoreceptors. This in turn may lead to an excess influx of calcium ions into the cells, which may consequently trigger a mitochondrial mediated apoptosis pathway (Krizaj and Copenhagen, 2002; Sancho-Pelluz et al., 2008). In addition, prolonged depolarization can increase metabolic stress in the cells and generate cytotoxic metabolic by-products, such as reactive oxygen species further deteriorating the structural integrity of the affected photoreceptors (Punzo et al., 2012). Together, all of this could ultimately cause degeneration of photoreceptors and thereby blindness in the mutant fish.

4.1.2. Deficiency in *gnb3b* leads to morphological defects in morphant and mutant cone photoreceptors

The morphology of photoreceptors was analyzed in zebrafish morphants and mutants to determine the consequences of *gnb3b* deficiency. Table 19 summarizes the observed morphologies. Four days old *gnb3b* morphants had aberrantly formed cone photoreceptors

while rods appeared to be morphologically normal. The observation that only cone cells are affected by the knock-down of *gnb3b* is not unexpected given that *gnb3b* expression has been shown to be restricted to this cell type (Lagman et al., 2015).

Table 19: Photoreceptor morphology in *gnb3b* morphants and mutants.

Cell type	Morphants (4 dpf)	*gnb3b*$^{del114-/-}$ (10 dpf)	*gnb3b*$^{del114+/-}$ (6 mths)
UV cones	Irregularly formed outer and inner segments	Shorter with missing outer segments and anomalous inner segments	Not tested
Double cones	Malformations in outer segments and shorter inner segments	Dysmorphic outer segments with varied inner segment length and morphology	Some deformities in outer and inner segments
Rods	Unaffected	Short and less developed outer segments	Unaffected

The gene knock-down results showed that rods were not affected, though this does not exclude that rod cells may be affected in the long run due to a possible 'bystander' effect. It was previously shown that in degenerative diseases of the retina, such as cone-rod dystrophies, the disease manifestation progresses from degenerating cones to rod cells (Hamel, 2007). Cells in close contact to a dying cell may be influenced into undergoing apoptosis (Ripps, 2002). How and when a 'healthy' cell succumbs to cell degeneration is determined by 1) the immediate environment (niche) where these cells reside, 2) the density of dying cells surrounding 'healthy' cells and 3) the type of the neighbouring dying cell, i.e. cones/rods, or 4) a combination of these factors (Lewis et al., 2010b; Saade et al., 2013). Taken together, it is possible that rod cells in *gnb3b* morphants undergo degeneration at a later stage, as a consequence of degenerating adjacent cone cells.

Structural deficits in cone cells were also observed in *gnb3b*$^{del114-/-}$ mutants at larval stages. In addition, the outer segment of rods was shorter and appeared less developed. The overall size of the mutant retina was slightly smaller than normal as well. *gnb3b*$^{del114-/-}$ mutants showed larval lethality and did not survive into adulthood. Heterozygous *gnb3b*$^{del114+/-}$ carriers at both larval and adult stages showed some deformed double cone cells but normal rods. I speculate

that the observed *gnb3b*$^{del114-/-}$ mutant phenotype could reflect 1) an arrested or delayed development of cone and rod photoreceptors, or 2) the beginning of ongoing degeneration of photoreceptors or 3) a combination of both effects. Due to larval lethality, the photoreceptor morphology could not be monitored at later time points to study the long-term consequences of the observed phenotype. Notably, heterozygous carriers showed an almost identical phenotype as the *gnb3b* morphants, as cones were affected but rods appeared normal. The morphology of rods however needs to be validated in depth by out-crossing to *Tg (Rho:EGFP)* fish, as this line demarcates individual rod cells. This will provide unambiguous evidence whether rod cell numbers or the length of individual outer segments are different between controls and heterozygous carriers. These carriers still have one functional copy of the *gnb3b* allele and in morphants, the *gnb3b* transcripts were knocked-down to approximately 57%. Hence, it is not surprising that both has similar phenotypes, although it should be kept in mind that morphants were analyzed at 4 dpf whereas heterozygotes were inspected as adults. Therefore, morphological differences that went unnoticed may still be present at comparable stages.

In addition, cGMP levels were quantified in retinas of adult heterozygous carriers. As the concentration of cGMP modulates depolarization and hyperpolarization of photoreceptors, measuring cGMP levels will provide some preliminary insight into the extent of active phototransduction. I hypothesized a reduction in cGMP levels in heterozygous mutants, as I expected reduced phototransduction activity, due to partial loss of *gnb3b*. Four independent fish were analysed and a 30% reduction in cGMP concentration was observed on average. This suggests a possible reduction in phototransduction activity in the morphologically defective photoreceptors. It is conceivable that the structural deficits observed in the outer segments of double cones could be a result of the phototransduction cascade being not fully functional, with subsequent alterations in cGMP concentrations. As described previously, dysregulation of the phototransduction cascade will consequently lead to imbalance in the intracellular cations resulting in increased metabolic stress and displacement of photoreceptor structural integrity.

However, a more thorough analysis of cGMP levels and the activity of the involved enzymes together with behavioural assays are needed in order to conclusively determine whether phototransduction and visual capacity are limited in heterozygous *gnb3b* carriers.

Interestingly, the photoreceptor phenotype in zebrafish *gnb3b* mutants at the larval stage differs from that in chicken and mouse *gnb3* mutants. Both chicken and mouse mutants do not show defects in the morphology of photoreceptors (Tummala et al., 2006; Nikonov et al., 2013). Instead, the synaptic termini of cones and rod photoreceptors become progressively disrupted in chickens, while in mice the synapses between rod cells and rod specific bipolar cells were affected (Tummala et al., 2006; Dhingra et al., 2012). It remains to be analysed whether the synaptic termini are disorganized in *gnb3b*$^{del114-/-}$ zebrafish mutants. In mice, the visual capacity was found to be still intact although the photoreceptor sensitivity to light was reduced (Nikonov et al., 2013). Additionally, minor reductions in Gα and Gγ expression levels, and minimal subcellular mislocalization of components of the phototransduction cascade were detected. Up to 7 months of age, cone cells did not show any defects and were functional (Dhingra et al., 2012). It was suggested that in the *Gnb3* mouse mutants, cone photoreceptors are functional because the Gα subunit might be able to function autonomously for signal transmission (Nikonov et al., 2013). However, these authors did not exclude other possibilities, such as 1) a role of different isoforms of Gβ subunits (i.e. Gβ1/ Gβ2 in cones), and/or 2) that the Gγ subunit alone was able to take over and function as a 'G$\beta\gamma$'. The difference between mouse and zebrafish *gnb3* mutant phenotypes might be linked to the inherent differences in the retina structure of both species. Mice are nocturnal, have a rod dominated retina and are dichromatic, while the zebrafish retina is cone dominant and tetrachromatic, and in this aspect more similar to the human retina (Huberman and Niell, 2011; Chhetri et al., 2014). Given that *gnb3* is expressed in cone cells (Ritchey et al., 2010), it is plausible that a *gnb3* loss causes less severe consequences in the rod dominated mouse retina, unlike the situation in zebrafish.

In chicken, a naturally occurring amino acid deletion ($D153^{del}$) mutation in *Gnb3* resulted in a retinopathy globe enlarged (Rge) phenotype (Montiani-Ferreira et al., 2003). It was predicted that the $D153^{del}$ mutation occurred within the β-propeller structure and disrupts correct protein folding, therefore leading to a non-functional protein that is likely to be degraded (Tummala et al., 2006; Tummala et al., 2011). These mutants have an enlarged retinal globe with abnormal ERG and suffer from a progressive loss of vision becoming completely blind by 8 weeks of age. The mutant retina had a disorganized outer plexiform layer and mislocalized endoplasmic reticulum in photoreceptors with disruptions observed in the synaptic terminals of rod and cone photoreceptors (Tummala et al., 2006). It was proposed that a haploinsufficiency in *Gnb3* caused by the instability of the mutant protein is the primary cause of the Rge disease phenotype. In chicken, *gnb3* is expressed in both cones and rods, which may explain the early onset of vision loss. Although chicken have a cone dominant retina, the phenotypical differences observed in *Gnb3* mutants across three species suggest the existence of species-specific expression differences and/or possibly functional divergence.

4.1.3. Does *gnb3b* have a non-retinal function?

Gnb3b homozygous mutants did not survive into adulthood and progressively died within one month after birth. This is different from findings in *Gnb3* chicken and mouse mutants, where at least a small number of homozygous mutants were able to survive. In the Rge chicken, the loss of *gnb3* resulted in glomerulopathy with the kidney glomerulus being enlarged and infiltrated by blood cells (Tummala et al., 2011). Based on previous RT-PCR studies, *Gnb3* is expressed in the chicken kidney (Tummala et al., 2006). Additionally, an increased embryonic mortality was observed in the Rge chicken, which was suggested to be due to an early embryonic expression of *Gnb3* (Tummala et al., 2006). *Gnb3* null mice also showed a high mortality rate with only 10% of the homozygous mutants surviving. These were able to grow up but were unable to breed for unknown reasons (Dhingra et al., 2012). Tummala et al. speculated that in humans, a GNB3

deficiency may lead to fetal miscarriages (Tummala et al., 2006). A single nucleotide polymorphism (SNP) in human GNB3 was shown to predispose carriers to metabolic diseases such as obesity, hypertension, dyslipidemia as well as tumors or Alzheimer's disease (Weinstein et al., 2006; Klenke et al., 2011). Together, all these findings suggest that *gnb3* possibly has non-retinal functions as well.

Previous studies conducted in *Gnb5* and *Gnb1* homozygous mouse mutants described high mortality rates and embryonic lethality, respectively (Chen et al., 2003; Kitamura et al., 2006). In *Gnb5* homozygous mutants, 66% mortality was observed and the surviving mice were small in size. As *Gnb5* is expressed in the brain as well as photoreceptors, the mortality rate was largely attributed to functional disruptions in neuronal development (Zhang et al., 2011). *Gnb1* is widely expressed in rod photoreceptors, brain, liver as well as other tissues, which was used to explain the increased homozygous lethality (Baehr and Frederick, 2009).

Taken together, these data point to the importance of Gβ subunits for general embryonic development and survival. It suggests that the loss of *gnb3b* in zebrafish not only affects photoreceptors but could have severe consequences on other tissues as well. As such, the lethality of *gnb3b*$^{del114-/-}$ zebrafish mutants could possibly be a consequence of systemic failure including a retina specific defect. Further experiments need to be conducted to analyse other tissues, e.g. the kidney in *gnb3b*$^{del114-/-}$ mutants in order to characterize the role of *gnb3b* in these tissues.

4.1.4. Where does *gnb3a* come into play in the *gnb3b* mutants?

Analysis of photoreceptor morphology at 20 dpf revealed that cone photoreceptors were still present throughout the retina. However, these cells were shorter and lacked a distinctly formed outer segment. The rod cells also had shorter outer segments. In fact, a much more severe retinal morphology was expected in the *gnb3b*$^{del114-/-}$ mutants such as extensively degenerating photoreceptors. As a possible explanation for the relatively mild retina defects observed in late

mutants, a compensatory mechanism was postulated in these mutants. *gnb3a*, the co-ortholog of *gnb3b*, proved to be a good candidate to test for a compensatory role, due to its reported expression in cone photoreceptors (Lagman et al., 2015). Low levels of *gnb3a* transcripts were detected in the retina of larvae and adults. Additionally, these authors described that a weak staining of *gnb3a* was observed throughout the entire embryo at early stages, after which the expression became restricted to the retina. It was concluded that the complementary expression patterns seen for *gnb3b* and *gnb3a* might be due to gene compartmentalization (Lagman et al., 2015).

To address a possible compensation, *gnb3a* expression levels were quantified in *gnb3b*$^{del114-/-}$ mutants at 3 dpf. On average, there was a 20% increase in *gnb3a* transcript levels in the mutants. It is speculated that the slight increase in *gnb3a* expression level could partially compensate and prevent photoreceptors from undergoing extensive degeneration. This could explain the presence of cone photoreceptors in mutant larvae at 20 dpf. On the other hand, this increase obviously was not sufficient to rescue larval lethality.

Based on my observation that *gnb3b* zebrafish mutants show a cone photoreceptor phenotype, it will be worthwhile to revisit *gnb3* as a suitable marker for inherited retinal diseases, in particular cone-rod dystrophies in human patients.

4.2. A role for *guk1b* in the phototransduction cascade

Bovine, rabbit and squirrel *guk1*, the ortholog of *guk1b*, have been reported to be expressed in photoreceptors (Hall and Kuhn, 1986; Fletcher, 2013). Within the phototransduction pathway, this gene is expected to play a downstream role in the signalling cascade, where it is required for the replenishment of cGMP. Thus far, human *guk1* has been mapped to a locus containing the retinal disease genes, autosomal recessive RP12 and USH2A, with GUK1 positioned in the same interval as USH2A (Fitzgibbon et al., 1996). Currently, functional data linking GUK1 to retinal

defects are not available. Thus, my study in zebrafish is the first to address the function of *guk1b* in the retina.

Brocher et al. (unpublished data) showed that *guk1b* expression is restricted to photoreceptors in zebrafish larvae at 4 dpf. It was also observed that *guk1b* is strongly expressed in the heart between 48 and 72 hpf. Based on the known requirement of Guk1 for catalysing GDP production during cGMP re-synthesis (Hall and Kuhn, 1986), it can be postulated that without functional Guk1b protein, cGMP will not be produced. Consequently, this will cause cGMP-gated ion channels in photoreceptors to remain closed and influx of cations will be inhibited. This should lead to constantly hyperpolarized photoreceptors. Earlier studies have shown that low cGMP levels or an equivalent 'light trigger' results in photoreceptor degeneration, although the exact mechanisms involved are yet to be elucidated (Fain and Lisman, 1993; Semple-Rowland et al., 1998).

The Guk1 protein folds into three structurally different domains, the CORE, LID and NMP binding region as reported in mice (Sekulic et al., 2002). Upon binding of GMP and ATP, all three domains come into close proximity, which allows catalytic activation and production of GDP. In my study, a mutant line carrying a 10 base pair deletion in *guk1b* (*guk1b*$^{del174-/-}$) was generated. Analysis of the deduced protein sequence revealed that the introduced mutation lies within the predicted CORE region of the guanylate kinase domain. I speculate that this mutation will lead to a disruption in the proper folding of the mutant protein and thereby may consequently affect the kinase activity. Without *guk1b*, the subsequent steps in cGMP recycling will possibly be hindered. In turn, this will result in a non-functional signal transduction in photoreceptors and consequently cause their degeneration.

4.2.1. *guk1b* morphants and mutants show structural deficits in photoreceptors

Preliminary analysis of *guk1b* morphants revealed degeneration of rod photoreceptors with intra-retinal pigment deposition, both being hallmarks of a RP phenotype (Brocher et al.,

unpublished). In these morphants, double cones were affected as well but to a lesser extent. These cone cells were slightly shorter and lacked properly formed outer segments. The *guk1b* morphant and mutant phenotypes are summarized in Table 20.

The *guk1b*$^{del174-/-}$ mutants, on the other hand, showed morphological defects in cone photoreceptors, while rods were only minimally affected. The UV and double cones had defects in their cell structure detectable at both larval and adult stages. Defects in the morphology of rod photoreceptors could not be observed at larval stages, while the outer segments were slightly shorter in adult rods.

Table 20: Photoreceptor phenotypes in *guk1b* morphants and mutants.

Cell type	Morphants (4 dpf)	*guk1b*$^{del174-/-}$ (4 dpf)	*guk1b*$^{del174-/-}$ (6 mths)
UV cones	Not tested	Outer segments and whole cells missing	Outer segment tips missing in some cells
Double cones	Shorter cells with outer segment defects	Inner and outer segments abnormal	Inner segments aberrantly formed; spaces between individual cells
Rods	Severe degeneration	Normal morphology	Outer segments shortened

Furthermore, EM imaging revealed that the folding of lamellar disks within the outer segments of rods and cones were generally intact. In some of the cone photoreceptors, the tips of the outer segment were irregularly formed to various degrees with some cells having uneven extensions of the lamellar disks. The adult *guk1b*$^{del174-/-}$ mutants were additionally tested for signs of retina degeneration and regeneration. There was no significant increase in the number of apoptotic or proliferating cells identified in the mutants, respectively. It was surprising to see that the aberrantly formed photoreceptors were not undergoing extensive degeneration. This does not exclude the possibility that the cells are in the process of slowly initiating degeneration or have already completed degeneration thus escaping the TUNEL staining. It is not unusual to detect low numbers of proliferating cells in mutants as without high numbers of apoptotic cells, there is no necessity to replace cells extensively by regeneration. Again, this does not exclude

that photoreceptors undergo extensive degeneration and regeneration at a later age in the mutants.

Evidence for the importance of cGMP levels come from studies of mutations in the gene encoding cone specific cyclic nucleotide-gated channel subunit 3 (CNGA3/B3), which have been shown to cause progressive cone dystrophies (Michaelides et al., 2006). These channels are involved in the phototransduction process, as their opening and closing modulates influx of ions into photoreceptors. Patients carrying defects in these genes are known to have progressively declining levels of cone function, color blindness and degeneration of cone photoreceptors (Wissinger et al., 2001; Michaelides et al., 2004). In a mouse *Cng3* mutant model, a progressive degeneration of cones with loss of vision was observed (Biel et al., 1999). Importantly, the retina of young mutant mice still contained cone photoreceptors and rod vision was unaffected. The authors postulated that the photoreceptor degeneration occurred as a secondary consequence of dysregulated calcium ions and cGMP levels in these mutants. Additionally, a long term disease progression and late onset of disease phenotype has also been described for other retinal degenerative diseases such as RP and AMD (Veleri et al., 2015).

Taken together, the phenotype observed in the adult *guk1b*$^{del174-/-}$ zebrafish mutants is suggestive for a possible slowly progressing cone-rod dystrophy. It can be speculated that the cone dystrophy observed may become more advanced over time and could lead to rod cell degeneration, leading to secondary cone-rod dystrophy. Analysing the photoreceptor morphology at various time points over two years could uncover whether the *guk1b*$^{del174-/-}$ mutants show a disease progression, especially in cone cells.

4.2.2. Do *guk1b*$^{del174-/-}$ mutants suffer from vision loss?

Guk1 is the kinase required for the first step of cGMP re-synthesis (Gaidarov et al., 1993). I hypothesized that upon loss of *guk1b*, cGMP will not be re-synthesized in photoreceptors of the zebrafish mutants. By measuring cGMP levels in the retina, an indirect measure of the functional

capacity of the mutant kinase was provided. Additionally, the analysed cGMP levels also provided indirect evidence for the extent of phototransduction, as cGMP levels determine the degree of hyperpolarization and depolarization of photoreceptors. It was expected that the adult *guk1b*$^{del174-/-}$ mutant retinas will have reduced levels of cGMP.

Surprisingly, there was no significant difference in cGMP levels between controls and mutants. Furthermore, in the wildtype and mutant fish tested, highly variable levels of cGMP were measured from individual fish. These observed differences in cGMP levels could possibly reflect inherent differences in cGMP requirement in individual fish. In addition, the absence of reduced cGMP levels could be explained by three possible reasons. Firstly, *guk1b* is the enzyme involved only in the first step of cGMP re-synthesis. Other alternative sources for GDP and GTP could exist to provide the substrate for the subsequent steps of cGMP synthesis (Abdulaev et al., 1998; Collery and Kennedy, 2010). Secondly, the generated *guk1b*$^{del174-/-}$ mutant could still have some residual kinase activity. Although unlikely based on the structural consequences, the mutant protein could still be able to convert GMP into GDP, possibly at a reduced rate. In yeast, it was shown that a mutation within the kinase domain of a membrane-associated guanylate kinase affected the binding affinity to GMP and therefore reduced the enzymatic activity (Olsen and Bredt, 2003; Zhang et al., 2015). As the guanylate kinase activity was not measured in this study, it will be worthwhile to analyse the *guk1b*$^{del174-/-}$ mutant protein activity. Thirdly, it is possible that compensation takes place in the homozygous mutants (Rossi et al., 2015). It was previously shown that the co-ortholog *guk1a* is expressed in the cardiovascular system of zebrafish at larval stages (Howe et al., 2013). To test for gene compensation, the expression levels of *guk1a* were quantified in *guk1b* mutants at 3 dpf. Interestingly, a 10% decrease in *guk1a* expression was found. This, together with the observation that *guk1a* and *guk1b* have different expression patterns in zebrafish makes any compensatory mechanism unlikely.

The mild reduction of *guk1a* expression levels observed in *guk1b* mutants opens the possibility of secondary vascular deficits in the mutants. It was reported that RP patients have a substantial reduction in ocular blood flow as well as alterations in the micro-circulation of the body (Cellini et al., 2010; Konieczka et al., 2012). These patients showed elevated levels of plasma endothelin-1 (ET-1), which is a vasoconstrictor that gets increased under hypoxic or oxidative stress. Though the exact cause is not known, it is postulated that a primary vascular dysregulation (PVD) syndrome could possibly be the contributing factor in these patients (Konieczka et al., 2012). The authors speculated that PVD syndrome leads to dysregulated autoregulation of ocular blood flow that increases oxidative stress and further aggravates the condition. However, a definitive link that PVD causes reduced ocular blood flow has yet to be established. It is also reported that patients with age related macular degeneration are seen with a reduction in ocular blood flow secondarily, which further contributes to disease pathogenesis (Ehrlich et al., 2008). It will be interesting to analyse in the retina of adult *guk1b*$^{del174-/-}$ mutants, whether potential secondary vascular defects are present.

The current study has revealed that a deficiency in *guk1b* results in photoreceptor defects, especially of cones. This provides a stepping stone to consider screening of patients with retinal degenerative diseases, such as progressive cone dystrophies and related cone dystrophies for mutations in *Guk1*.

4.3. Morpholino and CRISPR/Cas9 efficiency in gene knock-down and knock-out

In this study, MO mediated knock-down and CRISPR/Cas9 mediated knock-out were used for functional characterization of *gnb3b* and *guk1b*. MOs are a fast and easy way to temporarily reduce the expression levels of target genes of interest for functional analysis (Bill et al., 2009; Schulte-Merker and Stainier, 2014). This is particularly useful for the characterization of critical developmental genes that lead to embryonic lethality upon complete knock-out. MOs are known to elicit unspecific phenotypes due to potential off-target effects in some cases (Eisen

and Smith, 2008). By knocking-down *p53* in parallel, it has been shown that unspecific cell death can be blocked (Robu et al., 2007). *gnb3b* was knocked-down using splice-site specific MOs with an efficiency of 57%. This level of knock-down was sufficient to induce an abnormal cone photoreceptor phenotype in the morphants. To ensure that the *gnb3b* morphant phenotype observed was specific, I simultaneously knocked-down *p53* together with *gnb3b*. Based on the obtained TUNEL data, I concluded that unspecific cell death was induced by the *gnb3b* MOs at large scale, particularly in the trunk. This ambiguous MO phenotype as well as other limitations of MOs, such as limited MO stability, made it necessary to validate the observed phenotype in mutants as proposed earlier (Bedell et al., 2011).

Initially, the TALEN genome editing tool was utilized for generation of the *gnb3b* mutant line, however introduction of mutations in the genome of injected embryos or founders could not be detected. TALEN works by the dimerization of FokI nuclease monomers bound at the C-terminal end of two TALE arms, which leads to double stranded breaks at the target site in the genome (Gaj et al., 2013; Nemudryi et al., 2014). It is possible that the generated TALEN pairs did not come into close contact with the target site in the genome at the same place, at the same time, to elicit genome modifications. It is also reasonable to presume that the efficiency with which the two TALEN arms recognized and bound to the genome was low. Generally, the reported efficiency of TALEN for transmission of mutations is 35% at F_0 and 4% at F_1 (Varshney et al., 2015). This value was based on the analysis of 13 target genes for which TALEN was utilized. With such low levels of efficiency at F_0 and F_1, it is probable that large numbers of embryos have to be screened. In this study, a total of 250 embryos were screened for both TALEN pairs designed and this may not have been sufficient. Instead, the CRISPR/Cas9 system was used as an alternative for creating *gnb3b* and *guk1b* mutant lines.

The CRISPR/Cas9 technology was developed recently and has proven to be efficient in introducing mutations in the genome (Hwang et al., 2013; Sander and Joung, 2014). The

currently reported average efficacy in zebrafish for the introduction of mutations at the F_0 and F_1 levels is 53% and 28%, respectively (Varshney et al., 2015). These efficiency rates are based on a study, where 83 genes were analysed. The F_0 number represents the percentage of injected fish that were identified as positive for mutations in the germline and were able to transmit said mutations to the progeny. The F_1 number reflects the percentage of individual F_1 embryos that were positive for carrying the mutant allele. This quantifies the number of germ cell precursors that were modified in a positive founder fish. The efficiency of this system in introducing alterations at the genome level was measured for *gnb3b* and *guk1b* (summarized in Table 21). For *gnb3b*, the efficiency at F_0 was 73.3% and the F_1 germline transmission rate was 21.1%. *guk1b* had 100% F_0 efficacy and 17.6% efficiency at F_1. These values fall within the known range of efficacy.

Table 21: Knock-out efficiencies in *gnb3b* and *guk1b* mutants.

Mutant lines	F_0 Efficiency (%)	F_1 Germline transmission (%)
gnb3b	73.3	21.1
guk1b	100	17.6

The difference in the observed efficiencies between *gnb3b* and *guk1b* can be attributed to the binding affinity of the used guide RNAs (gRNAs). In a screen with 122 different gRNAs, it has been shown that the efficiency of a gRNA is variable for different genes (Gagnon et al., 2014). Importantly, the obtained efficiency was sufficient to successfully establish mutant lines for *gnb3b* and *guk1b* in this study. Another interesting observation was that particular types of mutations were introduced recurrently at high frequency. Two different types of 7 base pair deletions were seen in *gnb3b* and a 10 and 13 base pair deletion frequently occurred in *guk1b*. Gagnon et al., postulated that this predominance for certain alleles was due to a preferential way in which the DNA repair mechanism corrects the introduced mutations in the genome (Gagnon et al., 2014).

4.3.1 Do morphants recapitulate the mutant phenotype?

Comparing the photoreceptor morphologies of *gnb3b* morphants and mutants, similarities were seen. UV cones and double cones were shorter and part of the outer segments appeared to be missing or formed with defects. The rod photoreceptors of morphants had a similar morphology as the controls. The mutant rod photoreceptors were slightly underdeveloped but this could be a result of an overall smaller size of the mutants. It is possible that the phenotype seen in the morphant retina is specific, although the *gnb3b* MOs had additional off-target effects. Contradicting data were obtained when *guk1b* morphants and mutants were compared. In the morphants, the rod cells were degenerating extensively with disintegration of the retinal pigment epithelium. Contrarily, rod cells appeared close to normal with only slight shortening of the outer segments in the *guk1b* mutants. The outer segments of double cones were aberrantly formed in the morphants and mutants, with some cells missing in the mutants.

The disparities observed between morphants and mutants, especially for *guk1b*, could be attributed to the consequence of off-target effects elicited by the selected MOs, and the MO data generally should be approached with caution (Bedell et al., 2011; Gerety and Wilkinson, 2011). By performing additional rescue assays, the specificity of the retinal phenotype observed in *gnb3b* and *guk1b* morphants can be validated (Eisen and Smith, 2008). Importantly, in morphants, the gene is not completely down-regulated. Hence, there is still residual gene function, which could either be sufficient for 'normal' gene function or result in a 'partial' phenotype. Mutants are generated via modifications at the genome level, and subsequent outcrossing of the lines reduces the chance of unspecifically introduced off-target mutations. Also, in mutants due to a complete knock-out of the target gene, alternative pathways may be triggered to compensate for the loss of function, which is not the case after MO mediated gene knock-down (Rossi et al., 2015). Collectively, the data obtained from *gnb3b* and *guk1b* mutants likely provide a more representative and reliable scenario than the analysed morphants.

5. Future work

The current study mainly focused on phenotypes observed in photoreceptors of *gnb3b* and *guk1b* morphants and mutants. The obtained data allowed to raise new hypotheses about the roles of *gnb3b* and *guk1b* in the retina that need to be addressed in future experiments. One important experiment will be to confirm the described phenotypes in different mutant alleles. This study focused on data obtained from one mutant allele per gene and it will be important to recapitulate the observed phenotypes in different mutant variants of the same gene. The zebrafish retina comprises four different cone photoreceptors, red, green, blue and UV cones. Another part of the work should therefore be dedicated to analyse the phenotype of blue cone photoreceptors, e.g. by using antibodies detecting this cell type (Vihtelic et al., 1999; Takechi et al., 2008). This will provide a complete overview of the effects of gene deficiency on all different cones and rod photoreceptors. Additionally, as described above, *Gnb3* mutant mice and chicken are seen with defects in the synaptic termini. It will be worthwhile to address by EM whether the organization and formation of other cell types and formation of the synaptic termini are structurally normal in the mutant retina.

5.1. Quantification of visual capacity in mutants through behavioural assays

This study thoroughly analysed the morphology of photoreceptors, however, behavioural assays to determine visual capabilities were not performed. It is not yet known whether the visual capacity is intact in *gnb3b* and *guk1b* mutants. To quantify visual capacity, behavioural assays need to be carried out. For example, an optokinetic response (OKR) assay can be used to measure the visual activity in mutant larvae (Neuhauss, 2003). In this assay, a moving object triggers a reflex response in the larvae, which is measured in the form of saccadic eye movements. Previously tested *guk1b* zebrafish morphants at 4 dpf demonstrated a 54% reduction in OKR activity (Brocher et al., unpublished). It can be expected that in mutants, the

number of saccades is similarly reduced due to the defects observed in photoreceptors. This would in turn indicate that the mutants have reduced visual capacity as a consequence of aberrantly formed photoreceptors. Especially in the case of *gnb3b* mutants, this could provide additional support that vision loss is one of the causes for the observed larval death. The *guk1b*$^{del174-/-}$ adult mutants can also be subjected to ERG measurements (Chhetri et al., 2014). Readings from the ERG measurement can highlight whether the test subject has visual deficits and allow to differentiate photoreceptor defects and anomalies associated with the synaptic termini (Makhankov et al., 2004).

5.2. Generation of *gnb3b* and *guk1b* double mutants

Gnb3b acts upstream in the phototransduction cascade and *guk1b* is implicated further downstream in the same pathway. Therefore, it will be interesting to cross both mutant lines and observe photoreceptor morphology in double homozygous mutants. There are three possible outcomes: 1) an extremely severe photoreceptor morphology, particularly affecting cone cells with possibly increased cone-rod dystrophy that leads to accelerated vision loss, or 2) increased embryonic lethality as a consequence of systemic organ failure, or 3) minor morphological photoreceptor defects, if the double mutants are capable of modulating gene expression such that compensation allows the rescue of photoreceptor deficits. If larvae of double mutants are able to survive and grow up into adulthood, overall retina and specific photoreceptor morphology should be analyzed by immunostaining at different time points as described in this study. Secondly, an OKR assay should be carried out to measure the visual capacity in these double mutants. Depending on the outcome of these initial studies, similar experiments as those conducted in this current study should be performed in the double mutants.

6. Conclusion

In this study, I have shown for the first time, the effects of a loss of function of *gnb3b* and *guk1b* in zebrafish photoreceptors. Studies were conducted in morphants with a gene knock-down using splice-site specific MOs, and in mutants where genes were knocked-out using CRISPR/Cas9. As not much was known about the roles of *gnb3b* and *guk1b* in photoreceptors, the obtained data provide first insights towards the role of these genes for the structural integrity and maintenance of photoreceptors, particularly in cones. Based on the proposed biochemical functions of both proteins, my results suggest that the observed photoreceptor defects are a consequence of a dysregulated phototransduction signalling cascade (Fig. 46).

In the absence of *gnb3b*, the heterotrimeric G protein will not be formed properly, thus inhibiting the downstream activation of PDEs and subsequent hyperpolarization of the photoreceptors. This in turn will lead to constitutively depolarized photoreceptors. On the other hand, a *guk1b* deficiency will possibly prevent the re-synthesis of cGMP. Without sufficient cGMP levels, the photoreceptors will undergo constant hyperpolarization. A constant de- or hyperpolarization of photoreceptors will consequently lead to an intracellular imbalance of ions and increase their metabolic stress. This may result in a progressive degeneration of photoreceptors, especially of cones.

In this study, it was shown that a *gnb3b* deficiency causes larval lethality. It is postulated that *gnb3b*, being part of a G protein, may have roles outside the retina, which are yet to be determined. In contrast, *guk1b* mutants were able to grow into adults. Irregularities in cone photoreceptors were evident in these adults. The slow progression of photoreceptor degeneration could be the consequence of either a compensatory mechanism or of an extended time needed to manifest the disease phenotype.

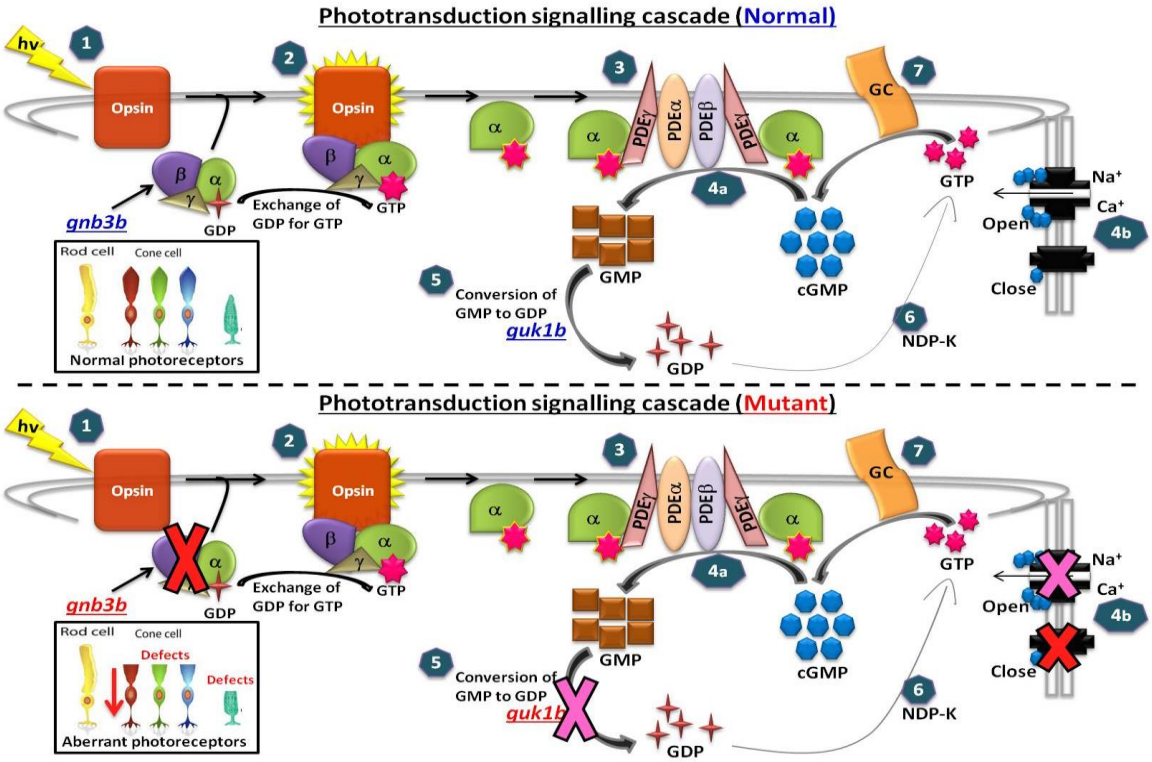

Figure 46: Schematic diagram summarizing the consequences of a loss of *gnb3b* and *guk1b* in zebrafish photoreceptors. Briefly, in the normal retina (top panel), absorption of a photon by opsins (1) triggers a conformational change, that leads to the activation of transducin (2). Subsequently, the activated Gα subunit dissociates from the Gβγ subunit and in turn activates PDEs (3). The PDEs hydrolyzes cGMPs into GMPs (4a), resulting in the closure of cGMP-gated ion channels (4b). This leads to the hyperpolarization of the photoreceptors. The photoreceptors return to their initial resting state through the restoration of cGMP concentration. *gnb3b* acts upstream in this pathway as it is the Gβ subunit of transducin. *guk1b* catalyzes the conversion of GMP into GDP (5), the first step towards cGMP re-synthesis. GTP is then produced from GDP by NDP-K (6). Finally, guanylyl cyclase converts GTP into cGMP (7). Introduction of mutations into *gnb3b* and *guk1b* leads to the dysregulation of the phototransduction pathway (bottom panel). Loss of functional *gnb3b* (red cross) will block the downstream signalling cascade, resulting in constantly depolarized photoreceptors. *guk1b* deficiency will inhibit re-synthesis of cGMP (pink arrow). Without cGMP, the photoreceptors will remain in a constitutively hyperpolarized state. Prolonged de- or hyperpolarization will lead to ionic imbalance and increase metabolic stress placed on these cells. This will lead to degeneration of photoreceptors (inset, boxed). hv: photon, Gαβγ: heterotrimeric G protein - transducin, PDE: phosphodiesterase, GC: guanylyl cyclase, NDP-K: nucleoside diphosphate kinase, *gnb3b*: G protein beta subunit 3b, *guk1b*: guanylate kinase 1b.

For *guk1b*, this is the first *in vivo* mutant model available in vertebrates that is functionally characterized. In this study, it was revealed that *gnb3b* and *guk1b* have critical roles within the retina and may be important genes implicated in the pathogenesis of cone dystrophies. Zebrafish has proven to be a suitable and efficient *in vivo* model for mimicking retinal disease phenotype.

7. References

Abdulaev NG, Karaschuk GN, Ladner JE, Kakuev DL, Yakhyaev AV, Tordova M, Gaidarov IO, Popov VI, Fujiwara JH, Chinchilla D, Eisenstein E, Gilliland GL, Ridge KD (1998) Nucleoside diphosphate kinase from bovine retina: purification, subcellular localization, molecular cloning, and three-dimensional structure. Biochemistry 37:13958-13967.

Altschul SF, Gish W, Miller W, Myers EW, Lipman DJ (1990) Basic local alignment search tool. Journal of molecular biology 215:403-410.

Anasagasti A, Irigoyen C, Barandika O, Lopez de Munain A, Ruiz-Ederra J (2012) Current mutation discovery approaches in Retinitis Pigmentosa. Vision research 75:117-129.

Auer TO, Del Bene F (2014) CRISPR/Cas9 and TALEN-mediated knock-in approaches in zebrafish. Methods 69:142-150.

Baehr W, Frederick JM (2009) Naturally occurring animal models with outer retina phenotypes. Vision research 49:2636-2652.

Bedell VM, Westcot SE, Ekker SC (2011) Lessons from morpholino-based screening in zebrafish. Briefings in functional genomics 10:181-188.

Benaglio P, San Jose PF, Avila-Fernandez A, Ascari G, Harper S, Manes G, Ayuso C, Hamel C, Berson EL, Rivolta C (2014) Mutational screening of splicing factor genes in cases with autosomal dominant retinitis pigmentosa. Molecular vision 20:843-851.

Biasini M, Bienert S, Waterhouse A, Arnold K, Studer G, Schmidt T, Kiefer F, Cassarino TG, Bertoni M, Bordoli L, Schwede T (2014) SWISS-MODEL: modelling protein tertiary and quaternary structure using evolutionary information. Nucleic acids research 42:W252-258.

Biel M, Seeliger M, Pfeifer A, Kohler K, Gerstner A, Ludwig A, Jaissle G, Fauser S, Zrenner E, Hofmann F (1999) Selective loss of cone function in mice lacking the cyclic nucleotide-gated channel CNG3. Proceedings of the National Academy of Sciences of the United States of America 96:7553-7557.

Bill BR, Petzold AM, Clark KJ, Schimmenti LA, Ekker SC (2009) A primer for morpholino use in zebrafish. Zebrafish 6:69-77.

Bilotta J, Saszik S (2001) The zebrafish as a model visual system. International journal of developmental neuroscience : the official journal of the International Society for Developmental Neuroscience 19:621-629.

Brady WA, Kokoris MS, Fitzgibbon M, Black ME (1996) Cloning, characterization, and modeling of mouse and human guanylate kinases. The Journal of biological chemistry 271:16734-16740.

Branchek T, Bremiller R (1984) The development of photoreceptors in the zebrafish, Brachydanio rerio. I. Structure. The Journal of comparative neurology 224:107-115.

Cayouette M, Poggi L, Harris WA (2006) Lineage in the vertebrate retina. Trends in neurosciences 29:563-570.

Cellini M, Strobbe E, Gizzi C, Campos EC (2010) ET-1 plasma levels and ocular blood flow in retinitis pigmentosa. Canadian journal of physiology and pharmacology 88:630-635.

Centanin L, Wittbrodt J (2014) Retinal neurogenesis. Development 141:241-244.

Cermak T, Doyle EL, Christian M, Wang L, Zhang Y, Schmidt C, Baller JA, Somia NV, Bogdanove AJ, Voytas DF (2011) Efficient design and assembly of custom TALEN and other TAL effector-based constructs for DNA targeting. Nucleic acids research 39:e82.

Chen CK, Eversole-Cire P, Zhang H, Mancino V, Chen YJ, He W, Wensel TG, Simon MI (2003) Instability of GGL domain-containing RGS proteins in mice lacking the G protein beta-subunit Gbeta5. Proceedings of the National Academy of Sciences of the United States of America 100:6604-6609.

Chen M, Manley JL (2009) Mechanisms of alternative splicing regulation: insights from molecular and genomics approaches. Nature reviews Molecular cell biology 10:741-754.

Chhetri J, Jacobson G, Gueven N (2014) Zebrafish--on the move towards ophthalmological research. Eye 28:367-380.

Chizzolini M, Galan A, Milan E, Sebastiani A, Costagliola C, Parmeggiani F (2011) Good epidemiologic practice in retinitis pigmentosa: from phenotyping to biobanking. Current genomics 12:260-266.

Collery RF, Kennedy BN (2010) Photoreceptor guanylate cyclases and cGMP phosphodiesterases in zebrafish. Advances in experimental medicine and biology 664:55-61.

Corpet F (1988) Multiple sequence alignment with hierarchical clustering. Nucleic acids research 16:10881-10890.

Dahlem TJ, Hoshijima K, Jurynec MJ, Gunther D, Starker CG, Locke AS, Weis AM, Voytas DF, Grunwald DJ (2012) Simple methods for generating and detecting locus-specific mutations induced with TALENs in the zebrafish genome. PLoS Genet 8:e1002861.

Daiger SP, Bowne SJ, Sullivan LS (2007) Perspective on genes and mutations causing retinitis pigmentosa. Archives of ophthalmology 125:151-158.

Dhingra A, Ramakrishnan H, Neinstein A, Fina ME, Xu Y, Li J, Chung DC, Lyubarsky A, Vardi N (2012) Gbeta3 is required for normal light ON responses and synaptic maintenance. The Journal of neuroscience : the official journal of the Society for Neuroscience 32:11343-11355.

Dolph PJ, Man-Son-Hing H, Yarfitz S, Colley NJ, Deer JR, Spencer M, Hurley JB, Zuker CS (1994) An eye-specific G beta subunit essential for termination of the phototransduction cascade. Nature 370:59-61.

Doyle EL, Booher NJ, Standage DS, Voytas DF, Brendel VP, Vandyk JK, Bogdanove AJ (2012) TAL Effector-Nucleotide Targeter (TALE-NT) 2.0: tools for TAL effector design and target prediction. Nucleic Acids Res 40:W117-122.

Driever W, Stemple D, Schier A, Solnica-Krezel L (1994) Zebrafish: genetic tools for studying vertebrate development. Trends in genetics : TIG 10:152-159.

Ehrlich R, Harris A, Kheradiya NS, Winston DM, Ciulla TA, Wirostko B (2008) Age-related macular degeneration and the aging eye. Clinical interventions in aging 3:473-482.

Eisen JS, Smith JC (2008) Controlling morpholino experiments: don't stop making antisense. Development 135:1735-1743.

Fadool JM, Dowling JE (2008) Zebrafish: a model system for the study of eye genetics. Progress in retinal and eye research 27:89-110.

Fain GL, Lisman JE (1993) Photoreceptor degeneration in vitamin A deprivation and retinitis pigmentosa: the equivalent light hypothesis. Experimental eye research 57:335-340.

Fain GL, Lisman JE (1999) Light, Ca2+, and photoreceptor death: new evidence for the equivalent-light hypothesis from arrestin knockout mice. Investigative ophthalmology & visual science 40:2770-2772.

Ferrari S, Di Iorio E, Barbaro V, Ponzin D, Sorrentino FS, Parmeggiani F (2011) Retinitis pigmentosa: genes and disease mechanisms. Current genomics 12:238-249.

Fitzgibbon J, Katsanis N, Wells D, Delhanty J, Vallins W, Hunt DM (1996) Human guanylate kinase (GUK1): cDNA sequence, expression and chromosomal localisation. FEBS letters 385:185-188.

Fletcher EL (2013) What neurochemistry tells us about the retina. Clinical & experimental optometry 96:257-258.

Gagnon JA, Valen E, Thyme SB, Huang P, Akhmetova L, Pauli A, Montague TG, Zimmerman S, Richter C, Schier AF (2014) Efficient mutagenesis by Cas9 protein-mediated oligonucleotide insertion and large-scale assessment of single-guide RNAs. PloS one 9:e98186.

Gaidarov IO, Suslov ON, Abdulaev NG (1993) Enzymes of the cyclic GMP metabolism in bovine retina. I. Cloning and expression of the gene for guanylate kinase. FEBS letters 335:81-84.

Gaj T, Gersbach CA, Barbas CF, 3rd (2013) ZFN, TALEN, and CRISPR/Cas-based methods for genome engineering. Trends in biotechnology 31:397-405.

Gao YQ, Danciger M, Akhmedov NB, Zhao DY, Heckenlively JR, Fishman GA, Weleber RG, Jacobson SG, Farber DB (1998) Exon screening of the genes encoding the beta- and gamma-subunits of cone transducin in patients with inherited retinal disease. Molecular vision 4:16.

Gasteiger E, Gattiker A, Hoogland C, Ivanyi I, Appel RD, Bairoch A (2003) ExPASy: The proteomics server for in-depth protein knowledge and analysis. Nucleic acids research 31:3784-3788.

Gerety SS, Wilkinson DG (2011) Morpholino artifacts provide pitfalls and reveal a novel role for pro-apoptotic genes in hindbrain boundary development. Developmental biology 350:279-289.

Gestri G, Link BA, Neuhauss SC (2012) The visual system of zebrafish and its use to model human ocular diseases. Developmental neurobiology 72:302-327.

Grainger RJ, Beggs JD (2005) Prp8 protein: at the heart of the spliceosome. Rna 11:533-557.

Guex N, Peitsch MC, Schwede T (2009) Automated comparative protein structure modeling with SWISS-MODEL and Swiss-PdbViewer: a historical perspective. Electrophoresis 30 Suppl 1:S162-173.

Hall SW, Kuhn H (1986) Purification and properties of guanylate kinase from bovine retinas and rod outer segments. European journal of biochemistry / FEBS 161:551-556.

Hamel C (2006) Retinitis pigmentosa. Orphanet journal of rare diseases 1:40.

Hamel CP (2007) Cone rod dystrophies. Orphanet journal of rare diseases 2:7.

Hartong DT, Berson EL, Dryja TP (2006) Retinitis pigmentosa. Lancet 368:1795-1809.

Howe DG et al. (2013) ZFIN, the Zebrafish Model Organism Database: increased support for mutants and transgenics. Nucleic acids research 41:D854-860.

Huang P, Xiao A, Zhou M, Zhu Z, Lin S, Zhang B (2011) Heritable gene targeting in zebrafish using customized TALENs. Nature biotechnology 29:699-700.

Huberman AD, Niell CM (2011) What can mice tell us about how vision works? Trends in neurosciences 34:464-473.

Hwang WY, Fu Y, Reyon D, Maeder ML, Tsai SQ, Sander JD, Peterson RT, Yeh JR, Joung JK (2013) Efficient genome editing in zebrafish using a CRISPR-Cas system. Nature biotechnology 31:227-229.

Jobling AI, Vessey KA, Waugh M, Mills SA, Fletcher EL (2013) A naturally occurring mouse model of achromatopsia: characterization of the mutation in cone transducin and subsequent retinal phenotype. Investigative ophthalmology & visual science 54:3350-3359.

Jurica MS, Moore MJ (2003) Pre-mRNA splicing: awash in a sea of proteins. Molecular cell 12:5-14.

Kim J, Lee E, Chang BS, Oh CS, Mun GH, Chung YH, Shin DH (2005) The presence of megamitochondria in the ellipsoid of photoreceptor inner segment of the zebrafish retina. Anatomia, histologia, embryologia 34:339-342.

Kitamura E, Danciger M, Yamashita C, Rao NP, Nusinowitz S, Chang B, Farber DB (2006) Disruption of the gene encoding the beta1-subunit of transducin in the Rd4/+ mouse. Investigative ophthalmology & visual science 47:1293-1301.

Klenke S, Kussmann M, Siffert W (2011) The GNB3 C825T polymorphism as a pharmacogenetic marker in the treatment of hypertension, obesity, and depression. Pharmacogenetics and genomics 21:594-606.

Kolb H (2011) Simple anatomy of the eye. In.

Konieczka K, Flammer AJ, Todorova M, Meyer P, Flammer J (2012) Retinitis pigmentosa and ocular blood flow. The EPMA journal 3:17.

Konrad M (1992) Cloning and expression of the essential gene for guanylate kinase from yeast. The Journal of biological chemistry 267:25652-25655.

Krizaj D, Copenhagen DR (2002) Calcium regulation in photoreceptors. Frontiers in bioscience : a journal and virtual library 7:d2023-2044.

Lagman D, Callado-Perez A, Franzen IE, Larhammar D, Abalo XM (2015) Transducin duplicates in the zebrafish retina and pineal complex: differential specialisation after the teleost tetraploidisation. PloS one 10:e0121330.

Larhammar D, Nordstrom K, Larsson TA (2009) Evolution of vertebrate rod and cone phototransduction genes. Philosophical transactions of the Royal Society of London Series B, Biological sciences 364:2867-2880.

Lenkowski JR, Raymond PA (2014) Muller glia: Stem cells for generation and regeneration of retinal neurons in teleost fish. Progress in retinal and eye research 40:94-123.

Lewis A, Williams P, Lawrence O, Wong RO, Brockerhoff SE (2010a) Wild-type cone photoreceptors persist despite neighboring mutant cone degeneration. J Neurosci 30:382-389.

Lewis A, Williams P, Lawrence O, Wong RO, Brockerhoff SE (2010b) Wild-type cone photoreceptors persist despite neighboring mutant cone degeneration. The Journal of neuroscience : the official journal of the Society for Neuroscience 30:382-389.

Lim S, Wang Y, Yu X, Huang Y, Featherstone MS, Sampath K (2013) A simple strategy for heritable chromosomal deletions in zebrafish via the combinatorial action of targeting nucleases. Genome biology 14:R69.

Linder B, Dill H, Hirmer A, Brocher J, Lee GP, Mathavan S, Bolz HJ, Winkler C, Laggerbauer B, Fischer U (2011) Systemic splicing factor deficiency causes tissue-specific defects: a zebrafish model for retinitis pigmentosa. Human molecular genetics 20:368-377.

Liu S, Rauhut R, Vornlocher HP, Luhrmann R (2006) The network of protein-protein interactions within the human U4/U6.U5 tri-snRNP. Rna 12:1418-1430.

Makarova OV, Makarov EM, Liu S, Vornlocher HP, Luhrmann R (2002) Protein 61K, encoded by a gene (PRPF31) linked to autosomal dominant retinitis pigmentosa, is required for U4/U6*U5 tri-snRNP formation and pre-mRNA splicing. The EMBO journal 21:1148-1157.

Makhankov YV, Rinner O, Neuhauss SC (2004) An inexpensive device for non-invasive electroretinography in small aquatic vertebrates. Journal of neuroscience methods 135:205-210.

McKie AB, McHale JC, Keen TJ, Tarttelin EE, Goliath R, van Lith-Verhoeven JJ, Greenberg J, Ramesar RS, Hoyng CB, Cremers FP, Mackey DA, Bhattacharya SS, Bird AC, Markham AF, Inglehearn CF (2001) Mutations in the pre-mRNA splicing factor gene PRPC8 in autosomal dominant retinitis pigmentosa (RP13). Human molecular genetics 10:1555-1562.

McLaren W, Pritchard B, Rios D, Chen Y, Flicek P, Cunningham F (2010) Deriving the consequences of genomic variants with the Ensembl API and SNP Effect Predictor. Bioinformatics 26:2069-2070.

Meighan PC, Peng C, Varnum MD (2015) Inherited macular degeneration-associated mutations in CNGB3 increase the ligand sensitivity and spontaneous open probability of cone cyclic nucleotide-gated channels. Frontiers in physiology 6:177.

Michaelides M, Hardcastle AJ, Hunt DM, Moore AT (2006) Progressive cone and cone-rod dystrophies: phenotypes and underlying molecular genetic basis. Survey of ophthalmology 51:232-258.

Michaelides M, Aligianis IA, Ainsworth JR, Good P, Mollon JD, Maher ER, Moore AT, Hunt DM (2004) Progressive cone dystrophy associated with mutation in CNGB3. Investigative ophthalmology & visual science 45:1975-1982.

Miller JC, Tan S, Qiao G, Barlow KA, Wang J, Xia DF, Meng X, Paschon DE, Leung E, Hinkley SJ, Dulay GP, Hua KL, Ankoudinova I, Cost GJ, Urnov FD, Zhang HS, Holmes MC, Zhang L, Gregory PD, Rebar EJ (2011) A TALE nuclease architecture for efficient genome editing. Nature biotechnology 29:143-148.

Montiani-Ferreira F, Li T, Kiupel M, Howland H, Hocking P, Curtis R, Petersen-Jones S (2003) Clinical features of the retinopathy, globe enlarged (rge) chick phenotype. Vision research 43:2009-2018.

Muto A, Orger MB, Wehman AM, Smear MC, Kay JN, Page-McCaw PS, Gahtan E, Xiao T, Nevin LM, Gosse NJ, Staub W, Finger-Baier K, Baier H (2005) Forward genetic analysis of visual behavior in zebrafish. PLoS genetics 1:e66.

Natarajan S (2011) Retinitis pigmentosa: a brief overview. Indian journal of ophthalmology 59:343-346.

Nemudryi AA, Valetdinova KR, Medvedev SP, Zakian SM (2014) TALEN and CRISPR/Cas Genome Editing Systems: Tools of Discovery. Acta naturae 6:19-40.

Neuhauss SC (2003) Behavioral genetic approaches to visual system development and function in zebrafish. Journal of neurobiology 54:148-160.

Nikonov SS, Lyubarsky A, Fina ME, Nikonova ES, Sengupta A, Chinniah C, Ding XQ, Smith RG, Pugh EN, Jr., Vardi N, Dhingra A (2013) Cones respond to light in the absence of transducin beta subunit. The Journal of neuroscience : the official journal of the Society for Neuroscience 33:5182-5194.

Oldham WM, Hamm HE (2008) Heterotrimeric G protein activation by G-protein-coupled receptors. Nature reviews Molecular cell biology 9:60-71.

Olsen O, Bredt DS (2003) Functional analysis of the nucleotide binding domain of membrane-associated guanylate kinases. The Journal of biological chemistry 278:6873-6878.

Pang JJ, Alexander J, Lei B, Deng W, Zhang K, Li Q, Chang B, Hauswirth WW (2010) Achromatopsia as a potential candidate for gene therapy. Advances in experimental medicine and biology 664:639-646.

Perrault I, Rozet JM, Calvas P, Gerber S, Camuzat A, Dollfus H, Chatelin S, Souied E, Ghazi I, Leowski C, Bonnemaison M, Le Paslier D, Frezal J, Dufier JL, Pittler S, Munnich A, Kaplan J (1996) Retinal-specific guanylate cyclase gene mutations in Leber's congenital amaurosis. Nature genetics 14:461-464.

Progatzky F, Dallman MJ, Lo Celso C (2013) From seeing to believing: labelling strategies for in vivo cell-tracking experiments. Interface focus 3:20130001.

Punzo C, Xiong W, Cepko CL (2012) Loss of daylight vision in retinal degeneration: are oxidative stress and metabolic dysregulation to blame? The Journal of biological chemistry 287:1642-1648.

Ridge KD, Abdulaev NG, Sousa M, Palczewski K (2003) Phototransduction: crystal clear. Trends in biochemical sciences 28:479-487.

Ripps H (2002) Cell death in retinitis pigmentosa: gap junctions and the 'bystander' effect. Experimental eye research 74:327-336.

Ritchey ER, Bongini RE, Code KA, Zelinka C, Petersen-Jones S, Fischer AJ (2010) The pattern of expression of guanine nucleotide-binding protein beta3 in the retina is conserved across vertebrate species. Neuroscience 169:1376-1391.

Robu ME, Larson JD, Nasevicius A, Beiraghi S, Brenner C, Farber SA, Ekker SC (2007) p53 activation by knockdown technologies. PLoS genetics 3:e78.

Rossi A, Kontarakis Z, Gerri C, Nolte H, Holper S, Kruger M, Stainier DY (2015) Genetic compensation induced by deleterious mutations but not gene knockdowns. Nature 524:230-233.

Saade CJ, Alvarez-Delfin K, Fadool JM (2013) Rod photoreceptors protect from cone degeneration-induced retinal remodeling and restore visual responses in zebrafish. The Journal of neuroscience : the official journal of the Society for Neuroscience 33:1804-1814.

Sancho-Pelluz J, Arango-Gonzalez B, Kustermann S, Romero FJ, van Veen T, Zrenner E, Ekstrom P, Paquet-Durand F (2008) Photoreceptor cell death mechanisms in inherited retinal degeneration. Molecular neurobiology 38:253-269.

Sander JD, Joung JK (2014) CRISPR-Cas systems for editing, regulating and targeting genomes. Nature biotechnology 32:347-355.

Sander JD, Maeder ML, Reyon D, Voytas DF, Joung JK, Dobbs D (2010) ZiFiT (Zinc Finger Targeter): an updated zinc finger engineering tool. Nucleic acids research 38:W462-468.

Schulte-Merker S, Stainier DY (2014) Out with the old, in with the new: reassessing morpholino knockdowns in light of genome editing technology. Development 141:3103-3104.

Schneider CA, Rasband WS, Eliceiri KW (2012) NIH Image to ImageJ: 25 years of image analysis. Nat Methods 9:671-675.

Sekulic N, Shuvalova L, Spangenberg O, Konrad M, Lavie A (2002) Structural characterization of the closed conformation of mouse guanylate kinase. The Journal of biological chemistry 277:30236-30243.

Semple-Rowland SL, Lee NR, Van Hooser JP, Palczewski K, Baehr W (1998) A null mutation in the photoreceptor guanylate cyclase gene causes the retinal degeneration chicken phenotype. Proceedings of the National Academy of Sciences of the United States of America 95:1271-1276.

Shichida Y, Matsuyama T (2009) Evolution of opsins and phototransduction. Philosophical transactions of the Royal Society of London Series B, Biological sciences 364:2881-2895.

Simo R, Villarroel M, Corraliza L, Hernandez C, Garcia-Ramirez M (2010) The retinal pigment epithelium: something more than a constituent of the blood-retinal barrier--implications for the pathogenesis of diabetic retinopathy. Journal of biomedicine & biotechnology 2010:190724.

Sprague J, Bayraktaroglu L, Clements D, Conlin T, Fashena D, Frazer K, Haendel M, Howe DG, Mani P, Ramachandran S, Schaper K, Segerdell E, Song P, Sprunger B, Taylor S, Van Slyke CE, Westerfield M (2006) The Zebrafish Information Network: the zebrafish model organism database. Nucleic acids research 34:D581-585.

Streisinger G, Walker C, Dower N, Knauber D, Singer F (1981) Production of clones of homozygous diploid zebra fish (Brachydanio rerio). Nature 291:293-296.

Takechi M, Seno S, Kawamura S (2008) Identification of cis-acting elements repressing blue opsin expression in zebrafish UV cones and pineal cells. The Journal of biological chemistry 283:31625-31632.

Tanackovic G, Ransijn A, Thibault P, Abou Elela S, Klinck R, Berson EL, Chabot B, Rivolta C (2011) PRPF mutations are associated with generalized defects in spliceosome formation and pre-mRNA splicing in patients with retinitis pigmentosa. Human molecular genetics 20:2116-2130.

Tarboush R, Chapman GB, Connaughton VP (2012) Ultrastructure of the distal retina of the adult zebrafish, Danio rerio. Tissue & cell 44:264-279.

Travis GH (1998) Mechanisms of cell death in the inherited retinal degenerations. American journal of human genetics 62:503-508.

Tsujikawa M, Malicki J (2004) Genetics of photoreceptor development and function in zebrafish. The International journal of developmental biology 48:925-934.

Tummala H, Ali M, Getty P, Hocking PM, Burt DW, Inglehearn CF, Lester DH (2006) Mutation in the guanine nucleotide-binding protein beta-3 causes retinal degeneration and embryonic mortality in chickens. Investigative ophthalmology & visual science 47:4714-4718.

Tummala H, Fleming S, Hocking PM, Wehner D, Naseem Z, Ali M, Inglehearn CF, Zhelev N, Lester DH (2011) The D153del mutation in GNB3 gene causes tissue specific signalling patterns and an abnormal renal morphology in Rge chickens. PloS one 6:e21156.

Vallazza-Deschamps G, Cia D, Gong J, Jellali A, Duboc A, Forster V, Sahel JA, Tessier LH, Picaud S (2005) Excessive activation of cyclic nucleotide-gated channels contributes to neuronal degeneration of photoreceptors. The European journal of neuroscience 22:1013-1022.

Varshney GK, Pei W, LaFave MC, Idol J, Xu L, Gallardo V, Carrington B, Bishop K, Jones M, Li M, Harper U, Huang SC, Prakash A, Chen W, Sood R, Ledin J, Burgess SM (2015) High-throughput gene targeting and phenotyping in zebrafish using CRISPR/Cas9. Genome research 25:1030-1042.

Veleri S, Lazar CH, Chang B, Sieving PA, Banin E, Swaroop A (2015) Biology and therapy of inherited retinal degenerative disease: insights from mouse models. Disease models & mechanisms 8:109-129.

Vihtelic TS, Doro CJ, Hyde DR (1999) Cloning and characterization of six zebrafish photoreceptor opsin cDNAs and immunolocalization of their corresponding proteins. Visual neuroscience 16:571-585.

Vithana EN, Abu-Safieh L, Allen MJ, Carey A, Papaioannou M, Chakarova C, Al-Maghtheh M, Ebenezer ND, Willis C, Moore AT, Bird AC, Hunt DM, Bhattacharya SS (2001) A human homolog of yeast pre-mRNA splicing gene, PRP31, underlies autosomal dominant retinitis pigmentosa on chromosome 19q13.4 (RP11). Molecular cell 8:375-381.

Wall MA, Coleman DE, Lee E, Iniguez-Lluhi JA, Posner BA, Gilman AG, Sprang SR (1995) The structure of the G protein heterotrimer Gi alpha 1 beta 1 gamma 2. Cell 83:1047-1058.

Weinstein LS, Chen M, Xie T, Liu J (2006) Genetic diseases associated with heterotrimeric G proteins. Trends in pharmacological sciences 27:260-266.

Wissinger B et al. (2001) CNGA3 mutations in hereditary cone photoreceptor disorders. American journal of human genetics 69:722-737.

Xu J, Morris L, Thapa A, Ma H, Michalakis S, Biel M, Baehr W, Peshenko IV, Dizhoor AM, Ding XQ (2013) cGMP accumulation causes photoreceptor degeneration in CNG channel deficiency: evidence of cGMP cytotoxicity independently of enhanced CNG channel function. The Journal of neuroscience : the official journal of the Society for Neuroscience 33:14939-14948.

Yin J, Brocher J, Fischer U, Winkler C (2011) Mutant Prpf31 causes pre-mRNA splicing defects and rod photoreceptor cell degeneration in a zebrafish model for Retinitis pigmentosa. Molecular neurodegeneration 6:56.

Yin J, Brocher J, Linder B, Hirmer A, Sundaramurthi H, Fischer U, Winkler C (2012) The 1D4 antibody labels outer segments of long double cone but not rod photoreceptors in zebrafish. Investigative ophthalmology & visual science 53:4943-4951.

Zhang JH, Pandey M, Seigneur EM, Panicker LM, Koo L, Schwartz OM, Chen W, Chen CK, Simonds WF (2011) Knockout of G protein beta5 impairs brain development and causes multiple neurologic abnormalities in mice. Journal of neurochemistry 119:544-554.

Zhang Y, Niu H, Li Y, Chu H, Shen H, Zhang D, Li G (2015) Mechanistic insight into the functional transition of the enzyme guanylate kinase induced by a single mutation. Scientific reports 5:8405.

Appendix 1 : Supplementary figures

Supplementary Figure 1

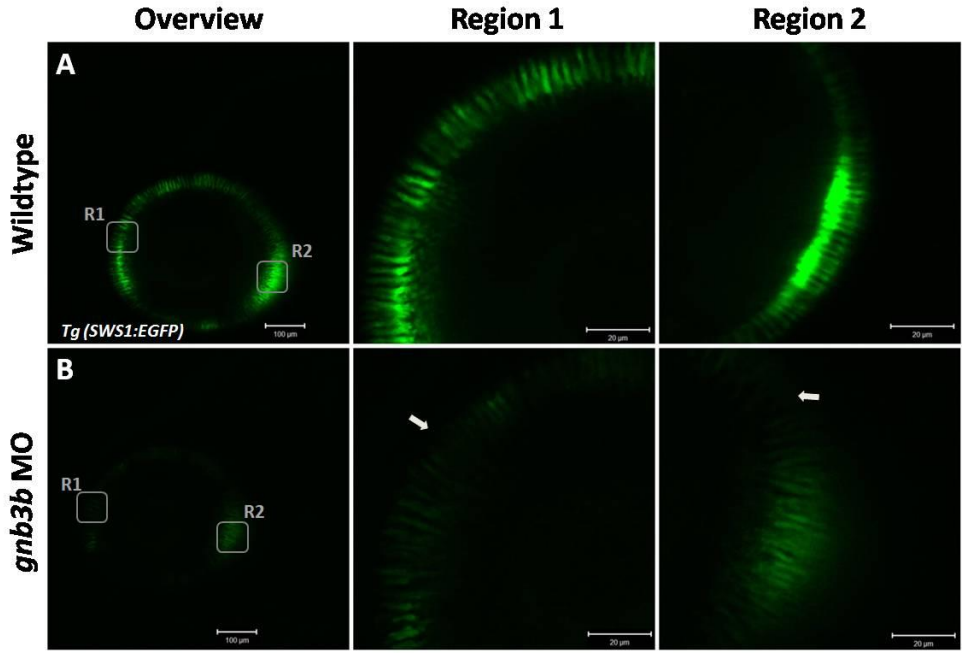

SP Figure 1: Live imaging of *gnb3b* Mo injected *Tg (SWS1:EGFP)* larvae at 4 dpf. A: The wildtype UV cones are observed throughout the retina of 4 days old larvae with clear EGFP signal. At higher magnifications, it was observed that the UV cones have an elongated morphology with strong EGFP signal towards the base of the inner segment (middle and right panels). B: In the *gnb3b* morphants, the EGFP expression in the UV cones were considerably reduced with aberrantly formed cells (middle and right panels). Additionally, in some regions cells are found to be missing (white arrows).

Appendix 2

List of primers used in this study.

Experiments used	5' - 3' sequence
***gnb3b* morphant screen**	
*gnb3b*E4up	TGG TCA GTG CAT CAC AGG AT
*gnb3b*E5do	GAG CAT CCA GCT CTT TCA CA
zf*gnb3b*I4	TGC TCC AGG ATC AAC ACA GA
TALEN mutant lines	
TALEN generation	
M13-47	CGC CAG GGT TTT CCC AGT CAC GAC
RV-M	AGC GGA TAA CAA TTT CAC ACA GGA
pCS-FokI_F1	GGT GGC GGG AGA GTT GAG AG
pCS-FokI_R3	CAA TGC TCT CCA GCG CCG GCC TG
pCS-FokI_R4	GCA TCC AGC GCA GGA CGT CC
TALEN mutant screening	
*gnb3b*I3For	CAC CAT GTT TTA ACC GTT GG
*gnb3b*E4Rev	ACC AAT GCA TGG CGT AGA TT
*gnb3b*I6for2	CAT AGC TTG GCA ACC AAT CA
*gnb3b*I7rev2	AAC CCT TCA GCG TTT TCT GA
CRISPR/Cas9 mutant lines	
Mutant screening	
guk1E616for	CAA TGG AGA TCC TGG TCA GC
guk1I7rev	TTT TGA TCC TTG CTC CTG GT
***gnb3b* gRNA preparation**	
*gnb3b*CROligo1	TAG GAA ATC TCG TGG CCA GCG G
*gnb3b*CROligo2	AAA CCC GCT GGC CAC GAG ATT T
Mutant screening	
1_FOR_*gnb3b*CrispR	TTG ATG ATG CAC AAA TGA AAA AG
2_FOR_*gnb3b*CrispR	AAA AAG CAC ACA TTA TTG CAT TGT A
3_FOR_*gnb3b*CrispR	TTT ACA AAA TCA TGA CGT GCT CTA A
4_FOR_*gnb3b*CrispR	CAC AGA TGT TGA TCG CAT TAT ACT T
6_FOR_*gnb3b*CrispR	AGA GCG TAA CTG GAA TGC TG
1_REV_*gnb3b*CrispR	TTG TTT GAT CTT CAG GTG TGT TC
2_REV_*gnb3b*CrispR	GAC GAT CTC AGT GTC ACT TAT GAA A
3_REV_*gnb3b*CrispR	TCA GCG TTC TCT ATT TTA GCA GAT T
4_REV_*gnb3b*CrispR	GCG AGA AAG TAA AGT CTC TTG TTT G
Co-ortholog test	
*guk1a*_For1	AGG CCT GTG GTG ATG AGT G
*guk1a*_Rev1	GGA AGT GAA CGG AGA GAG G
*gnb3a*_For1	CGG AGA AGC TGA AGG ATG AC
*gnb3a*_Rev1	GGC GAG GGA CAT ACA GTC TC

Experiments used	5' - 3' sequence
Probes generation	
*gnb3b*exonup	TGG TCA GTG CAT CAC AGG AT
*gnb3b*exondown	GCC AGA AAG CAC ACC AAC TT
Housekeeping gene (loading control)	
*bActin*2FOR	ATC GTG ATG GAC TCT GGT GA
*bActin*2REV	AAG AAG GAT GGC TGG AAC AG
Sequencing of cloned samples	
M13 Forward (-20)	GTA AAA CGA CGG CCA G
M13 Reverse	CAG GAA ACA GCT ATG AC
pJET1.2 forward	CGA CTC ACT ATA GGG AGA GCG GC
pJET1.2 reverse	AAG AAC ATC GAT TTT CCA TGG CAG
Sp6	ATT TAG GTG ACA CTA TAG